

AD-A130 071

CURING OF GRAPHITE/EPOXY COMPOSITES(U) MICHIGAN UNIV
ANN ARBOR DEPT OF MECHANICAL ENGINEERING AND APPLIED
MECHANICS A C LOOS ET AL. MAR 83 AFWAL-TR-83-4040

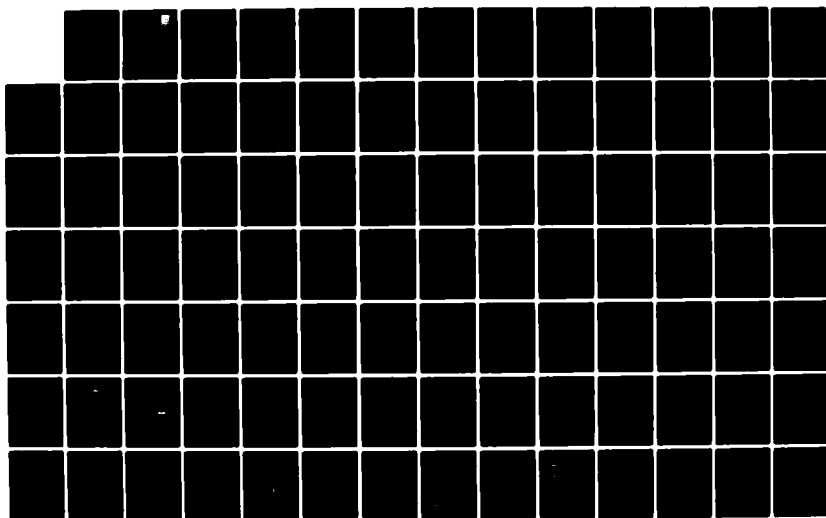
1/2

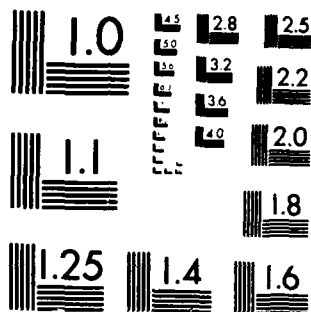
UNCLASSIFIED

F33615-81-C-5050

F/G 11/4

NL





MICROCOPY RESOLUTION TEST CHART
NATIONAL BUREAU OF STANDARDS-1963-A

ADA130071

AFWAL-TR-83-4040

CURING OF GRAPHITE/EPOXY COMPOSITES

Alfred C. Loos
George S. Springer

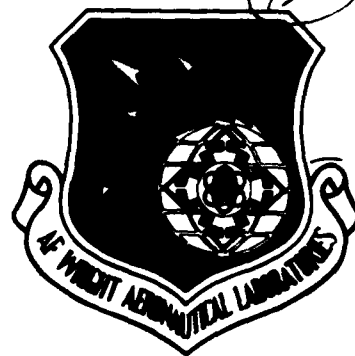
Department of Mechanical Engineering and Applied Mechanics
The University of Michigan
Ann Arbor, MI. 48109

March 1983

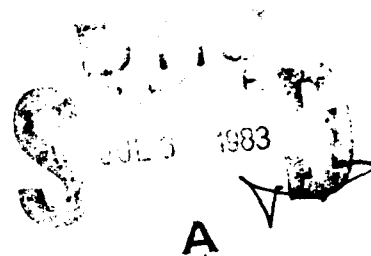
Interim Report for Period June 1982-March 1983

Approved for Public Release; Distribution Unlimited

MATERIALS LABORATORY
AIR FORCE WRIGHT AERONAUTICAL LABORATORIES
AIR FORCE SYSTEMS COMMAND
WRIGHT-PATTERSON AFB, OHIO 45433



DTIC FILE COPY



83 07 6 102

NOTICE

When Government drawings, specifications, or other data are used for any purpose other than in connection with a definitely related Government procurement operation, the United States Government thereby incurs no responsibility nor any obligation whatsoever; and the fact that the Government may have formulated, furnished, or in any way supplied the said drawings, specifications, or other data, is not to be regarded by implication or otherwise as in any manner licensing the holder or any other person or corporation, or conveying any rights or permission to manufacture, use, or sell any patented invention that may in any way be related thereto.

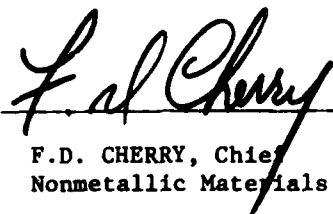
This report has been reviewed by the Office of Public Affairs (ASD/PA) and is releasable to the National Technical Information Service (NTIS). At NTIS, it will be available to the general public, including foreign nations.

This technical report has been reviewed and is approved for publication.



S.W. Tsai, Project Engineer & Chief
Mechanics and Surface Interactions Branch
Nonmetallic Materials Division

FOR THE COMMANDER



F.D. CHERRY, Chief
Nonmetallic Materials Division

"If your address has changed, if you wish to be removed from our mailing list, or if the addressee is no longer employed by your organization please notify AFWAL/MLBM, W-PAFB, Ohio 45433 to help us maintain a current mailing list.

Copies of this report should not be returned unless return is required by security considerations, contractual obligations, or notice on a specific document.

Unclassified

SECURITY CLASSIFICATION OF THIS PAGE (When Data Entered)

REPORT DOCUMENTATION PAGE		READ INSTRUCTIONS BEFORE COMPLETING FORM
1. REPORT NUMBER AFWAL-TR-83 -4040	2. GOVT ACCESSION NO. AD-A130071	3. RECIPIENT'S CATALOG NUMBER
4. TITLE (and Subtitle) CURING OF GRAPHITE/EPOXY COMPOSITES		5. TYPE OF REPORT & PERIOD COVERED June, 1982-March 1983
		6. PERFORMING ORG. REPORT NUMBER
7. AUTHOR(s) Alfred C. Loos George S. Springer		8. CONTRACT OR GRANT NUMBER(s) F33615-81-C-5050
9. PERFORMING ORGANIZATION NAME AND ADDRESS Department of Mechanical Engineering and Applied Mechanics, The University of Michigan Ann Arbor, MI. 48109		10. PROGRAM ELEMENT, PROJECT, TASK AREA & WORK UNIT NUMBERS FY1457-81-02013
11. CONTROLLING OFFICE NAME AND ADDRESS Materials Laboratory (AFWAL/MLBM) Air Force Wright Aeronautical Laboratories, AFSC Wright-Patterson, AFB, OH. 45433		12. REPORT DATE March 1983
14. MONITORING AGENCY NAME & ADDRESS (if different from Controlling Office)		13. NUMBER OF PAGES 158
		15. SECURITY CLASS. (of this report) Unclassified
		15a. DECLASSIFICATION/DOWNGRADING SCHEDULE
16. DISTRIBUTION STATEMENT (of this Report) Approved for public release, distribution unlimited		
17. DISTRIBUTION STATEMENT (of the abstract entered in Block 20, if different from Report)		
18. SUPPLEMENTARY NOTES		
19. KEY WORDS (Continue on reverse side if necessary and identify by block number) Composite Materials Curing Manufacturing		
20. ABSTRACT (Continue on reverse side if necessary and identify by block number) Models were developed which describe the curing process of composites constructed from continuous fiber-reinforced, thermosetting resin matrix prepreg materials. On the basis of the models, a computer code was developed, which for flat-plate composites cured by a specified cure cycle, provides the temperature distribution, the degree of cure of the resin, and the resin viscosity, inside the composite. In addition, the computer code can be used to determine the amount of resin flow out of the composite and the resin content of the composite and the bleeder.		

DD FORM 1 JAN 73 1473

Unclassified

SECURITY CLASSIFICATION OF THIS PAGE (When Data Entered)

Unclassified

SECURITY CLASSIFICATION OF THIS PAGE(When Data Entered)

Tests were performed measuring the temperature distribution in and the resin flow out of composites constructed from Hercules AS/3501-6 graphite/epoxy prepreg tape. The data was compared with results calculated with the computer code for the conditions employed in the tests. Good agreement was found between the data and the results of the computer code indicating that the model describes adequately the temperature distribution and resin flow.

A parametric study was also performed to illustrate how the model and the associated computer code can be used to determine the appropriate cure cycle for a given application, which results in a composite that is cured uniformly in the shortest amount of time.

Unclassified

SECURITY CLASSIFICATION OF THIS PAGE(When Data Entered)

FOREWORD

This report was prepared by Alfred C. Loos and George S. Springer, Department of Mechanical Engineering and Applied Mechanics, The University of Michigan for the Mechanics and Surface Interactions Branch (AFWAL/MLBM), Nonmetallic Materials Division, Materials Laboratory, Air Force Wright Aeronautical Laboratories, Wright-Patterson AFB, Ohio. The work was performed under Contract Number F 33617-81-C5050, Project number FY1457-~~81~~-02013.

This report covers work accomplished during the period June, 1982-March 1983.

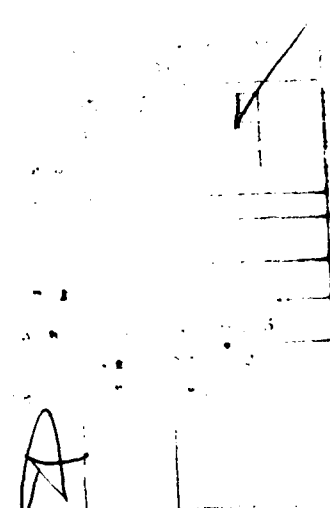


TABLE OF CONTENTS

Section	Page
I. INTRODUCTION	1
II. MODEL	4
2.1 Problem Statement	5
2.2 Thermo-Chemical Model	7
2.3 Resin Flow Model	11
2.3.1 Resin Flow Normal to the Tool Plate	14
2.3.2 Resin Flow Parallel to the Tool Plate	18
2.3.3 Total Resin Flow	23
2.4 Calculation of the Prepreg Properties	24
2.5 Use of the Model in Establishing the Cure Cycle	27
III. INPUT PARAMETERS	28
3.1 Compacted Prepreg Ply Thickness and Resin Content	31
3.2 Apparent Permeability (S_c) and Flow Coefficient (B')	32
3.3 Heat of Reaction and Degree of Cure	33
3.4 Viscosity	33
3.5 Bleeder Properties	34
IV. NUMERICAL	36
4.1 Grid	36
4.2 Numerical Solution to the Thermo-Chemical Model	38
4.3 Numerical Solution to the Resin Flow Model	41
4.4 Properties at the Grid Points	48
4.5 Computer Code	49
V. EXPERIMENTAL	54
5.1 Heated Platens	54

5.2	Pneumatic Press	57
5.3	Temperature Controller	60
5.4	Test Specimens	63
5.5	Experimental Procedure	65
VI.	RESULTS	66
6.1	Comparisons Between the Results of the Model and Data	66
6.2	Selection of the Cure Cycle	73
VII.	SUMMARY AND CONCLUSION	98
	APPENDICES	101
A.	Heat of Reaction and Degree of Cure Measurements for Hercules 3501-6 Resin	102
B.	Properties of Hercules AS/3501-6 Prepreg and Mochburg CW 1850 Thermal Fiber Bleeder Cloth	122
C.	Additional Temperature Controller Information	126
D.	Relationship Between Platen Force and Cylinder Pressure	132
	REFERENCES	135

LIST OF FIGURES

Figure

1.	Geometry of the Composite-Bleeder System.....	6
2.	Resin Flow Model.....	10
3.	Illustration of the Resin Flow Process Normal to the Tool Plate.....	13
4.	Simultaneous Resin Flow Both Normal and Parallel to the Tool Plate.....	15
5.	Geometry of the Resin Flow Model Parallel to the Tool Plate.....	20
6.	Arrangement of the Grid Points.....	37
7.	Model of the Resin Flow Processes Normal and Parallel to the Tool Plate.....	42
8.	Temperature Distribution as a Function of Time. Comparison Between the Computer and Analytical Solutions.....	50
9.	Degree of Cure as a Function of Time. Comparison Between the Computer and Analytical Solutions.....	51
10.	Resin Flow as a Function of Time Normal to the Tool Plate (top) and Parallel to the Tool Plate (bottom). Comparison Between the Computer and Pocket Calculator Solutions.....	53
11.	Geometry of the Heated Platens.....	55
12.	Temperature Distribution Across the Surface of the Lower Platen as a Function of Time. Symbols Represent the Location of the Thermocouples on the Platen Surface.....	58
13.	Schematic of the Pneumatic Press.....	59
14.	Schematic of the Temperature Controller Circuit.....	61
15.	The Temperatures Measured on the Surfaces of 16, 32, and 64-Ply Composites During Cure.....	67

List of Figures (cont.)

Figure

16. Temperature as a Function of Time at Three Positions Inside a 64-Ply Composite. Comparisons Between the Data and the Results Computed by the Model. The Temperature Cure Cycle is Shown in Figure 15. The Cure Pressure and the Bleeder Pressure were Constant at 586 kPa (85 psi) and 101 kPa (14.7 psi) Respectively..... 69
17. The Mass Loss, Normal to the Tool Plate (bottom), Parallel to the Tool Plate (center), and the Total Mass Loss (top) as a Function of Time for a 64-Ply Composite. Comparisons Between the Data and the Results Computed by the Model for Different Cure Pressures. The Temperature Cure Cycle is Shown in Figure 15. The Bleeder Pressure was Constant at 101 kPa (14.7 psi). The Initial Resin Content was 42%..... 70
18. The Mass Loss, Normal to the Tool Plate (bottom), Parallel to the Tool Plate (center), and the Total Mass Loss (top) as a Function of Time. Comparisons Between the Data and the Results Computed by the Model for 16, 32, and 64-Ply Composites. The Temperature Cure Cycle is Shown in Figure 15. The Cure and Bleeder Pressures were Constant at 586 kPa (85 psi) and 101 kPa (14.7 psi) Respectively. The Initial Resin Content was 42%..... 71
19. The Mass Loss, Normal to the Tool Plate (bottom), Parallel to the Tool Plate (center), and the Total Mass Loss (top) as a Function of Time for a 64-Ply Composite. Comparisons Between the Data and the Results Computed by the Model for Different Initial Resin Contents (39% and 42%). The Temperature Cure Cycle is Shown in Figure 15. The Cure and Bleeder Pressures were Constant at 586 kPa (85 psi) and 101 kPa (14.7 psi) Respectively..... 72
20. Illustration of the Cure Cycle Used in the Parametric Study..... 75
21. Manufacturer's Recommended Cure Cycle for Hercules AS/3501-6 Prepreg [38]..... 76
22. Temperature Distribution as a Function of Time for Different Heating Rates and Different Thicknesses. a) 64-Ply, $\dot{T}_0 = 2.8^\circ\text{C/min}$ (left), b) 64-Ply, $\dot{T}_0 = 27.8^\circ\text{C/min}$ (right). Results Obtained by the Model..... 78

List of Figures (cont.)

Figure

23. Number of Compacted Plies, n_s , as a Function of Time for Different Cure Pressures and Different Composite Thicknesses. a) 16-Ply (bottom), b) 32-Ply (center), and c) 64-Ply (top). Results Obtained by the Model..... 80
24. Number of Compacted Plies, n_s , as a Function of Time for a) Different Maximum Cure Temperatures, T_{max} (bottom) and b) Different Heating Rates, \dot{T}_0 (top). Results Obtained by the Model..... 81
25. The Time Required, t_y , to Squeeze Excess Resin Out of Every Ply of a 32-Ply Composite at a) Different Maximum Cure Temperatures, T_{max} (left) and b) Different Heating Rates, \dot{T}_0 (right). Results Obtained by the Model... 83
26. Number of Compacted Plies, n_s , as a Function of Time for a Composite Cured by the Cure Cycle Recommended by the Prepreg Manufacturer (Figure 21). Results Obtained by the Model..... 84
27. The Maximum Number of Compacted Plies, $(n_s)_{max}$, at the End of the Cure as a Function of Cure Pressure, P_0 . Results Obtained by the Model..... 86
28. Viscosity Distribution at Different Times Inside a 32-Ply Composite. Results Obtained by the Model..... 87
29. The Maximum Viscosity, μ_{max} , Inside a 32-Ply Composite as a Function of Time. Gel is Assumed to Occur When the Viscosity Reaches 100 Pa.s. Results Obtained by the Model..... 88
30. Number of Compacted Plies, n_s , as a Function of Time for a) Different Cure Pressures, P_0 (left) and b) Different Heating Rates, \dot{T}_0 (right). The Pressure Should be Applied Before Time $t_{p,0}$. Results Obtained by the Model. 90
31. Degree of Cure Distribution as a Function of Time. a) 64-Ply Composite, $\dot{T}_0 = 2.8^\circ\text{C/min}$ (left). b) 128-Ply Composite, $\dot{T}_0 = 27.8^\circ\text{C/min}$ (right). Results Obtained by the Model..... 91

List of Figures (cont.)

Figure

32. Illustration of the Minimum Value of the Degree of Cure, α_{\min} , Inside the Composite as a Function of Time. The Cure is Considered Complete When the Degree of Cure Reaches a Specified Value, α^* , at Every Point in the Composite..... 93
33. Minimum Degree of Cure, α_{\min} , as a Function of Time for a 32-Ply Composite at a) Different Maximum Cure Temperatures, T_{\max} (left) and b) Different Heating Rates, \dot{T}_0 (right). Results Obtained by the Model..... 95
34. Cure Time, t_c , as a Function of a) Maximum Cure Temperature, T_{\max} (left) and b) Heating Rate, \dot{T}_0 (right), for a 32-Ply Composite. Results Obtained by the Model.....
35. Minimum Degree of Cure, α_{\min} , as a Function of Time for a 32-Ply Composite Cured by the Manufacturer's Recommended Cure Cycle (Figure 21). Results Obtained by the Model
- A.1 Illustration of Rate of Heat Generation versus Time Curves Measured by Differential Scanning Calorimetry Using Dynamic Scanning and Isothermal Scanning..... 105
- A.2 A Typical Rate of Heat Generation versus Time Curve Provided by Dynamic Scanning Experiments. Sample Size 4.3 mg. Temperature Scale Constructed from the Known Value of the Scanning Rate which was 20 K/min. 107
- A.3 Cure Rate versus Degree of Cure. Solid Lines were Calculated Using Equations (A.6)-(A.8) and the Constants given in Table A.2. Note the Difference in Scales on the Vertical Axes of the Figures on the Left and Right..... 108
- A.4 The Parameters, K_1 , K_2 and K_3 (Equations A.6-A.8), as a Function of Inverse Absolute Temperature. Solid Lines were Calculated by a Least Square Curve Fit to the Data..... 111
- C.1 Output Voltage of the RTD Circuit as a Function of Resistance..... 127
- C.2 RTD Temperature as a Function of RTD Resistance. Calibration Curve was Constructed from Data Provided by the RTD Manufacturer [47]..... 128
- C.3 Output Voltage of the RTD Circuit as a Function of RTD Temperature..... 129

List of Figures (cont.)

Figure

- C.4 Relationship Between the Digital Input to the D/A Converter
and the Analog Voltage Output..... 130
- C.5 Temperature Controller Circuit Diagram..... 131
- D.1 Force Generated by the Cylinder Ram on the Press Platens
as a Function of Indicated Cylinder Air Pressure..... 133

LIST OF APPENDICES

Appendix

- A. Heat of Reaction and Degree of Cure Measurements
for Hercules 3501-6 Resin 102
- B. Properties of Hercules AS/3501-6 Prepreg and
Mochburg CW 1850 Thermal Fiber Bleeder Cloth. . . 122
- C. Additional Temperature Controller Information . . 126
- D. Relationship Between Platen Force and Cylinder
Pressure. 132

NOMENCLATURE

a	thermal diffusivity, m^2/s
A	cross sectional area, m^2
A_x	cross sectional area perpendicular to the x axis, m^2
A_z	cross sectional area perpendicular to the z axis, m^2
A_1, A_2, A_3	pre-exponential factors, min^{-1}
B	constant defined in Equation (A.6)
B_k	constant defined in Equation (2.49)
B_l	constant defined in Equation (2.20)
B'	flow coefficient of the prepreg parallel to the fibers
C	specific heat per unit mass of the composite, $kJ/(kg \cdot K)$
C_f	specific heat per unit mass of the fiber, $kJ/(kg \cdot K)$
C_n	specific heat per unit mass of the nth prepreg ply, $kJ/(kg \cdot K)$
C_r	specific heat per unit mass of the resin, $kJ/(kg \cdot K)$
d_n	thickness of the nth channel between the n and n-1 prepreg plies
dQ/dt	rate of heat generation measured by differential scanning calorimetry, $kJ/(kg \cdot min)$
dx/dt	cure rate, min^{-1}
$\Delta E_1, \Delta E_2, \Delta E_3$	activation energies, J/mol
f	functional relationship between cure rate, temperature, and degree of cure.
F	applied force along the channel surface, N
g	functional relationship between resin viscosity, temper- ature, and degree of cure

$G(t)$	parameter defined in Equation (2.16)
h_b	instantaneous depth of resin in the bleeder, m
h_c	thickness of the compacted plies, m
h_1	thickness of one compacted prepreg ply, m
H	amount of heat released, measured by differential scanning calorimetry, kJ/kg
H_r	heat of reaction per unit mass of the resin, J/kg
H_R	total or ultimate heat of reaction during cure, J/kg
$(H_R)_n$	heat of reaction per unit mass of the nth prepreg ply, J/kg
$H(t)$	heat evolved from the beginning of the reaction to some intermediate time t , J/kg
\dot{H}	rate of heat generation by chemical reactions, J/(kg·s)
k	thermal conductivity perpendicular to the plane of the composite (z direction), W/(m·K)
k_n	thermal conductivity of the nth prepreg ply normal to the fibers (z direction), W/(m·K)
k_f	thermal conductivity of the fiber, W/(m·K)
k_r	thermal conductivity of the resin, W/(m·K)
K_1, K_2, K_3	reaction rate constants, min^{-1}
L	thickness of the composite, m
L_b	thickness of the bleeder, m
L_i	initial thickness of the composite, m
\dot{m}_{rz}	resin mass flow rate normal to the tool plate (z direction), kg/s
$(\dot{m}_{rx})_n$	resin mass flow rate of the nth channel parallel to the fibers (x direction), kg/s
m^*	measured total mass loss of the composite, percent
m_E^*	measured mass loss due to resin flow parallel to the tool plate (x direction), percent

m_T^*	measured mass loss due to resin flow normal to the tool plate (z direction), percent
M	total mass of the composite, kg
M_{com}	mass of one compacted prepreg ply, kg
M_E	total amount of resin flow parallel to the tool plate (x direction), kg
$(M_E)_n$	amount of resin leaving the nth prepreg ply in time t parallel to the tool plate (x direction), kg
M_f	mass of the fibers in one prepreg ply, kg
M_i	initial mass of the composite, kg
M_L	measured mass of the fluid contained in the pores of the bleeder, kg
M_n	mass of the nth prepreg ply, kg
M_r	total mass of resin in the composite, kg
$(M_r)_{com}$	mass of resin in one compacted prepreg ply, kg
$(M_r)_n$	mass of resin in the nth prepreg ply, kg
M_T	mass of resin that leaves the composite and enters the bleeder (z direction), kg
\bar{M}_r	mass of the resin in the volume surrounding an "interior" grid point, kg
n_s	number of compacted plies
$(n_s)_{max}$	maximum number of compacted plies
N	total number of prepreg plies
P	pressure, Pa
P_b	pressure in the bleeder, Pa
P_c	pressure in the composite at position h_c , Pa
P_H	pressure at the vertical centerline of the nth channel, Pa
P_L	pressure at the channel exit, Pa

P_o	applied cure pressure, Pa
P_u	pressure at the interface between the composite and the bleeder, Pa
R	universal gas constant, J/(mol·K)
RE_n	Reynolds number, defined for the nth channel in Equation (2.23)
\dot{R}	reaction rate, s^{-1}
S	apparent permeability, m^2
S_b	apparent permeability of the bleeder, m^2
S_c	apparent permeability of the composite, m^2
t	time, min
t_c	cure time, min
t_N	time required to squeeze excess resin out of every ply in the composite, min
t_p	time of pressure application, min
t_{gel}	gel time, min
Δt	time step size
T	temperature, °C or K
T_i	initial temperature, °C
T_L	boundary temperature on the lower surface of the composite, °C
T_{max}	maximum cure temperature, °C
T_o	applied cure temperature, °C
T_u	boundary temperature on the upper surface of the composite, °C
T^*	maximum temperature limit, °C
\dot{T}_o	heating rate, °C/min
U	parameter defined in Equation (4.6)
v	velocity, m/s

v_b	velocity of the resin in the bleeder, normal to the tool plate (z direction), m/s
$(v_x)_n$	velocity of the resin in the nth channel, parallel to the tool plate (x direction), m/s
v_z	velocity of the resin in the composite, normal to the tool plate (z direction), m/s
V	volume, m^3
V_B	bulk volume of the bleeder, m^3
V_f	volume of the fibers in one prepreg ply, m^3
V_n	volume of the nth prepreg ply, m^3
V_p	volume of the pores in the bleeder, m^3
$(V_r)_n$	volume of the resin in the nth prepreg ply, m^3
W	width of the composite or prepreg, m
x	horizontal coordinate parallel to the tool plate
x_L	channel length, m
z	vertical coordinate normal to the tool plate
Δz_n	grid spacing in the vertical direction (Figure 6)

GREEK SYMBOLS

α	degree of cure
α_{min}	lowest value of the degree of cure in the composite at any time
α^*	specified degree of cure
λ	parameter defined in Equation (2.22)
μ	resin viscosity, Pa·s
μ_b	viscosity of the resin in the bleeder, Pa·s
μ_{max}	maximum resin viscosity at any point inside the composite at any time, Pa·s
μ_n	viscosity of the resin in the nth channel, Pa·s

$\bar{\mu}_l$	average resin viscosity across the l-th prepreg ply, Pa-s
$(v_f)_n$	fiber volume fraction of the nth prepreg ply
$(v_r)_n$	resin volume fraction of the nth prepreg ply
ρ	density of the composite, kg/m ³
ρ_{com}	density of one compacted prepreg ply, kg/m ³
ρ_f	fiber density, kg/m ³
ρ_L	density of the fluid contained in the pores of the bleeder, kg/m ³
ρ_n	density of the nth prepreg ply, kg/m ³
ρ_r	resin density, kg/m ³
ϕ_b	porosity of the bleeder

SUBSCRIPTS

b	conditions in the bleeder
c	conditions in the composite at position h_c
com	denotes compacted ply
f	denotes the fiber
i	initial condition
j	denotes a grid point in the z direction
l	denotes a grid point of the l-th ply (Equation 4.12)
n	denotes the nth prepreg ply
o	applied cure condition
q	denotes the time level
r	denotes the resin
u	interface between the composite and the bleeder
x	horizontal coordinate parallel to the tool plate
z	vertical coordinate normal to the tool plate

SUPERSCRIPTS

q denotes the time step

★ measured or specified value

SECTION I

INTRODUCTION

Composite parts and structures constructed from continuous fiber-reinforced thermosetting resin matrix prepreg materials are manufactured by arranging the uncured fiber resin mixture into the desired shape and then curing the material. The curing process is accomplished by exposing the material to elevated temperatures and pressures for a predetermined length of time. The elevated temperatures applied during the cure provide the heat required for initiating and maintaining the chemical reactions in the resin which cause the desired changes in the molecular structure. The applied pressure provides the force needed to squeeze excess resin out of the material and to consolidate individual plies.

The elevated temperatures and pressures to which the material is subjected are referred to as the cure temperature and the cure pressure. The magnitudes and durations of these temperatures and pressures applied during the curing process (denoted as the cure cycle) significantly affect the performance of the finished product. Therefore, the cure cycle must be selected carefully for each application. Some major considerations in selecting the proper cure cycle for a given composite material are:

- 1) the temperature inside the material must not exceed a preset maximum value at any time during cure,
- 2) at the end of cure, all the excess resin is squeezed out from every ply of the composite and the resin distribution is uniform,
- 3) the material is cured uniformly and completely, and
- 4) the curing process is achieved in the shortest amount of time.

At the present time, no method exists which relates the cure cycle to the thermal, chemical, and physical processes occurring in continuous fiber-reinforced composites during cure which could be used to establish the most appropriate cure cycle in any given application.

Presently, the cure cycle is generally selected empirically by curing small composite structures and evaluating the quality of the structure after cure. Such empirical methods have several drawbacks: a) an extensive experimental program is usually required to determine the proper cure cycle for a given material, b) a cure cycle found to satisfactorily cure a given material under one set of conditions may not apply for a different set of conditions, and c) they do not ensure that the composite was cured completely in the shortest amount of time. The results obtained by empirical methods do not shed light on the importance of various parameters which affect cure.

The shortcoming of the empirical approach could be overcome by use of analytical models. Unfortunately, no complete model exists that would simulate the entire curing process. Therefore, the first and major objective of this study was to develop models which relate the cure temperature and cure pressure and the properties of the material to the thermal, chemical, and physical processes occurring

in the composite during cure. The second objective was to obtain test data which can be used to validate the models. The third and final objective was to demonstrate the use of the models in establishing the cure cycle for continuous fiber composites which results in a part that is cured uniformly and in the shortest time.

SECTION II

MODEL

In this section, a model is described which can be used for calculating the following parameters during cure:

- a) the temperature, T , inside the composite as a function of position and time;
- b) the degree of cure of the resin, α , as a function of position and time;
- c) the resin viscosity, μ , as a function of position and time;
- d) the number of compacted prepreg plies, n_s , as a function of time;
- e) the amount of resin in the bleeder as a function of time; and
- f) the thickness and the mass of the composite as a function of time.

A model providing the above-mentioned information is developed below in two parts. The first part of the model, referred to as the "thermo-chemical model," yields the temperature, the degree of cure, and the viscosity. The second part, referred to as the "flow model," gives the resin flow out of the composite and the resin content of the composite and the bleeder. Details of the two models are presented in Sections 2.2 and 2.3. First, a brief description of the problem is given.

2.1. Problem Statement

Consider a fiber-reinforced epoxy resin matrix composite of initial thickness L_c (Figure 1). The composite is constructed from unidirectional "prepreg" tape. The "prepreg" consists of unidirectional continuous fibers embedded in an uncured epoxy resin matrix. An absorbent material (referred to as a "bleeder") is placed on one or both sides of the composite. The thickness of the bleeder is L_b . The composite-bleeder system is placed on a metal tool plate ready for processing. A sheet of nonporous teflon release cloth is placed between the composite and the tool plate, and a sheet of porous teflon release cloth is placed between the composite and the bleeder, to prevent sticking.

Initially (time < 0), the resin is uncured and the bleeder contains no resin. Starting at time $t = 0$, the composite-bleeder system is exposed to a known temperature T_0 . The cure temperature, T_0 , may be the same or may be different on the two sides of the composite-bleeder system. At some time t_p ($t_p \geq 0$), a known pressure, P_0 , is applied to the system, squeezing excess resin from the composite. Both the cure temperature, T_0 , and the cure pressure, P_0 , may vary with time in an arbitrary manner. The objective is to determine the parameters listed in points a) - f) above.

In formulating the model, resin is allowed to flow in the directions both perpendicular and parallel to the plane of the composite. However, resin flow in the plane of the composite is allowed only in the direction parallel to the fibers as described in Section 2.3. In the analysis, the composite properties are assumed to vary only in the z direction. The properties in the plane of the composite are taken

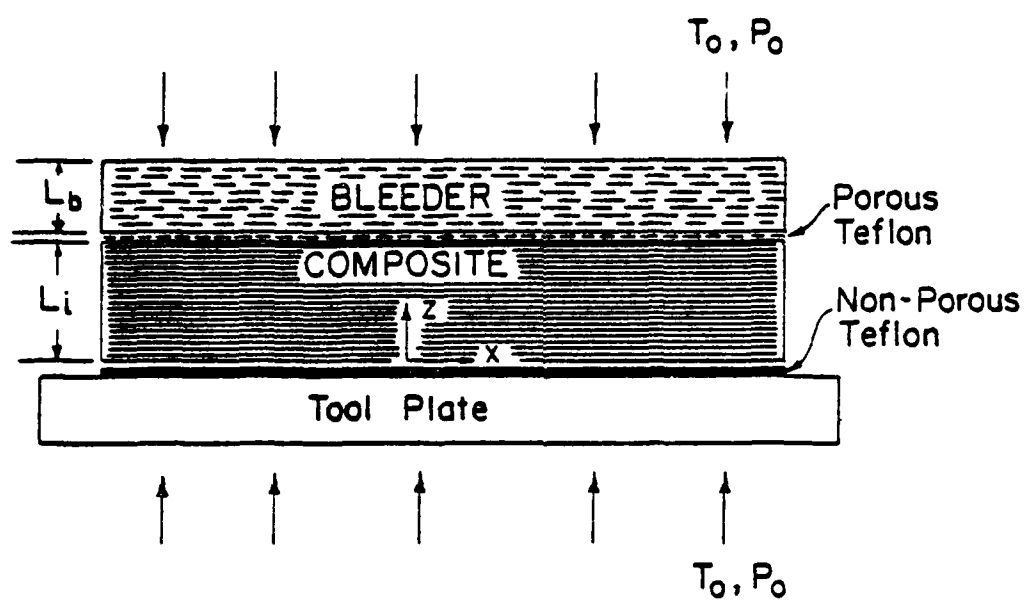


Figure 1 Geometry of the Composite-Bleeder System.

to be constant.

2.2 Thermo-Chemical Model

The temperature distribution, the degree of cure of the resin, and the resin viscosity inside the composite depend on the rate at which heat is transmitted from the environment into the material. Previous investigators have shown that the temperature inside the composite can be calculated using the law of conservation of energy together with an appropriate expression for the cure kinetics [1 - 10]. The law of conservation of energy for a small volume element dV inside the composite is

$$\begin{array}{l} \text{Rate of change} \\ \text{of energy in } dV = \end{array} \begin{array}{l} \text{Net rate of energy} \\ \text{transfer into } dV \\ \text{by conduction} \end{array} + \begin{array}{l} \text{Net rate of} \\ \text{energy transfer} \\ \text{into } dV \text{ by} \\ \text{convection} \end{array} + \begin{array}{l} \text{Rate of energy} \\ \text{liberated (or} \\ \text{absorbed) in} \\ dV \text{ by chemical} \\ \text{reactions} \end{array} \quad (2.1)$$

By neglecting energy transfer by convection, the energy equation may be expressed as

$$\frac{\partial \rho C T}{\partial t} = \frac{\partial}{\partial z} k \frac{\partial T}{\partial z} + \rho \dot{H} \quad (2.2)$$

where ρ and C are the density and specific heat of the composite, k is the thermal conductivity in the direction perpendicular to the plane of the composite, and T is the temperature. \dot{H} is the rate of heat generated by chemical reactions and is defined in the following manner

$$\dot{H} = \dot{R} H_R \quad (2.3)$$

H_R is the total or ultimate heat of reaction during cure and \dot{R} is the reaction or cure rate. Following the work of previous investigators [5,7 - 29], the degree of cure of the resin (denoted as the degree of cure, α) is defined as

$$\alpha = \frac{H(t)}{H_R} \quad (2.4)$$

$H(t)$ is the heat evolved from the beginning of the reaction to some intermediate time, t . For an uncured material, $\alpha = 0$, and for a completely cured material, α approaches unity. By differentiating Equation (2.4) with respect to time, the following expression is obtained

$$\dot{H} = \frac{d\alpha}{dt} H_R \quad (2.5)$$

A comparison of Equations (2.3) and (2.5) shows that in this formulation, $d\alpha/dt$ is the reaction or cure rate. If diffusion of chemical species is neglected, the degree of cure at each point inside the material can be calculated once the cure rate is known in the following way:

$$\alpha = \int_0^t \left(\frac{d\alpha}{dt} \right) dt \quad (2.6)$$

In order to complete the model, the dependence of the cure rate on the temperature and on the degree of cure must be known. This dependence may be expressed symbolically as

$$\frac{d\alpha}{dt} = f(T, \alpha) \quad (2.7)$$

The functional relationship in Equation (2.7), along with the value of the heat of reaction H_R for the prepreg material under consideration, can be determined experimentally by the procedures described in Section 3.3. Solutions to Equations (2.2) and (2.5) - (2.7) can be obtained once the initial and boundary conditions are specified. The initial conditions require that the temperature and degree of cure inside the composite be given before the start of the cure (time $t < 0$). The boundary conditions require that the temperatures on the top and bottom surfaces of the composite be known as a function of time during cure (time $t \geq 0$). Accordingly, the initial and boundary conditions corresponding to Equations (2.2) and (2.5) - (2.7) are

Initial conditions:

$$\left. \begin{array}{l} T = T_i(z) \\ \alpha = 0 \end{array} \right\} \begin{array}{l} 0 \leq z \leq L \\ t < 0 \end{array} \quad (2.8)$$

T_i is the initial temperature in the composite.

Boundary conditions:

$$\left. \begin{array}{l} T = T_L(t) \text{ at } z = 0 \\ T = T_u(t) \text{ at } z = L \end{array} \right\} t \geq 0 \quad (2.9)$$

where T_u and T_L are the temperatures on the top and bottom surfaces of the composite, respectively (Figure 2).

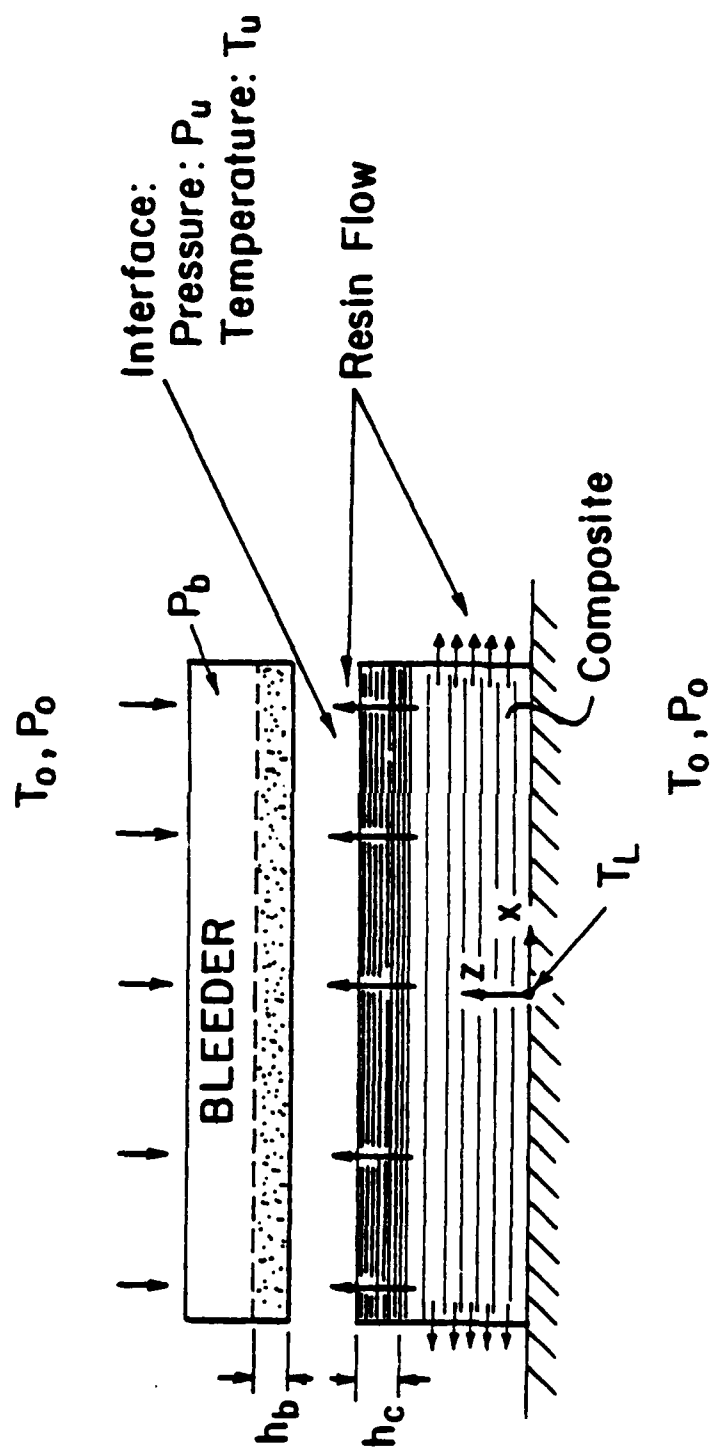


Figure 2 Resin Flow Model.

Solutions to Equations (2.2) and (2.5) - (2.7) yield the temperature T , the cure rate $d\alpha/dt$, and the degree of cure, α , as functions of position and time inside the composite.

Once these parameters are known, the resin viscosity can be calculated, provided a suitable expression relating resin viscosity to its temperature and degree of cure is available. If the resin viscosity is assumed to be independent of shear rate, then the relationship between viscosity, temperature, and degree of cure can be represented in the form:

$$\mu = g(T, \alpha) \quad (2.10)$$

The manner in which the relationship between viscosity, temperature, and degree of cure can be established is described in Section 3.4.

2.3 Resin Flow Model

At some time t_p ($t_p \geq 0$), pressure is applied to the composite-bleeder system (Figure 2). As a result of this pressure, resin flows from the composite into the bleeders. The resin flow rate depends on a) the magnitude of the applied pressure P_0 , b) the air pressure in the bleeders P_b , c) the viscosity of the resin in the composite and in the bleeder, d) the porosity of the bleeder and, e) the thicknesses of the composite and the bleeders. Resin flow in the direction parallel to the plane of the composite can be neglected if a) both the width and the length of the composite are large compared to the thickness L , and b) if restraints are placed around the sides of the composite. This situation is generally encountered in practice. When modelling the curing process of systems where the aforementioned

conditions are met, only resin flow normal to the tool plate needs to be taken into account. However, under some conditions, resin flow along the fibers cannot be prevented. This situation may occur when the length of the composite is similar to the thickness. Under these circumstances, resin flow both normal and parallel to the tool plate takes place simultaneously. The model must then consider resin flow in both directions. In the model that is developed below, resin flow both normal and parallel to the tool plate is taken into account.

Before the resin flow model is established, the behavior of the prepreg plies during the squeezing action (cure pressure application) is examined.

The resin flow process normal to the tool plate was demonstrated by Springer [10] to occur by the following mechanism. As pressure is applied, the first (top) ply ($n_s = 1$, Figure 3) moves toward the second ply ($n_s = 2$), while resin is squeezed out from the space between the plies. The resin seeps through the fiber bundles of the first ply. When the fibers in the first ply get close to the fibers in the second ply, the two plies move together toward the third ply, squeezing the resin out of the space between the second and the third ply. This sequence of events is repeated for the subsequent plies. Thus, the interaction of the fibers proceeds down the prepreg in a wavelike manner (Figure 3).

Note that there are essentially two regions in the composite. In region 1, the plies are squeezed together and contain no excess resin, while in region 2 the plies have not moved and have the original resin content. Some compacting of the fibers within the individual plies may also occur, but as a first approximation, this effect is neglected here.

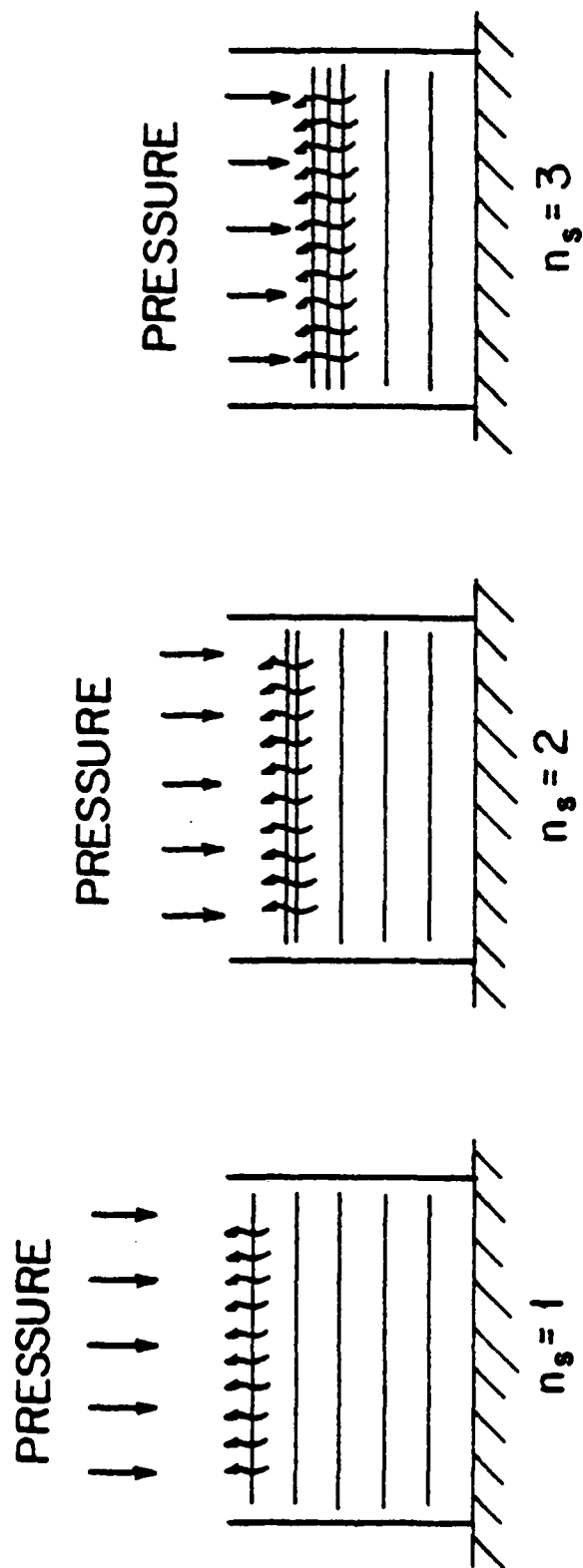


Figure 3 Illustration of the Resin Flow Process Normal to the Tool Plate.

It is noted that there is a pressure drop only across those plies through which resin flow takes place. The pressure is constant (and equal to the applied pressure P_0) across the remaining layers of prepreg.

When there is resin flow in both the normal and parallel directions, resin is squeezed out from between every ply continuously, as long as there is excess resin between adjacent plies. In this case, the thicknesses between different plies vary and change with time, as illustrated in Figure 4.

Although the resin flow in the normal and parallel directions are related, to facilitate the calculations in the model, the two phenomena are decoupled. Hence, separate models are described below for the resin flow in directions normal and parallel to the tool plate.

The model developed predicts changes in the dimensions of the composite only due to changes in the resin content. Shrinkage due to changes in the molecular structure of the resin during cure is not considered.

2.3.1 Resin Flow Normal to the Tool Plate

Owing to the complex geometry, the equations describing the resin flow through the composite normal to the tool plate (z direction) and into the bleeder cannot be established exactly. Nevertheless, an approximate formulation of the problem is feasible by treating the resin flow through both the composite and bleeder as flow through porous media. Such an approach was proposed by Bartlett [30] for studying resin flow through glass fabric prepreg, and by Loos and Springer [9] for resin flow in continuous fiber prepreps. In the model,

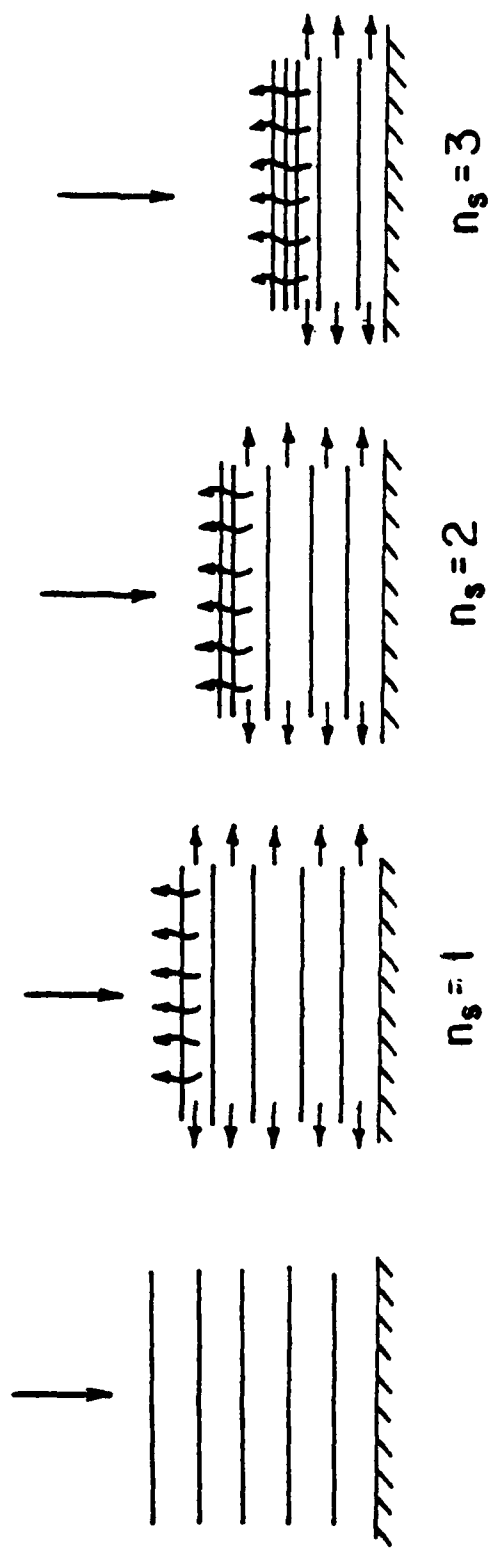


Figure 4 Simultaneous Resin Flow both Normal and Parallel to the Tool Plate.

inertia forces are considered to be negligible compared to viscous forces. Then, at any instant of time, the resin velocities in the prepreg and in the bleeder may be represented by Darcy's law [31]

$$v = -\frac{S}{\mu} \frac{dP}{dz} \quad (2.11)$$

where S is the apparent permeability, μ is the viscosity, and dP/dz is the pressure gradient. The law of conservation of mass (together with Equation (2.11)) gives the following expression for the rate of change of mass M in the composite:

$$\frac{dM}{dt} = -\rho_r A_z v_z = -\rho_r A_z S_c \frac{P_c - P_u}{\int_0^{h_c} \mu dz} \quad (2.12)$$

where ρ_r is the resin density, A_z is the cross sectional area perpendicular to the z axis, h_c is the thickness of the compacted plies, i.e., the thickness of the layer through which resin flow takes place (Figure 2). P_u is the pressure at the interface between the composite and the bleeder. The subscript c refers to conditions in the composite at position h_c . Accordingly, P_c is the pressure at h_c and is the same as the applied pressure ($P_c = P_o$) [32].

At any instant of time, the resin flow rate through the composite is equal to the resin flow rate into the bleeder:

$$\rho_r A_z v_z = \rho_r A_b v_b \quad (2.13)$$

The temperature, and hence the viscosity, of the resin inside the bleeder is assumed to be independent of position (but not of time). Thus, Equations (2.11) and (2.13) yield

$$\rho_r A_z v_z = \rho_r A_z \frac{S_b}{\mu_b} \frac{P_u - P_b}{h_b} \quad (2.14)$$

where h_b is the instantaneous depth of resin in the bleeder. The subscript b refers to conditions in the bleeder. In developing the above expressions, the pressure drop across the porous teflon sheet between the bleeder and the composite was neglected.

Noting that the mass of the fibers in the composite remains constant, Equations (2.12) - (2.14) may be rearranged to yield the following expression for the rate of change of resin mass in the composite:

$$\frac{dM_r}{dt} = -\frac{\rho_r A_z S_c}{\int_0^{h_c} \mu dz} \left[\frac{P_0 - P_b}{1 + G(t)} \right] \quad (2.15)$$

where $G(t)$ is a parameter defined as

$$G(t) = \frac{S_c}{S_b} \frac{\mu_b h_b}{\int_0^{h_c} \mu dz} \quad (2.16)$$

M_r is the mass of resin in the composite at any instant of time. The mass of resin that leaves the composite and enters the bleeder in time t is

$$M_T = \int_0^t \frac{dM_r}{dt} dt \quad (2.17)$$

The instantaneous resin depth in the bleeder is related to the mass of resin that enters the bleeder by the expression

$$h_b = \frac{1}{\rho \phi_b A_z} \int_0^t \frac{dM_r}{dt} dt \quad (2.18)$$

where ϕ_b is the porosity of the bleeder and represents the volume (per unit volume) which can be filled by resin. The thickness of the compacted plies is

$$h_c = n_s h_1 \quad (2.19)$$

where h_1 is the thickness of one compacted prepreg ply and n_s is the number of compacted prepreg plies. The thickness of one compacted prepreg ply can be determined using the procedure described in Section 3.1. The value of n_s varies with time, depending on the amount of resin that has been squeezed out of the composite.

Equations (2.12) - (2.19) are the relationships needed for calculating the resin flow normal to the tool plate.

2.3.2. Resin Flow Parallel to the Tool Plate

In principle, in the plane of the composite, resin may flow along the fibers and in the direction perpendicular to the fibers. In practice, resin flow perpendicular to the fibers is small because of a) the resistance created by the fibers and b) the restraints placed around the edges of the composite. If such restraints were not provided fiber spreading ("wash out") would occur, resulting in a non-uniform distribution of fibers in the composite. Therefore, in this section, only resin flow along the fibers is considered.

It is assumed that resin flow along the fibers and parallel to the tool plate can be characterized as developing viscous flow between two

parallel plates separated by a distance d_n ("channel flow", Figure 5). The distance, d_n , separating the plates is small compared to the thickness of the composite ($d_n < L$). Therefore, the variation in resin properties perpendicular to the boundaries of the channel (z direction) is neglected, and the resin properties along the channel (x direction) are taken to be constant. The pressure drop between the center of any given channel and the channel exit, ($P_H - P_L$, Figure 5), can be expressed as [33]

$$\frac{2(P_H - P_L)}{\rho_r (v_x^2)_n} = \lambda \frac{X_L}{d_n} + B_1 \quad (2.20)$$

where $(v_x)_n$ is the average resin velocity in the channel, X_L is the channel length, and B_1 is a constant. The subscript n refers to the channel located between the n and n-1 prepreg plies (i.e., beneath the fiber bundles of prepreg ply n). The thickness of nth channel is calculated by assuming that a) there is one channel per ply and b) all the excess resin is contained in the channel. Accordingly, the thickness of the channel is given by the following expression:

$$d_n = \frac{M_n}{\rho_n A_z} - \frac{M_{com}}{\rho_{com} A_z} \quad (2.21)$$

where M_n and ρ_n are the mass and density of prepreg ply, n, respectively. The manner in which M_n and ρ_n can be calculated is described in Section 2.4. M_{com} and ρ_{com} are the mass and density of a compacted prepreg ply (i.e. a prepreg ply with all excess resin squeezed out), respectively. The technique used to determine M_{com} is described in Section 3.1, along with an appropriate expression for determining ρ_{com} .

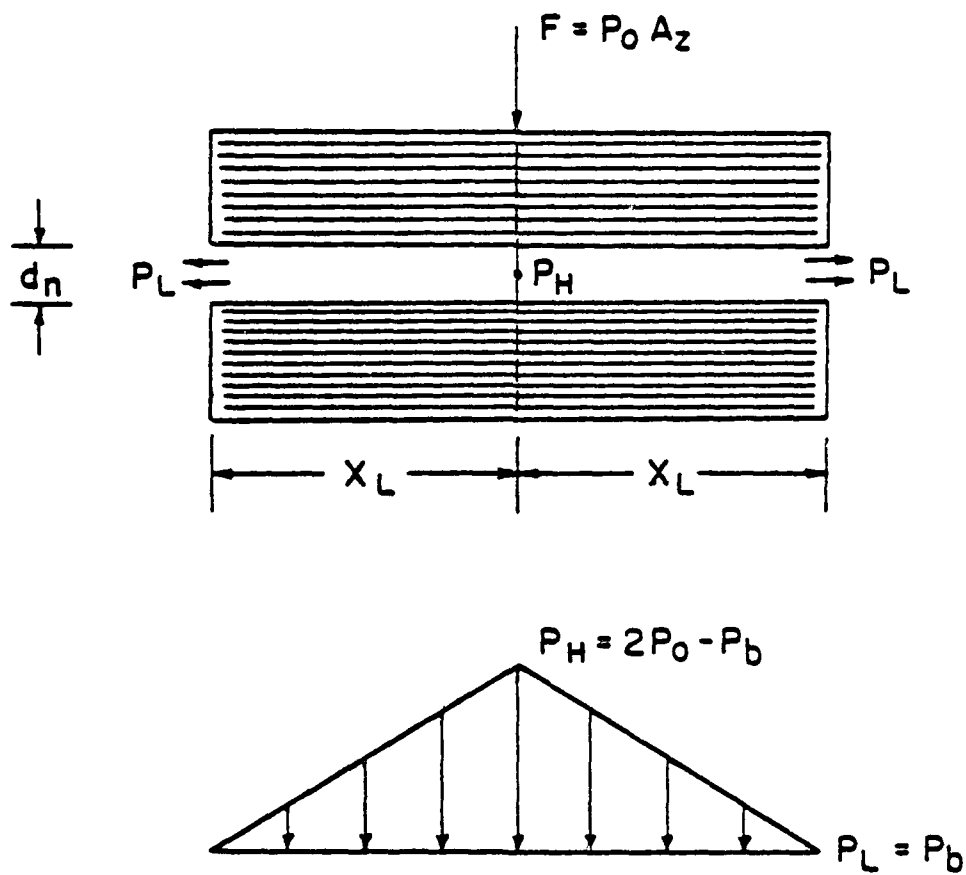


Figure 5 Geometry of the Resin Flow Model Parallel to the Tool Plate.

For laminar flow between parallel plates, λ is defined as

$$\lambda = \frac{96}{RE_n} \quad (2.22)$$

where RE_n is the Reynolds number

$$RE_n = \frac{\rho_r (v_x)_n d_n}{\mu_n} \quad (2.23)$$

where μ_n is the viscosity of the resin in the channel.

Substitution of Equations (2.22) and (2.23) into Equation (2.20) yields the following expression for the average velocity in the channel:

$$(v_x)_n = \frac{1}{B'} \frac{d_n^2}{\mu_n} \frac{(P_H - P_L)}{X_L} \quad (2.24)$$

where B' is a constant which must be determined experimentally. The resin mass flow rate is

$$(\dot{m}_{rx})_n = \rho_r A_x (v_x)_n \quad (2.25)$$

where A_x is the cross sectional area defined as the product of the channel width, W , and thickness, d_n .

The law of conservation of mass together with Equation (2.25) gives the following expression for the rate of change of mass M_n in the n th prepreg ply:

$$\frac{dM_n}{dt} = -2(\dot{m}_{rx})_n = -2\rho_r A_x (v_x)_n \quad (2.26)$$

The right hand side of Equation (2.26) is multiplied by a factor of 2 to account for resin flow in two directions away from the centerline of the channel. Equations (2.24) and (2.26) result in the following expression for the rate of change in resin content $(M_r)_n$ of the nth prepreg ply:

$$\frac{d(M_r)_n}{dt} = \frac{-2}{B'} \frac{d_n^3}{\mu_n} \rho_r W \frac{(P_H - P_L)}{X_L} \quad (2.27)$$

The amount of resin leaving the nth prepreg ply in time t is

$$(M_E)_n = \int_0^t \frac{d(M_r)_n}{dt} dt \quad (2.28)$$

The total amount of resin flow parallel to the tool plate can be determined by summing Equation (2.28) over all plies containing excess resin

$$M_E = \sum_{n=1}^{N-n_s} (M_E)_n \quad (2.29)$$

where N is the total number of prepreg plies.

The pressure at the centerline of the channel, P_H , can be estimated from the force balance applied along the boundaries of the channel. Assuming that the pressure gradient in the x direction is linear, and that the centerline pressure P_H is the same in each ply,

the pressure distribution of each channel may be expressed as

$$P = \left(\frac{P_L - P_H}{X_L} \right) x + P_H \quad (2.30)$$

where P_L is the pressure at the exit of the channel and is assumed to be equal to the pressure of the environment surrounding the composite P_b . A force balance applied along the channel surface gives (Figure 5)

$$F = \int_A P \cdot dA = 2W \int_0^{X_L} P dx \quad (2.31)$$

where F is the applied force. The force can be related to the cure pressure P_o as

$$F = P_o A_z = 2P_o W X_L \quad (2.32)$$

Equations (2.30) - (2.32) yield the centerline pressure

$$P_H = 2P_o - P_b \quad (2.33)$$

Equations (2.20) - (2.33) are the relationships needed for calculating the resin flow in the direction along the fibers.

2.3.3 Total Resin Flow

The total resin flow out of the composite in time t is the sum of the resin flows both normal and parallel to the tool plate. The law of conservation of mass gives the following expression for the total rate of change of mass M in the composite:

$$\frac{dM}{dt} = -\dot{m}_{rz} + -2 \sum_{n=1}^{N-n_s} (\dot{m}_{rx})_n \quad (2.34)$$

where \dot{m}_{rz} and \dot{m}_{rx} are the resin mass flow rates normal to the tool plate (z direction) and parallel to the tool plate (x direction), respectively.

The total mass of the composite at time t is

$$M = M_i + M_T + M_E \quad (2.35)$$

where M_T and M_E are defined by Equations (2.17) and (2.29) and M_i is the initial mass of the composite. The composite thickness at time t is

$$L = \frac{M}{\rho 2X_L W} \quad (2.36)$$

where ρ is the density of the composite.

2.4 Calculation of the Prepreg Properties

Solution of the thermo-chemical model described in Section 2.2 requires that the density ρ , specific C , heat of reaction H_R , and the thermal conductivity k of the prepreg be known. These properties depend upon the local resin and fiber contents of each prepreg ply. The resin content varies in the composite with position and time. Hence ρ , C , H_R , and k also vary with position and time. The thermo-chemical and resin flow models provide the variation in resin content of the composite. With this information, the aforementioned properties can be calculated using the rule of mixtures described below.

The mass of the nth prepreg ply is

$$M_n = (M_r)_n + M_f \quad (2.37)$$

where $(M_r)_n$ and M_f are the masses of the resin and the fiber in the nth prepreg ply, respectively. The mass of the fiber is the same for each prepreg ply, and remains constant during the resin flow process. By expressing the mass in terms of volume and density

$$M = \rho V \quad (2.38)$$

Equation (2.37) can be rewritten as

$$\rho_n V_n = \rho_r (V_r)_n + \rho_f V_f \quad (2.39)$$

where V_n , $(V_r)_n$, and V_f are the volumes of the prepreg, the resin, and the fiber, respectively. ρ_f is the density of the fiber. The volume fraction of the resin and the volume fraction of the fiber can be defined for the nth prepreg ply as

$$(V_r)_n = \frac{(V_r)_n}{V_n} = \frac{(V_r)_n}{(V_r)_n + V_f} \quad (2.40)$$

$$(V_f)_n = \frac{V_f}{V_n} = \frac{V_f}{(V_r)_n + V_f} \quad (2.41)$$

Substitution of Equation (2.38) into Equation (2.40) and (2.41) gives

$$(V_r)_n = \frac{1}{1 + \frac{\rho_r}{\rho_f} \frac{M_f}{(M_r)_n}} \quad (2.42)$$

$$(V_f)_n = \frac{1}{1 + \frac{\rho_f}{\rho_r} \frac{(M_r)_n}{M_f}} \quad (2.43)$$

Equations (2.39), (2.42), and (2.43) yield the following expression for the density

$$\rho_n = \frac{\rho_r}{1 + \frac{\rho_r}{\rho_f} \frac{M_f}{(M_r)_n}} + \frac{\rho_f}{1 + \frac{\rho_f}{\rho_r} \frac{(M_r)_n}{M_f}} \quad (2.44)$$

It should be noted that values of ρ_r and ρ_f can be determined readily. The mass of resin in each prepreg ply $(M_r)_n$ can be calculated from the resin flow models described in Section 2.3.

The specific heat of the nth prepreg ply is taken to be the sum of the specific heat of the resin C_r and the specific heat of the fibers C_f

$$M_n C_n = (M_r)_n C_r + M_f C_f \quad (2.45)$$

By rearranging Equation (2.45), the prepreg specific heat per unit mass, C_n , can be written as

$$C_n = \frac{(M_r)_n}{M_n} C_r + \frac{M_f}{M_n} C_f \quad (2.46)$$

The heat of reaction for the nth prepreg ply can be expressed as

$$(H_R)_n = \frac{(M_r)_n}{M_n} H_r \quad (2.47)$$

where H_R is the heat of reaction per unit mass for the prepreg and H_r is the heat of reaction per unit mass for the resin. Equation (2.47)

assumes that the fibers do not participate in the reaction and do not affect the chemical reactions occurring in the resin. In Equations (2.46) and (2.47) the resin and fiber properties are specified and the fiber mass is known for each ply. The variation in resin mass with position and time is given as part of the numerical solution described in Chapter 4.

The thermal conductivity normal to the fibers (z direction, Figure 1) may be estimated from the expression [34]

$$(K)_n = \left(1 - 2\sqrt{\frac{(V_f)_n}{\pi}}\right) K_r + \frac{K_r}{B_K} \left[\pi - \frac{4}{\sqrt{1 - \left(\frac{B_K^2 (V_f)_n}{\pi}\right)}} \right. \\ \left. \tan^{-1} \frac{\sqrt{1 - \frac{B_K^2 (V_f)_n}{\pi}}}{1 + B_K \sqrt{\frac{(V_f)_n}{\pi}}} \right] \quad (2.48)$$

where B_K is defined as

$$B_K \equiv 2 \left(\frac{K_r}{K_f} - 1 \right) \quad (2.49)$$

Here k_r and k_f are the thermal conductivities of the resin and the fibers, respectively. Values of k_r and k_f are known and the fiber volume fraction of the nth prepreg ply can be calculated by Equation (2.43).

2.5 Use of the Model in Establishing the Cure Cycle

The models developed in this section can be used to select the appropriate cure cycle in a given application. The procedures to be used in selecting a cure cycle are discussed in Section 6.2.

SECTION III

INPUT PARAMETERS

Solution of the equations in Chapter 2 require that the input parameters be specified. The parameters may be categorized into six major groups: a) Geometry, b) Initial and Boundary Conditions, c) Prepreg Properties, d) Resin Properties, e) Fiber Properties, and f) Bleeder Properties. A complete list of the input parameters is given in Table 1.

The parameters pertaining to the geometry (Group A, Table 1), along with the initial and boundary conditions (Group B, Table 1), are specified by the user of the prepreg. The initial prepreg ply thickness and the initial prepreg resin mass fraction (parameters 9 and 10 of Group C, Table 1) are usually specified by the manufacturer for a given prepreg material. The resin and fiber properties (Group D and Group E, Table 1) are either specified by the prepreg manufacturer or can often be found in the published literature. The remaining parameters, marked by an asterisk in Table 1, are generally not known. In the following, a brief description is given of the methods used to determine these parameters.

TABLE 1

Input Parameters Required for Solutions of the
Thermo-Chemical and Resin Flow Models.

A. Geometry

- 1) Length of the composite
- 2) Width of the composite
- 3) Number of plies in the composite

B. Initial and Boundary Conditions

- 4) Initial temperature distribution in the composite
- 5) Initial degree of cure of the resin in the composite
- 6) Cure temperature as a function of time
- 7) Cure pressure as a function of time
- 8) Pressure in the bleeder

C. Prepreg Properties

- 9) Initial thickness of one ply
- 10) Initial resin mass fraction
- 11) Resin content of one compacted ply*
- 12) Compacted ply thickness*
- 13) Apparent permeability of the prepreg normal to the plane of the composite*
- 14) Flow coefficient of the prepreg parallel to the fibers*

Table 1 (continued)

D. Resin Properties

- 15) Density
- 16) Specific heat
- 17) Thermal conductivity
- 18) Heat of reaction*
- 19) Relationship between the cure rate, temperature, and degree of cure*
- 20) Relationship between the viscosity, temperature, and degree of cure*

E. Fiber Properties

- 21) Density
- 22) Specific heat
- 23) Thermal conductivity

F. Bleeder Properties

- 24) Apparent permeability*
- 25) Porosity*

3.1 Compacted Prepreg Ply Thickness and Resin Content

The compacted prepreg ply thickness and the compacted prepreg ply resin content can be determined by the following procedure. A thin (4 - 16 ply) composite panel is constructed from the prepreg. The panel is cured employing a cure cycle that will ensure that all the excess resin is squeezed out of every ply in the composite (i.e., all plies are consolidated $n_s = N$). The total mass of the composite M is measured after cure. The resin content of one compacted prepreg ply $(M_r)_{com}$ is related to the composite mass by the expression

$$(M_r)_{com} = \frac{M}{N} - M_f \quad (3.1)$$

M_f is the fiber mass of one prepreg ply, and N is the total number of plies in the composite. The compacted prepreg ply thickness h_1 can be calculated in the following manner:

$$h_1 = \frac{M/N}{\rho_{com} A_z} \quad (3.2)$$

where ρ_{com} is the compacted ply density and can be determined from Equation (2.44) as

$$\rho_{com} = \frac{\rho_r}{1 + \frac{\rho_r}{\rho_f} \frac{M_f}{(M_r)_{com}}} + \frac{\rho_f}{1 + \frac{\rho_f}{\rho_r} \frac{(M_r)_{com}}{M_f}} \quad (3.3)$$

A_z is the cross sectional area normal to the plane of the composite.

The compacted ply resin content is determined by Equation (3.1) above.

3.2 Apparent Permeability (S_c) and Flow Coefficient (B')

The apparent permeability of the prepreg normal to the fibers (S_c) can be determined by curing a thin (4 to 8 ply) composite specimen for a predetermined length of time. During the cure, the resin squeezed out through the plane of the composite normal to the tool plate is collected in the bleeder placed on the top of the composite. After the cure is terminated, the amount of resin in the bleeder (i.e. the resin flow into the bleeder) is determined by measuring the difference between the original bleeder weight (mass) and the final weight (mass) of the resin-soaked bleeder. An initial value for the apparent permeability is estimated, and the resin flow normal to the fibers is calculated using the model presented in Section 2.3.1. The value of the permeability is adjusted and the calculations are repeated until the calculated and measured resin flows match.

The flow coefficient of the prepreg parallel to the fibers (B') can be determined from the following procedure. A thick composite (approximately 30 - 60 ply thick) is cured for a predetermined length of time. Resin squeezed out from between the individual plies (parallel to the fibers) is collected by bleeders placed around the edges of the composite. The resin flow through the edges is calculated by measuring the difference between the original weight of the "edge" bleeders and the final weight of the resin-soaked bleeders. Assuming a value for the flow coefficient, the resin flow parallel to the fibers is calculated using the model presented in Section 2.3.2. The value of the flow coefficient is adjusted and the calculations are repeated until the measured resin flow matches the calculated resin flow.

3.3 Heat of Reaction and Degree of Cure

The thermo-chemical model requires that the heat of reaction of the prepreg and the relationship between the cure rate, the temperature, and the degree of cure be specified. Different experimental techniques have been used in the past to obtain the above parameters. One frequently used technique, that has the advantage of simultaneously measuring both the heat of reaction and the cure kinetics, is differential scanning calorimetry (DSC). The particular experimental methods employed with DSC measurements vary, depending on the material system being studied. An experimental procedure which may be used to measure the above parameters for a resin typically used in commercial prepreps (Hercules 3501-6 epoxy resin) is described in Appendix A. The measurements yield the heat of reaction, H_r , of the resin and a relationship between the rate of cure, $d\alpha/dt$, the temperature, T , and the degree of cure, α .

The measured values of the rate of cure, the temperature, and the degree of cure of the resin can be used in the thermo-chemical model directly in tabular form or can be fit to a mathematical equation. An empirical expression relating $d\alpha/dt$ to T and α is given in Appendix A for Hercules 3501-6 epoxy resin.

3.4 Viscosity

A relationship between the resin viscosity, the temperature, and the degree of cure of the resin is required in calculating the resin flow.

The resin viscosity can be measured at a constant shear rate on a viscometer or at a constant angular frequency on a mechanical spectrometer. The measurements are generally performed at a constant temperature for specified periods of time. The data provide the viscosity as a function of temperature and time:

$$\mu = \mu(T, t) \quad (3.4)$$

Measurements such as those described in Section 3.3 give the degree of cure of the resin as a function of temperature and time:

$$\alpha = \alpha(T, t) \quad (3.5)$$

By combining the viscosity - temperature - time data (Equation 3.4) with the degree of cure - temperature - time data (Equation 3.5), a relationship between viscosity, temperature, and degree of cure is obtained.

$$\mu = g(T, \alpha) \quad (2.10)$$

Such a relationship can be in tabular form or can be fit to a mathematical equation for use in the numerical calculations, as shown in Appendix B.

3.5 Bleeder Properties

The bleeder can be characterized by two parameters denoted as the apparent permeability (S_b) and the porosity (ϕ_b). The permeability of the bleeder can be determined by measuring the flow rate of a fluid (e.g., air) through a bleeder of known thickness and the corresponding pressure drop across the bleeder. By substituting the measured values

for the fluid flow rate, the pressure drop, and the bleeder thickness into Equation (2.11), the apparent permeability of the bleeder is calculated.

The porosity of the bleeder is defined as

$$\phi_b = \frac{V_p}{V_B} \quad (3.6)$$

where V_B is the bulk volume of the bleeder (product of the cross-sectional area and the thickness), and V_p is the volume of the pores. The volume of the pores can be estimated by saturating the bleeder with a fluid (e.g., resin). By measuring the difference in weights between the empty bleeder and the fluid-saturated bleeder, the amount of fluid contained in the pores of the bleeder is obtained. Assuming that the bleeder does not absorb the fluid, the volume of the pores can be estimated from the expression

$$V_p = \frac{M_L}{\rho_L} \quad (3.7)$$

where M_L is the measured mass of the fluid contained in the bleeder pores and ρ_L is the fluid density.

A more detailed description of the experimental techniques available for measuring the permeability and porosity of porous media can be found in Collins [31].

SECTION IV

NUMERICAL

Solutions to the thermo-chemical and resin flow models must be obtained by numerical methods. The numerical procedures used to obtain solutions to the model and the associated computer code are summarized below. In the final section of this chapter, four sample problems with known analytical solutions were solved by the computer code. The solution generated by the computer code for each test problem is compared to the solution obtained by analytical methods.

4.1 Grid

The composite was divided into a one dimensional grid, as illustrated in Figure 6. The grid points were located at the interfaces of two adjacent plies. In addition, grid points were placed on the lower surface of the prepreg ply adjacent to the tool plate and on the top surface of the prepreg ply next to the bleeder. Accordingly, the total number of grid points is $N + 1$, where N is the total number of prepreg plies in the composite.

The distance between any two grid points, denoted as Δz_n , is approximately equal to the thickness of the n th prepreg ply. The grid spacing, Δz_n , is not constant, but varies with time depending on the resin content of the n th ply. Each grid point is indicated by the

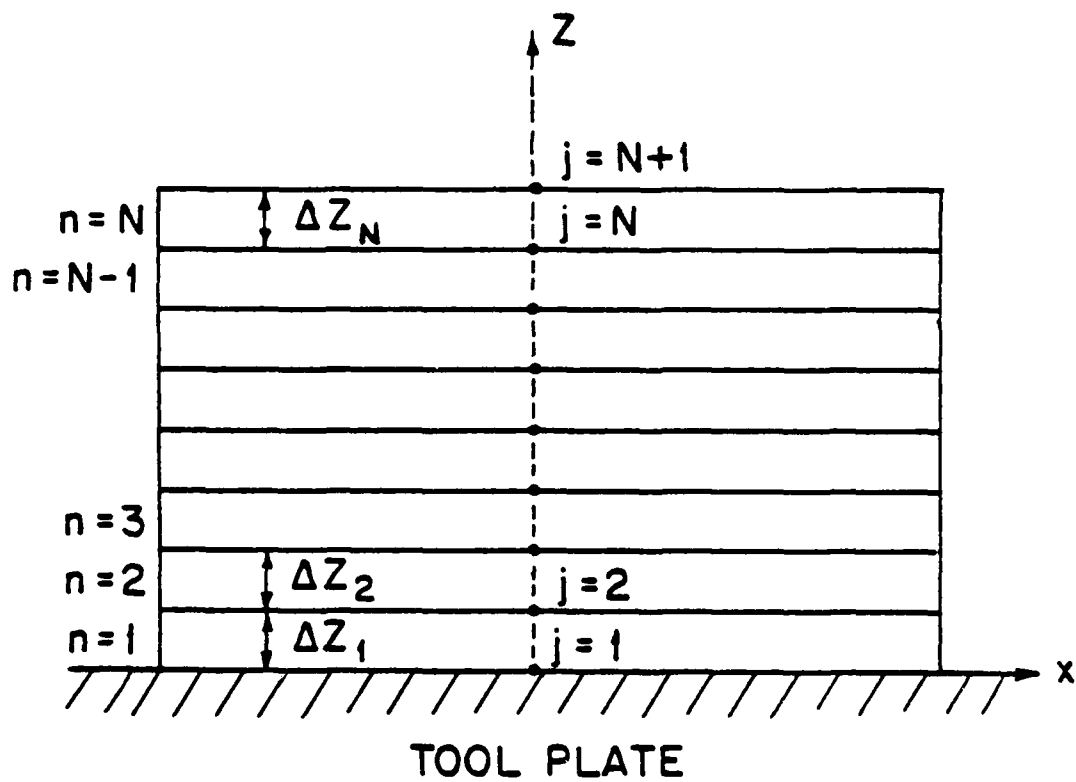


Figure 6 Arrangement of the Grid Points.

subscript j and time is designated by the superscript q .

4.2 Numerical Solution to the Thermo-Chemical Model

In order to determine the temperature, the degree of cure, and the resin viscosity of the composite as a function of position and time, the equations described in Section 2.2 must be solved numerically.

Equation (2.2), together with Equation (2.5), give the following expression for the energy equation:

$$\frac{\partial \rho C T}{\partial t} = \frac{\partial}{\partial z} K \frac{\partial T}{\partial z} + \rho \left(\frac{d\alpha}{dt} \right) H_R \quad (4.1)$$

This equation is expressed in finite difference form suitable for numerical solution. At any "interior" grid point, ($2 \leq j \leq N$), the term on the left hand side of Equation (4.1) is approximated by

$$\frac{\partial \rho C T}{\partial t} \doteq \rho_j^q C_j^q \left(\frac{T_j^{q+1} - T_j^q}{\Delta t} \right) \quad (4.2)$$

where Δt is a time step equal to the time between T_j^{q+1} and T_j^q . The first term on the right hand side of Equation (4.1) is approximated by [35]

$$\begin{aligned} \frac{\partial}{\partial z} K \frac{\partial T}{\partial z} \doteq K_j^q & \left[\frac{2 T_{j+1}^{q+1}}{\Delta Z_n^q (\Delta Z_n^q + \Delta Z_{n-1}^q)} - \frac{2 T_j^{q+1}}{\Delta Z_n^q \Delta Z_{n-1}^q} \right. \\ & \left. + \frac{2 T_{j-1}^{q+1}}{\Delta Z_{n-1}^q (\Delta Z_n^q + \Delta Z_{n-1}^q)} \right] \quad (4.3) \end{aligned}$$

where Δz_n^q is the distance between the grid points j and $j + 1$ at time t_q , and Δz_{n-1}^q is the distance between the grid points j and $j - 1$ at time t_q .

Combining Equations (4.1) - (4.3) gives the following algebraic expression as an approximation to the original partial differential equation:

$$\begin{aligned} & \frac{-2a_j^q \Delta t}{\Delta z_{n-1}^q (\Delta z_n^q + \Delta z_{n-1}^q)} T_{j-1}^{q+1} + \left(1 + \frac{2a_j^q \Delta t}{\Delta z_n^q \Delta z_{n-1}^q} \right) T_j^{q+1} \\ & - \frac{2a_j^q \Delta t}{\Delta z_n^q (\Delta z_n^q + \Delta z_{n-1}^q)} T_{j+1}^{q+1} = T_j^q + U_j^q \Delta t \end{aligned} \quad (4.4)$$

where a_j^q the thermal diffusivity is defined as

$$a_j^q = \frac{k_j^q}{\rho_j^q C_j^q} \quad (4.5)$$

and U_j^q is defined as

$$U_j^q = \frac{(H_R)_j^q}{C_j^q} \left(\frac{d\alpha}{dt} \right)_j \quad (4.6)$$

Equation (4.4) represents $N-1$ linear equations corresponding to the $N-1$ interior grid points. This set of equations, called a tridiagonal system, can be solved for the temperature of each grid point at the new time (T_j^{q+1}) using a Gaussian elimination method. An algorithm for

the solution of the above tridiagonal system is given by Carnahan et al. [36].

The temperatures at the lower (T_1^{q+1}) and upper (T_{N+1}^{q+1}) boundary grid points are specified by the boundary conditions. The boundary temperatures may vary with time in an arbitrary manner. The arbitrary variation of temperature with time was approximated by straight line segments.

It is noted that the numerical procedure outlined previously is an implicit method of solution. The implicit method does not impose a limit on the size of the time step (Δt), which can be used with a desired grid spacing (Δz) to ensure stability of the numerical solution. Therefore, a stability criterion is not required for the above numerical procedure, and the time step size can be chosen arbitrarily.

Once the temperature (T_j^{q+1}) is known at each grid point, the resin degree of cure can be determined at each grid point. The functional relationship between cure rate, temperature, and degree of cure is given by

$$\frac{d\alpha}{dt} = f(T, \alpha) \quad (2.7)$$

By approximating the cure rate by the difference equation

$$\frac{d\alpha}{dt} \doteq \frac{\alpha_j^{q+1} - \alpha_j^q}{\Delta t} \quad (4.7)$$

and substituting Equation (4.7) into Equation (2.7), we obtain the following expression for the degree of cure at the new time t_{q+1}

$$\alpha_j^{q+1} = \alpha_j^q + f(T_j^{q+1}, \alpha_j^q) \Delta t \quad (4.8)$$

The viscosity of the resin can be determined at each grid point and at time t_{q+1} once the temperature (T_j^{q+1}) and the degree of cure (α_j^{q+1}) are known. The exact relationship between viscosity, temperature, and degree of cure depends on the resin system being studied (Equation 2.10). A symbolic relationship between the viscosity at each grid point (μ_j^{q+1}), the temperature (T_j^{q+1}), and the degree of cure (α_j^{q+1}) can be expressed as

$$\mu_j^{q+1} = g(T_j^{q+1}, \alpha_j^{q+1}) \quad (4.9)$$

4.3 Numerical Solution to the Resin Flow Model

As was discussed in Section 2.3, resin flow takes place both perpendicular and parallel to the tool plate (x and z directions, Figure 2). The resin flow in the z direction takes place across n_s plies, where n_s is the number of compacted plies. Once a ply reaches its compacted resin content, $(M_r)_{com}$, no additional resin can be squeezed out from the ply. Therefore, at any given time t , the resin in the z direction that flows across the n_s plies comes from the $n=N-n_s$ ply only (Figure 7).

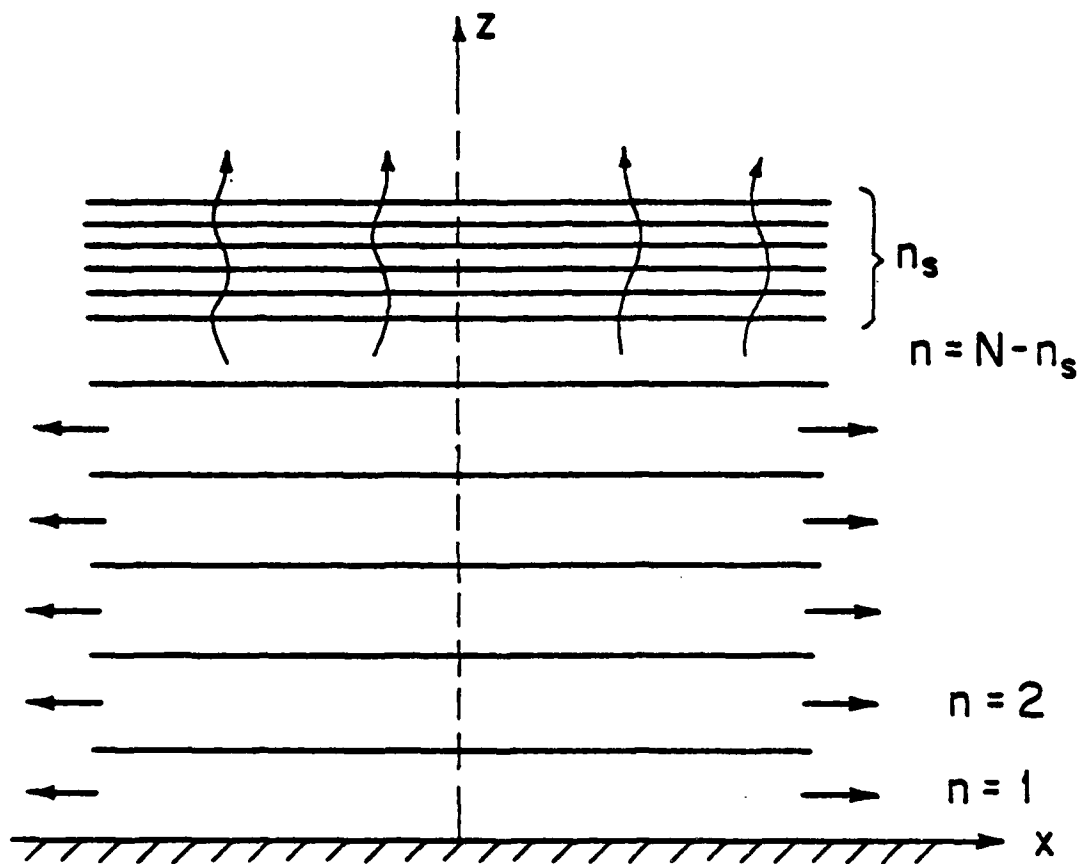


Figure 7 Model of the Resin Flow Processes Normal and Parallel to the Tool Plate.

Resin flow along the plane of the composite in the x direction takes place simultaneously across all the plies beneath the $N-n_s$ ply. Resin flow from the $N-n_s$ ply in the x direction is neglected in the calculations that follow.

The change in resin mass of the composite due to resin flow normal to the tool plate (z direction) is given by Equation (2.17). For one time step Δt (between t_q and t_{q+1}), this equation may be approximated as

$$(M_r)_{N-n_s}^{q+1} = \int_t^{t+\Delta t} \left(\frac{dM_r}{dt} \right) dt \doteq \frac{\Delta t}{2} \left[\left(\frac{dM_r}{dt} \right)_{N-n_s}^q + \left(\frac{dM_r}{dt} \right)_{N-n_s}^{q+1} \right] \quad (4.10)$$

where the subscript $N-n_s$ signifies that during any given time step, the resin content of the composite due to flow in the z direction changes only in the $N-n_s$ ply. The integral in Equations (2.15) and (2.16) is approximated by

$$\int_0^{h_c} \mu dz \doteq h_1 \sum_{l=1}^{n_s+1} \bar{\mu}_l \quad (4.11)$$

where $\bar{\mu}_l$ is the average viscosity across the l -th ply

$$\bar{\mu}_l \doteq \frac{\mu_{l+1} + \mu_l}{2} \quad (4.12)$$

where μ_{l+1} and μ_l are the viscosities of the upper and lower grid points

of layer l , h_1 is the thickness of one compacted ply, and n_s is the number of compacted plies. Equations (2.15), (2.16), (4.10), and (4.11) give the following expression:

$$(M_T)_{N-n_s}^{q+1} \doteq \frac{-\rho_r A_z \Delta t}{2} \left[\frac{(P_o^q - P_b^q)}{\left(\frac{\mu_{N+1}^q h_b^{q-1}}{S_b} + \frac{h_1}{S_c} \sum_{l=1}^{n_s+1} \bar{\mu}_l^q \right)} + \frac{(P_o^{q+1} - P_b^{q+1})}{\left(\frac{\mu_{N+1}^{q+1} h_b^q}{S_b} + \frac{h_1}{S_c} \sum_{l=1}^{n_s+1} \bar{\mu}_l^{q+1} \right)} \right] \quad (4.13)$$

At time $t + \Delta t$, the resin content of the $N-n_s$ ply is

$$(M_r)_{N-n_s}^{q+1} = (M_r)_{N-n_s}^q + (M_T)_{N-n_s}^{q+1} \quad (4.14)$$

and the total (resin plus fiber) mass in the $N-n_s$ ply is

$$(M)_{N-n_s}^{q+1} = (M_r)_{N-n_s}^{q+1} + M_f \quad (4.15)$$

where M_f is the fiber mass in one prepreg ply. At time $t + \Delta t$, the new thickness of ply $N-n_s$ is

$$(\Delta Z)_{N-n_s}^{q+1} = \frac{(M)_{N-n_s}^{q+1}}{\rho_{N-n_s}^{q+1} A_z} \quad (4.16)$$

where the density $\rho_{N-n_s}^{q+1}$ is given by Equation (2.44). The instantaneous resin depth in the bleeder (Equation (2.18)) at time $t + \Delta t$ is

$$h_b^{q+1} = \frac{1}{\rho_r \phi_b A_z} (M_r)_{N-n_s}^{q+1} + h_b^q \quad (4.17)$$

The value of n_s at time $t + \Delta t$ is determined from the following expressions:

$$n_s^{q+1} = n_s^q \quad \text{when} \quad (M_r)_{N-n_s}^{q+1} < (M_r)_{\text{com}} \quad (4.18)$$

$$n_s^{q+1} = n_s^q + 1 \quad \text{when} \quad (M_r)_{N-n_s}^{q+1} \geq (M_r)_{\text{com}} \quad (4.19)$$

The total resin loss in the z direction from the beginning of resin flow to the end of resin flow can be determined by summing Equation (4.13) over all time steps.

The resin flow in the plane of the composite parallel to the fibers (x direction) is given by Equation (2.27). Combining Equation (2.27) with Equation (2.33) gives the rate of change in the resin content of the n th prepreg ply as

$$\left(\frac{dM_r}{dt}\right)_n = -\frac{4\rho_r W}{B'} \frac{d_n^3}{\mu_n} \frac{(P_o - P_b)}{X_L} \quad (4.20)$$

where the subscript n refers to a resin-rich ply, ($n < (N - n_s)$). In time Δt , the amount of resin loss in the x direction from the n th ply is

$$(M_E)_n^{q+1} = \int_t^{t+\Delta t} \left(\frac{dM_r}{dt}\right)_n dt \doteq \frac{\Delta t}{2} \left[\left(\frac{dM_r}{dt}\right)_n^q + \left(\frac{dM_r}{dt}\right)_n^{q+1} \right] \quad (4.21)$$

Equations (4.20) and (4.21) yield

$$\begin{aligned} (M_E)_n^{q+1} = & -\frac{2\rho_r W}{B' X_L} \Delta t \left[\frac{(d_n^3)^{q-1}}{\mu_n^q} (P_o^q - P_b^q) \right. \\ & \left. + \frac{(d_n^3)^q}{\mu_n^{q+1}} (P_o^{q+1} - P_b^{q+1}) \right] \end{aligned} \quad (4.22)$$

The resin content of the n th ply at time $t + \Delta t$ is

$$(M_r)_n^{q+1} = (M_r)_n^q + (M_E)_n^{q+1} \quad (4.23)$$

The total mass of the n th prepreg ply is

$$(M)_n^{q+1} = (M_r)_n^{q+1} + M_f \quad (4.24)$$

At time $t + \Delta t$, the thickness of the n th ply is

$$\Delta z_n^{g+1} = \frac{(M_n)^{g+1}}{\rho_n^{g+1} A_z} \quad (4.25)$$

where the density is given by Equation (2.44). The channel thickness, d_n , was previously defined by Equation (2.21). Combining Equations (2.21), (3.2), and (4.25) gives the following expression for the channel thickness at time $t + \Delta t$:

$$d_n^{g+1} = \Delta z_n^{g+1} - h_1 \quad (4.26)$$

The mass of the entire composite at time $t + \Delta t$ is obtained by summing the masses of the individual prepreg plies

$$M^{g+1} = \sum_{n=1}^{N-n_s} M_n^{g+1} + n_s M_{com} \quad (4.27)$$

where M_{com} is the total mass of one compacted prepreg ply. The thickness of the composite at time $t + \Delta t$ is

$$L^{g+1} = \sum_{n=1}^{N-n_s} \Delta z_n^{g+1} + n_s h_1 \quad (4.28)$$

4.4 Properties at the Grid Points

Solution of Equation (4.4) requires that the density ρ , the specific heat C , the heat of reaction H_R , and the thermal conductivity k at each grid point be known. Once the mass of resin and the mass of fiber in the volume surrounding a grid point has been determined, the aforementioned properties can be calculated from Equations (2.44) through (2.48).

The mass of resin $(\bar{M}_r)_j^{q+1}$ in the volume surrounding an "interior" grid point ($2 \leq j \leq N$) is calculated from the following expression

$$(\bar{M}_r)_j^{q+1} = \frac{(M_r)_n^{q+1} + (M_r)_{n-1}^{q+1}}{2} \quad (4.29)$$

where $(M_r)_n^{q+1}$ and $(M_r)_{n-1}^{q+1}$ are the resin masses in the n and $n-1$ plies, respectively. At the two boundary grid points ($j=1$ and $j=N+1$), the resin masses are calculated from the following expressions:

$$(\bar{M}_r)_1^{q+1} = \frac{(M_r)_1^{q+1}}{2} ; \quad (\bar{M}_r)_{N+1}^{q+1} = \frac{(M_r)_N^{q+1}}{2} \quad (4.30)$$

In calculating the grid point properties above, the properties of the resin (ρ_r, C_r, H_r, k_r) and the properties of the fiber (ρ_f, C_f, k_f) are assumed to be independent of temperature and degree of cure of the resin. Variations in any of the above properties with temperature or degree of cure could be incorporated in the calculation of the grid point properties.

4.5 Computer Code

A computer code was developed to implement the foregoing numerical procedures given in Sections 4.2 - 4.4. To test the accuracy of the computer code, results were obtained to four problems for which known solutions exist. The properties of Hercules AS/3501-6 prepreg material given in Appendix B were used in the calculations.

In the first problem, a flat 64-ply composite, initially at ambient temperature (21°C), is suddenly exposed to a step change in temperature (152°C) at its boundaries. The temperature distribution was calculated by assuming no heat generation by chemical reactions inside the material and no resin flow. The temperature distribution as a function of time calculated by the computer code was compared with the temperature distribution calculated using an analytical solution given in Carslaw and Jaeger [37]. The results (Figure 8) show a good agreement between the computer solution and the analytical solution.

The second problem concerned a 4-ply composite exposed to a constant and uniform temperature (152°C or 177°C). The degree of cure as a function of time was calculated both by the computer code and by the analytical solution given in reference [29]. A comparison of the two solutions shows excellent agreement between the computer and the analytical results (Figure 9).

The third and fourth problems dealt with resin flows in the directions normal and parallel to the tool plate. Using the computer code, the resin flows in an 8-ply composite were calculated taking both the temperature and the resin viscosity inside the composite to be uniform and constant and by assuming no internal heat generation due

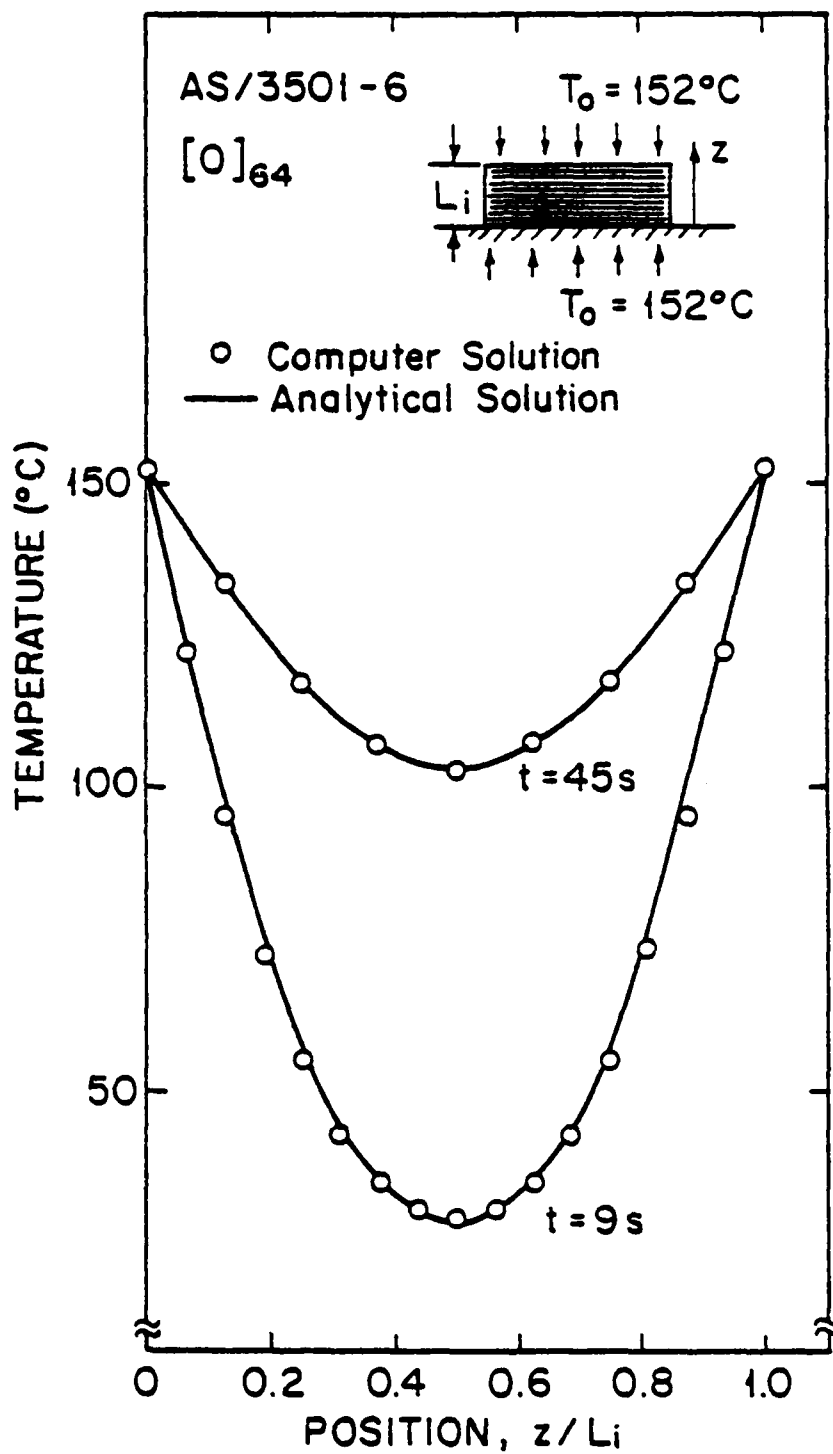


Figure 8 Temperature Distribution as a Function of Time. Comparison Between the Computer and Analytical Solutions.

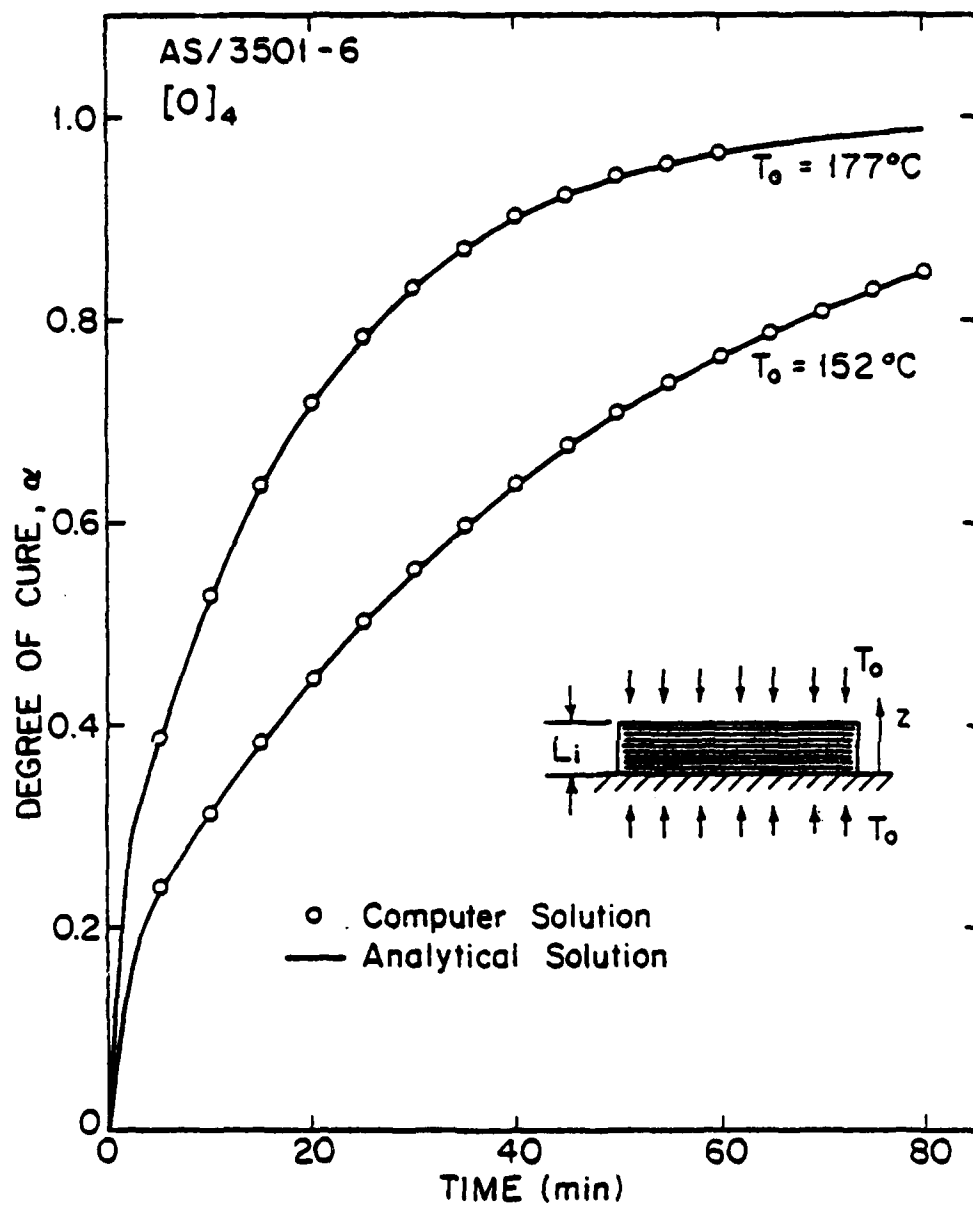


Figure 9 Degree of Cure as a Function of Time. Comparison Between the Computer and Analytical Solutions.

to chemical reactions. In the one case, resin flow only normal to the tool plate was considered, while in the other case, resin flow parallel to the tool plate was taken into account. The same problems as described above were solved using the equations for the resin flows in Section 2.3. These solutions were calculated manually with the aid of a pocket calculator. The resin flows calculated by the computer code and by the pocket calculator are shown in Figure 10. The resin mass flows shown in these figures were normalized with respect to the original ($t=0$) mass of the composite. As can be seen there is good agreement between the computer solution and the pocket calculator solution.

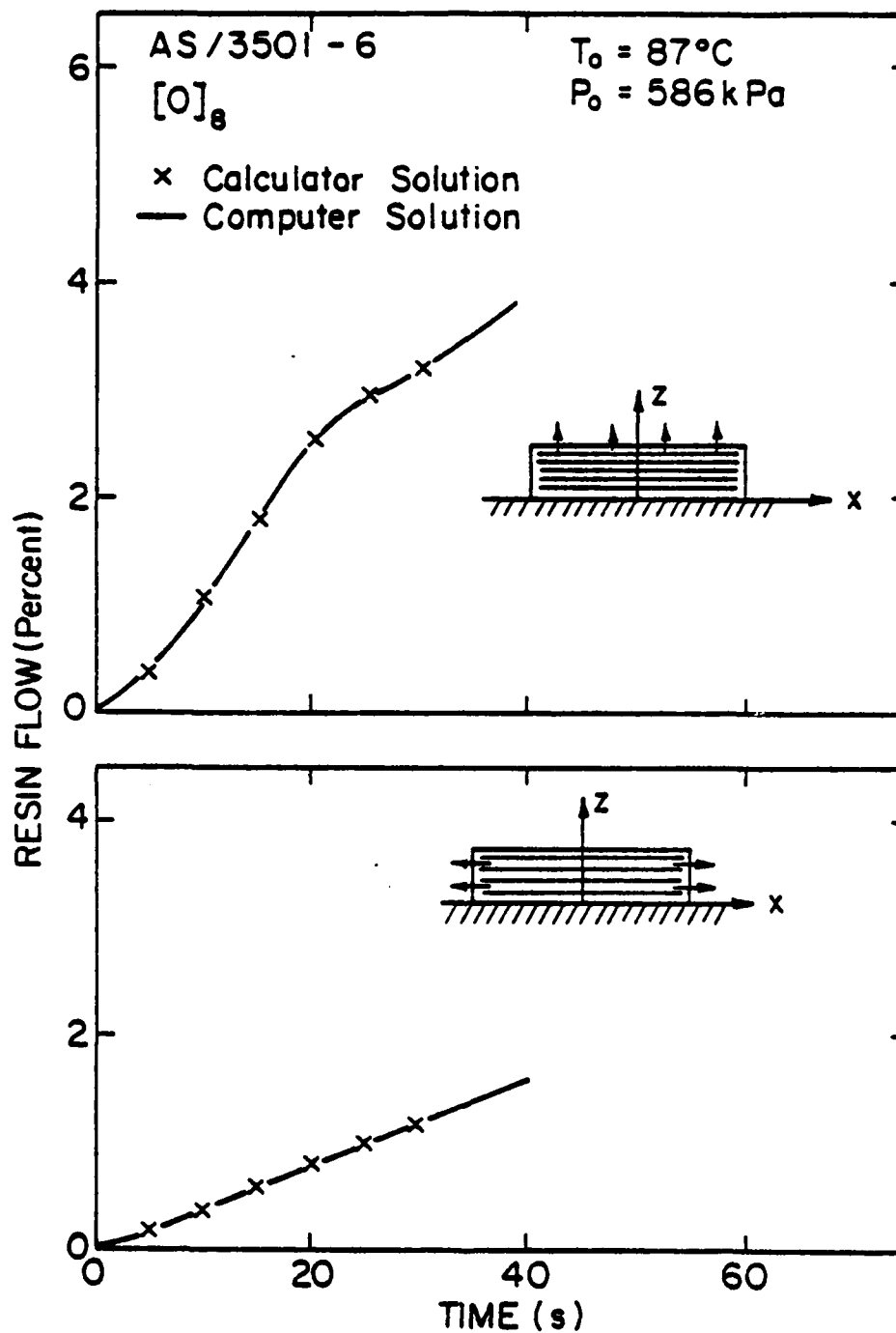


Figure 10 Resin Flow as a Function of Time Normal to the Tool Plate (top) and Parallel to the Tool Plate (bottom). Comparison Between the Computer and Pocket Calculator Solutions.

SECTION V

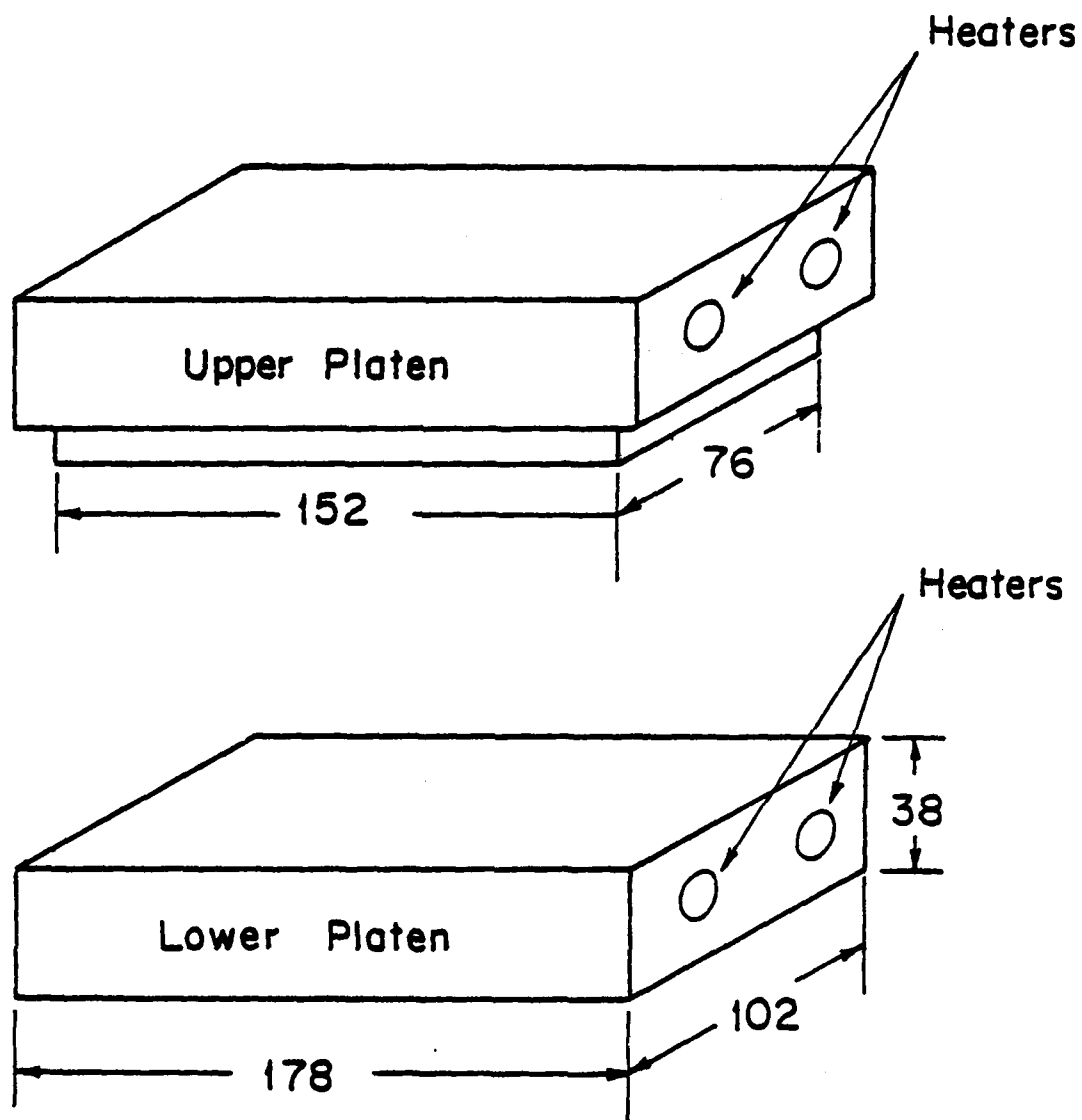
EXPERIMENTAL

In this chapter, the experimental apparatus and procedures which are described were used to cure the composite test specimens and to measure the temperature distribution and the resin flow of the composite during cure.

The apparatus consisted of three major components: the heated press platens, the pneumatic press, and the heater controller. Each of the three systems is described below. In addition, a brief description is given of the method used to construct the test specimens.

5.1 Heated Platens

The material (prepreg) was placed between two 102 mm wide, 178 mm long, and 38 mm thick aluminum platens (Figure 11). The platens were identical except that a 12.7 mm wide, 6.4 mm deep groove was machined around the edges of the top platen heating surface. Two 9.5 mm diameter holes (165 mm deep) were drilled into the side of each platen. The centers of the two holes were symmetric with respect to the vertical and horizontal centerlines of the platen. A 250 watt (at 120 V) Chromalox cartridge heater (Model No. CIR-2061) was inserted into each hole and was held firmly in place with a cap screw. Power to the heaters was controlled by the circuit described in Section 5.3.



All Dimensions in mm

Figure 11 Geometry of the Heated Platens.

6.4 mm and 12.7 mm thick hard board insulation was fastened to the sides and to the bottom of each platen, respectively.

A 2.38 mm diameter hole was drilled into each platen to accommodate a temperature sensor. The hole terminated at approximately 3.18 mm beneath the heating surface of the platen. The purpose of the sensors was to provide information regarding the temperature of the heating surfaces. An Omega RTD (Model No. W2103, 2.0 mm diameter, 7.0 mm long) temperature sensor, coated with a high thermal conductivity grease (Omega Omegatherm 201 silicone paste), was firmly embedded in each hole.

The RTD temperature sensor operates on the principle that a change in the temperature of the sensor produces a proportional change in the resistance of the sensor. The temperature vs. resistance relationship was provided by the manufacturer and is shown in Figure C.2 of Appendix C. The sensors were powered by a constant current source operating at approximately 3mA. To verify that the current source did not cause appreciable self heating of the sensor, the aluminum platen (with the sensor installed) was placed in a constant temperature oven. After the steady state condition was reached, the temperature indicated by the sensor was measured and was compared to the oven temperature. The oven temperature and the temperature of the sensor were within 0.6°C, indicating that the temperature of the sensor did not increase appreciably due to the current passing through the sensor. The output of each RTD was fed to the heater control circuit, as discussed in Section 2.3.

In order to determine the temperature distribution across the platen surface, five thermocouples were temporarily mounted on the surface of the lower platen. A 6.4 mm thick asbestos sheet was placed on the platen surface to minimize heat transfer from the surface of the platen. The heaters were turned on, and the outputs of the thermocouples were recorded as a function of time. These measurements were made for a transient heating rate of 6.7°C/min (80% heater power), from room temperature to 99°C. It was found that the temperature across the surface varied less than 3°C when the center-line temperature was 99°C (Figure 12). Measurements also showed that the difference between the platen surface temperature and the temperature indicated by the RTD sensor was less than 0.5°C. The thermocouples on the surface were removed when composites were cured.

5.2 Pneumatic Press

The aluminum platens were mounted onto the upper and lower surfaces of a Danly four post rectangular die set (Figure 13). The function of the die set is to keep the upper and lower platen surfaces parallel and to act as a guide when compressing a test specimen. The die set was securely installed in a rigid 89 kN (10 ton) press frame. Force to the die set (and consequently to the platens) was provided by a 203 mm diameter pneumatic cylinder operating on the shop air supply (621 kPa max.). A pressure regulator was installed between the air supply and the cylinder. Air pressure in the cylinder was indicated on a Heise 0-689 kPa (0 - 100 psi) pressure gauge. Pressure could be read off this gauge to within 6.9 kPa (1 psi) accuracy.

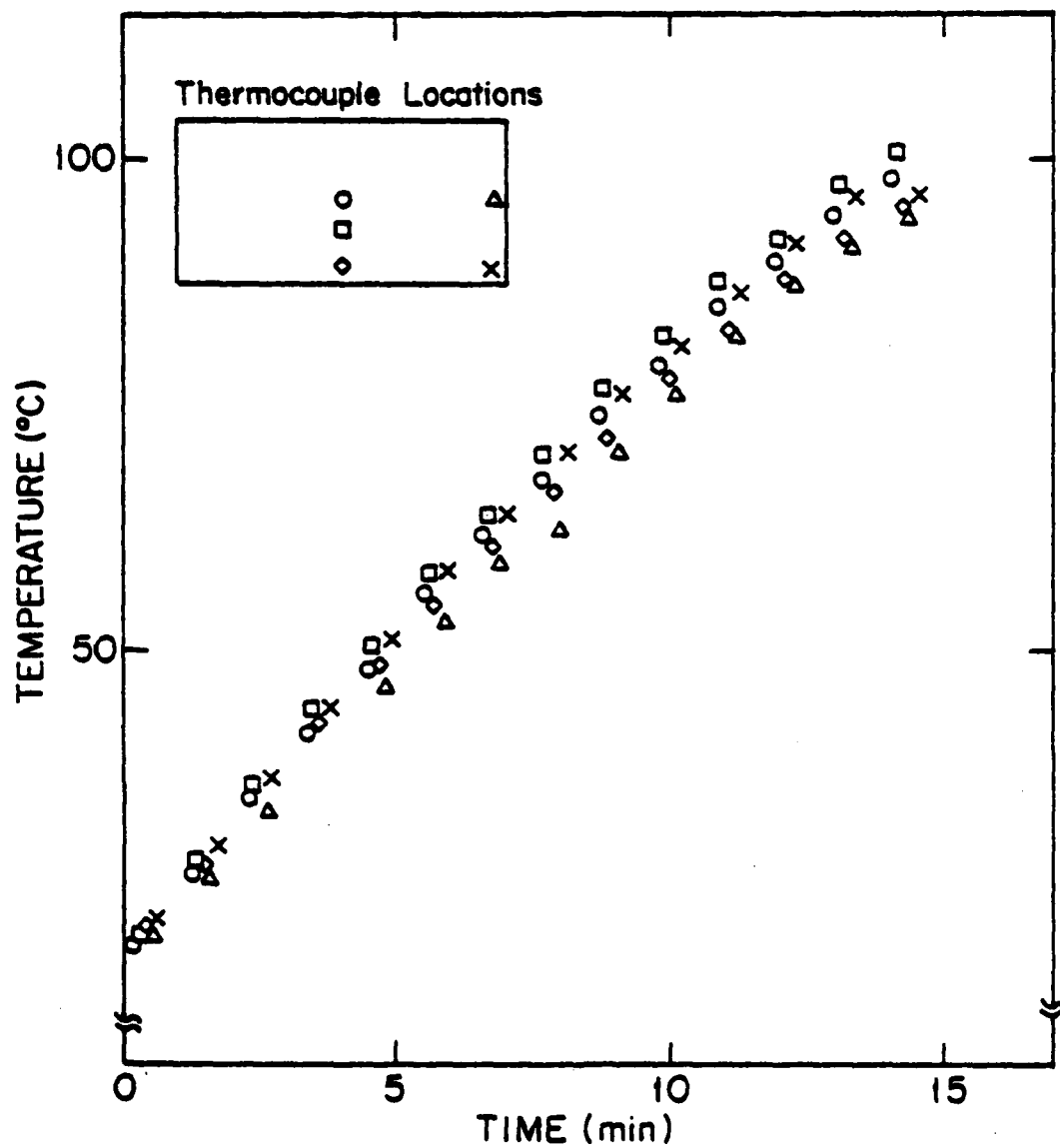


Figure 12 Temperature Distribution Across the Surface of the Lower Platen as a Function of Time. Symbols Represent the Location of the Thermocouples on the Platen Surface.

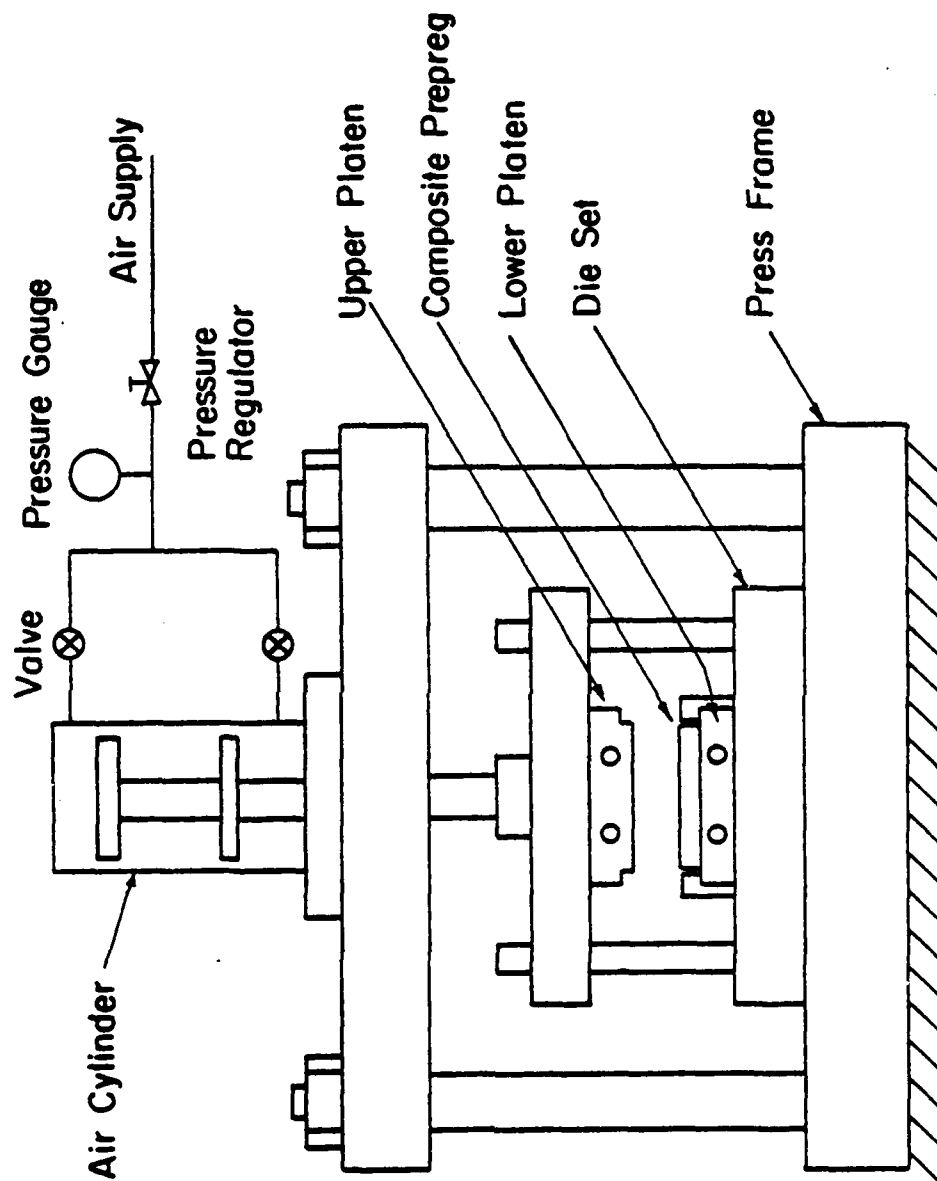


Figure 13 Schematic of the Pneumatic Press.

The cylinder ram was securely bolted on the center line of the upper die set surface. The relationship between the force generated by the cylinder ram on the upper platen and the cylinder air pressure was determined using a calibrated Baldwin (Model SR-4) 8.9 kN (2000 lbf.) load cell. The load cell was centered between the upper and lower platens and measurements were made of the force vs. the indicated cylinder air pressure. The results are presented in Figure D.1 (Appendix D). The relationship between force and pressure was checked between tests and found to be within $\pm 6\%$ of the values in Figure D.1.

5.3 Temperature Controller

The surface temperature of the upper and lower platens was controlled by regulating the voltage inputs to the heaters installed in the upper and lower platens. This task was accomplished by the controller described below.

The major components of the controller included a Texas Instruments TM 990/189 microcomputer, a 1 Hz timer, a 10 bit digital-to-analog converter (D/A), two comparators, and two proportional heater controllers. A schematic of the circuit is shown in Figure 14. A detailed circuit diagram of the controller is given in Appendix C.

The following two relationships were stored in the computer a) the required surface temperature as a function of time and b) the relationship between the RTD output voltage and its temperature. The manner in which the relationship between the RTD voltage and the temperature was obtained will be discussed subsequently.

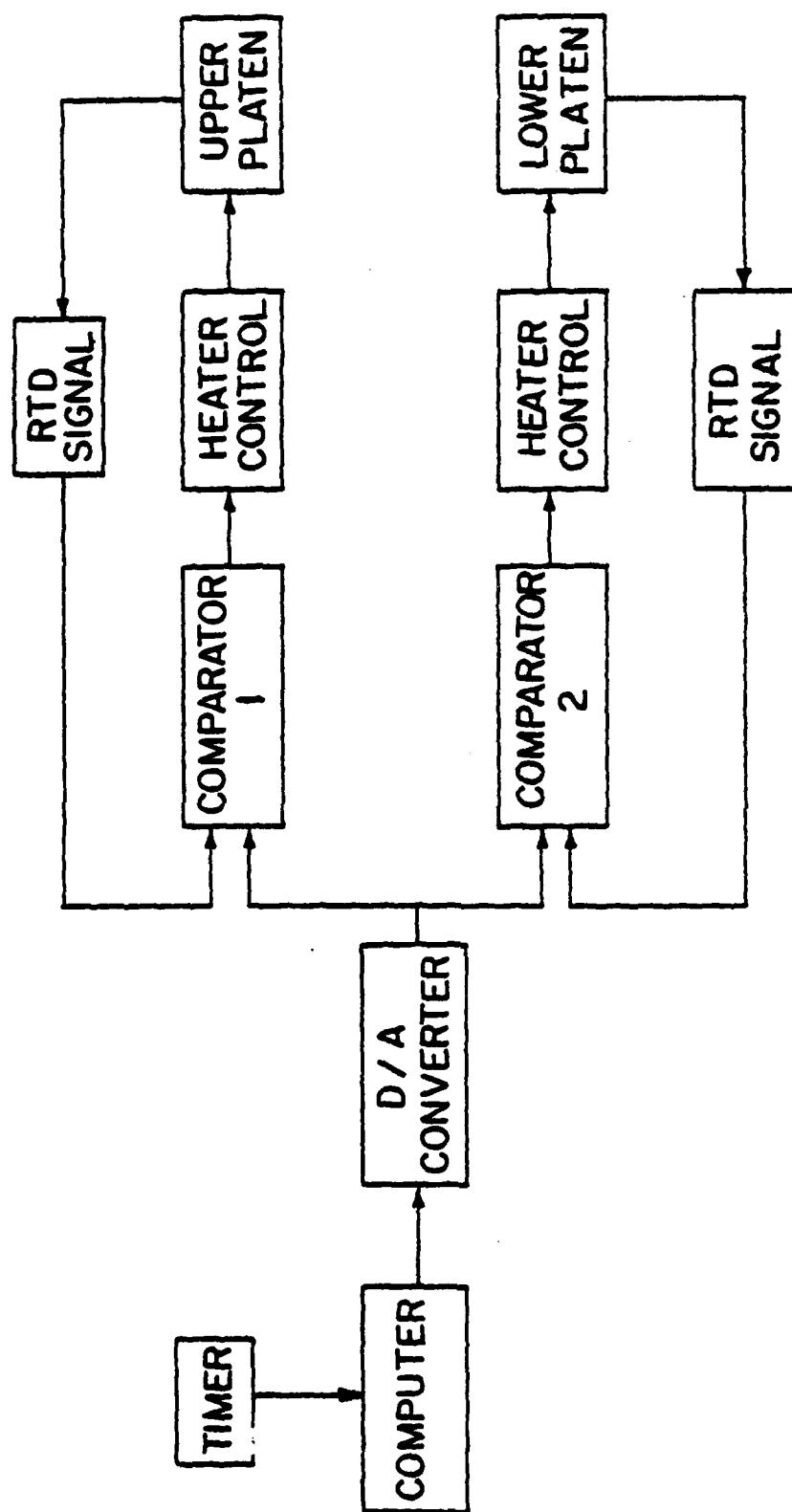


Figure 14 Schematic of the Temperature Controller Circuit.

The timer was started and its output signal was fed into the computer. At one-second intervals, the computer calculated the required platen temperature. From the RTD output voltage vs. temperature table stored in the computer, the voltage corresponding to the calculated temperature was selected. This voltage signal was sent to both comparators through the D/A converter. The voltage output of each RTD sensor was also fed into the appropriate comparator. Each comparator compared the voltage signal from the RTD element (which is proportional to the actual surface temperature) and the voltage signal from the D/A (which is proportional to the required surface temperature) and generated an output voltage proportional to the difference between the two signals. The output voltage from each comparator was fed directly into the heater controller, which regulates the power input to each bank of heaters.

As indicated in the preceding, the controller required that the RTD temperature vs. RTD voltage relationship be known and stored in the computer. This relationship was obtained by the following procedure. Each RTD was removed from the circuit and was replaced with a variable-resistance box. With the constant current source operating, the voltage drop across the circuit was measured as a function of resistance (Figure C.1, Appendix C). The results thus obtained (i.e. voltage drop vs. resistance) were combined with the temperature vs. resistance relationship of the RTD provided by the manufacturer (Figure C.2, Appendix C). This resulted in the required relationship between RTD temperature and output voltage (Figure C.3, Appendix C). Note that this is the voltage signal that was stored in the computer.

The voltage output from the computer which is input to the D/A was in the form of a digital signal. The relationship between the digital input to the D/A converter and the analog voltage output was obtained by sending a known digital signal into the D/A converter and measuring the output with a voltmeter. The results are shown in Figure C.4 of Appendix C.

In order to check that each RTD circuit maintained a constant voltage-versus-temperature relationship, two calibration resistors ($126\ \Omega$ and $159.6\ \Omega$) were installed in each circuit. Calibration checks were performed periodically by switching the RTD sensors out of the circuit and measuring the output voltage of the circuit with the resistors in place. Minor changes in the circuit characteristics were corrected with adjustable potentiometers installed in each circuit.

5.4 Test Specimens

Test specimens were constructed from 305 mm wide, 0.165 mm thick unidirectional graphite fiber epoxy matrix prepreg tape. The prepreg was cut into 76 mm by 152 mm rectangular sheets with the fibers parallel to the 152 mm side. The individual sheets were stacked on top of each other to form a lay-up with the required number of plies. The lay-up was placed on the lower platen.

One sheet of nonporous teflon-coated release cloth and one sheet of porous teflon cloth were placed between the lower platen and the composite to prevent sticking. One sheet of porous teflon was placed on top of the composite lay-up, followed by a Mochburg (CW 1850) thermal fiber bleeder cloth. For every three-ply of prepreg, one sheet

of bleeder cloth was used. The bleeder cloth was cut to the same rectangular dimensions (76 mm by 152 mm) as the prepreg. One sheet each of nonporous teflon and porous teflon separated the bleeder from the top platen.

Two rigid aluminum bars were placed along the sides of the composite lay-up parallel to the fibers (Figure 13). These bars were securely fastened to the lower heater platen to prevent resin flow and fiber "washout".

Additional bleeder cloths were placed along the edges of the composite, perpendicular to the fibers. These "edge" bleeders were held in place by aluminum bars fastened to the lower platen. One sheet of porous teflon was placed between the bleeder and the composite. For 16-ply composite lay-ups, each bleeder consisted of 12 sheets of 76 mm long, 13 mm high Mochburg cloth. The 32-ply composites required 45 (76 mm by 9.5 mm) sheets of Mochburg cloth. The number of Mochburg sheets required for 64-ply composites varied from 40 to 57 sheets (76 mm by 13 mm) for each bleeder, depending on the resin content of the prepreg.

In order to measure the temperature distribution in the composite during cure, thermocouples were embedded in and attached to the surfaces of selected 64-ply specimens. One thermocouple each was on the top and bottom surfaces of the composite. Three thermocouples were embedded in the composite between plies 8 and 9, plies 16 and 17, and plies 32 and 33. Each thermocouple was mounted near the centerline of the material.

The thermocouples were constructed from No. 32 gauge (2 mm diameter) copper and constantan wire and were coated with Glyptol to prevent electrical contact with the graphite fibers. The calibration of each thermocouple (provided by thermocouple reference tables) was checked at the freezing and boiling points of water. Output of the thermocouples was measured by a Honeywell (Type 153 "ELECTRONIK") multipoint chart recorder, providing a record of temperature vs. time.

5.5 Experimental Procedure

Before each test, the composite lay-up and the bleeders were weighed on either a Mettler (Model H51AR) analytical balance or on an Ohaus (2610 gram) triple-beam balance. The composite specimen was placed into the press and the bleeders were installed in the proper locations. The desired force was applied to the specimen, and the heaters were turned on. At preselected times, the heaters were turned off and the pressure was released. After the composite-bleeder assembly was cooled to room temperature, it was removed from the press, and the weights of the composite and the bleeders were measured.

SECTION VI

RESULTS

In this chapter, comparisons between the results of the models and the data are presented, and the use of the model in establishing the proper cure cycle for a given application is discussed.

6.1 Comparisons Between the Results of the Model and Data

Experiments were performed to verify the thermo-chemical and resin flow models. In the experiments, temperature distributions and resin flows perpendicular and parallel to the tool plate of unidirectional composites were measured. The experiments were performed using Hercules AS/3501-6 graphite, fiber-reinforced, epoxy resin matrix prepreg tape. The same cure temperature was used in every test. The cure temperatures on the lower and upper surfaces of the composite (as measured by thermocouples) are shown in Figure 15. The pressure was applied at the beginning of the cure cycle and remained constant for the duration of the cure. Tests were performed with different applied pressures ranging from 103 kPa (15 psi) to 724 kPa (105 psi). The pressure in the bleeder was taken to be equal to the ambient pressure of 101 kPa (14.7 psi).

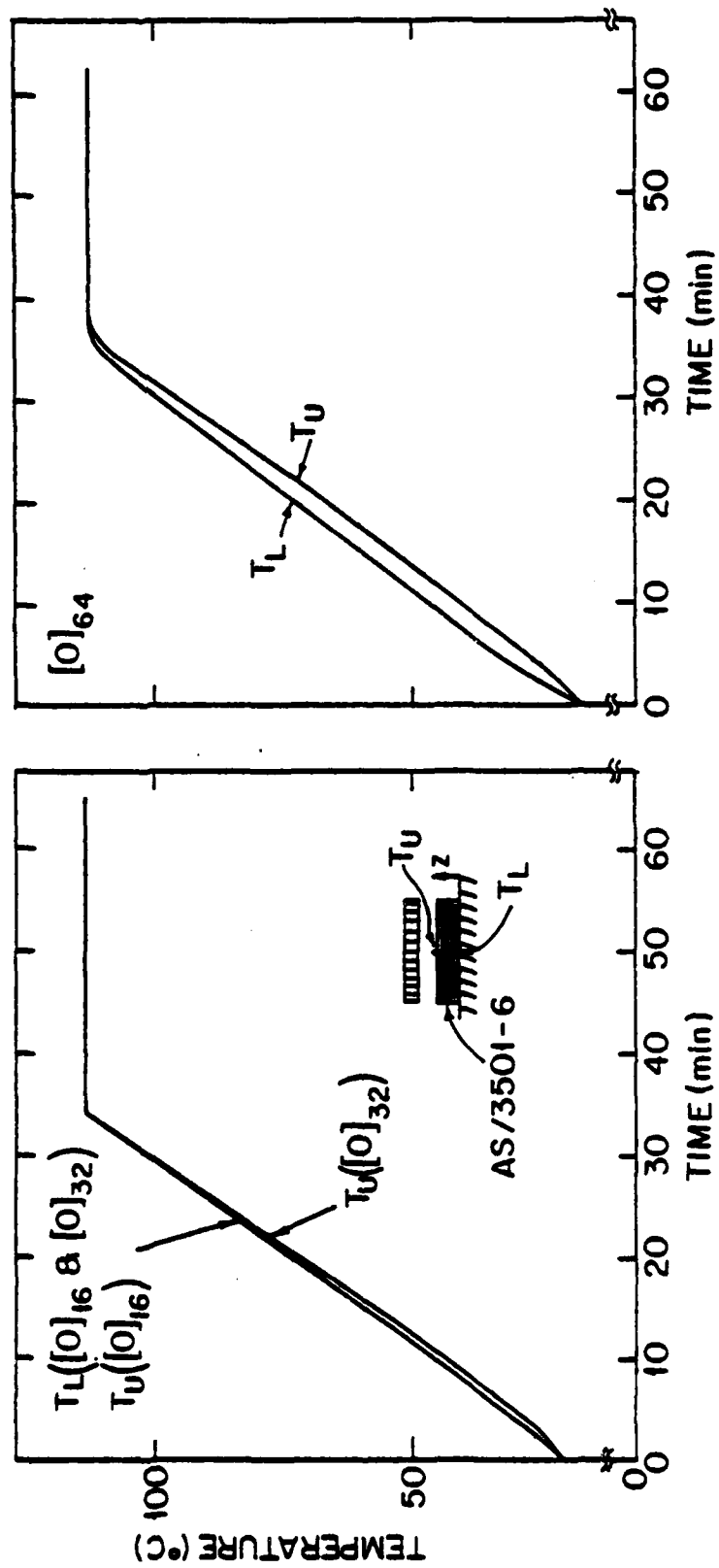


Figure 15 The Temperatures Measured on the Surfaces of 16, 32, and 64-Ply Composites During Cure.

The temperature as a function of time was measured at three locations inside a 64 ply composite. Results of the temperature measurements are presented in Figure 16.

Resin flow measurements were made with different cure pressures (103 kPa (15 psi), 345 kPa (50 psi), 586 kPa (85 psi), and 724 kPa (105 psi)), different ply thicknesses (16, 32, and 64 plies), and different initial prepreg resin contents (39% and 42%). The results are shown in Figures 17 - 19. In these figures, time, t , is plotted on the abscissa. The ordinates represent either the total mass loss, m^* , of the composite or the mass losses due to resin flow in the directions normal (m_T^*) and parallel (m_E^*) to the tool plate in time t . The mass losses shown in Figures 17 - 19 represent the mass loss with respect to the initial mass of the composite:

$$m^* = \frac{\text{mass loss}}{\text{initial mass}} \times 100 \quad (\text{percent})$$

The temperature distribution in the composite and the resin flow were calculated by the models using the same cure temperatures (Figure 15) and cure pressures which were employed in the tests. The prepreg and bleeder properties used in the calculations are listed in Appendix B.

The results of the models are represented by solid lines in Figures 16 - 19. As can be seen, the calculated and measured temperatures and the calculated and measured resin mass losses agree well. These agreements, which exist for wide ranges of applied cure pressures, composite thicknesses, and initial prepreg resin contents, tend to confirm the validity of the thermo-chemical and resin flow models.

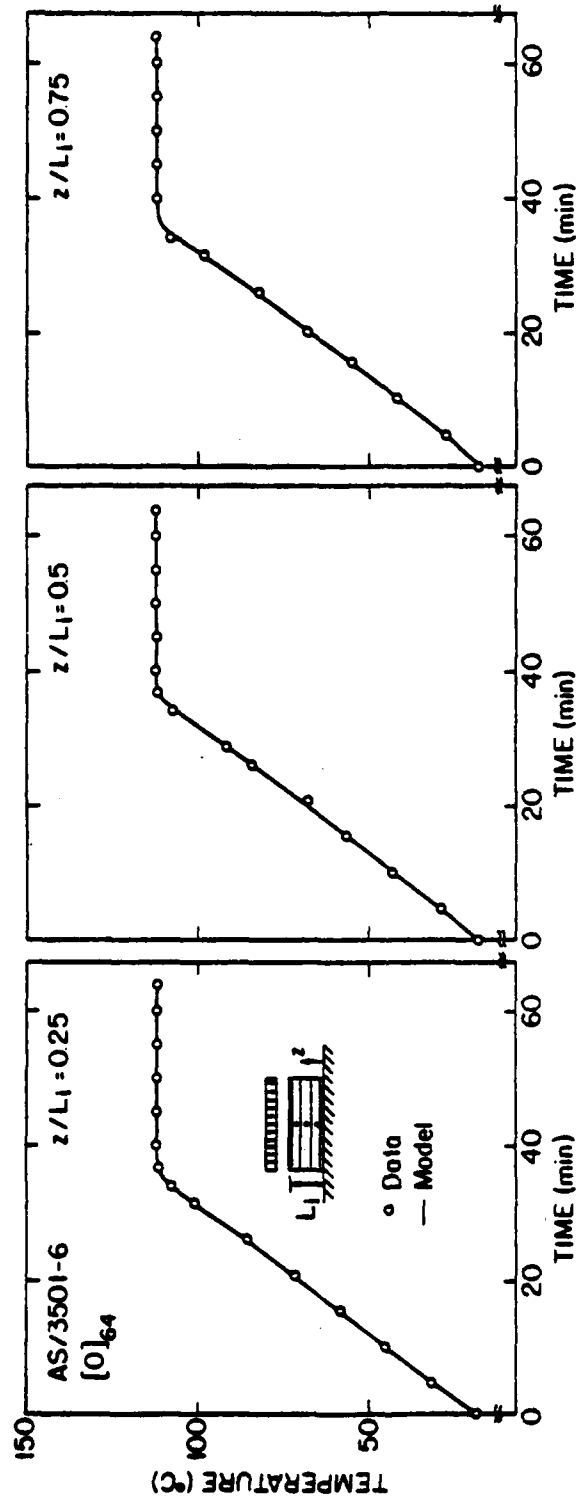


Figure 16 Temperature as a Function of Time at Three Positions Inside a 64-Ply Composite. Comparisons Between the Data and the Results Computed by the Model. The Temperature Cure Cycle is Shown in Figure 15. The Cure Pressure and the Bleeder Pressure were Constant at 586 kPa (85 psi) and 101 kPa (14.7 psi) Respectively.

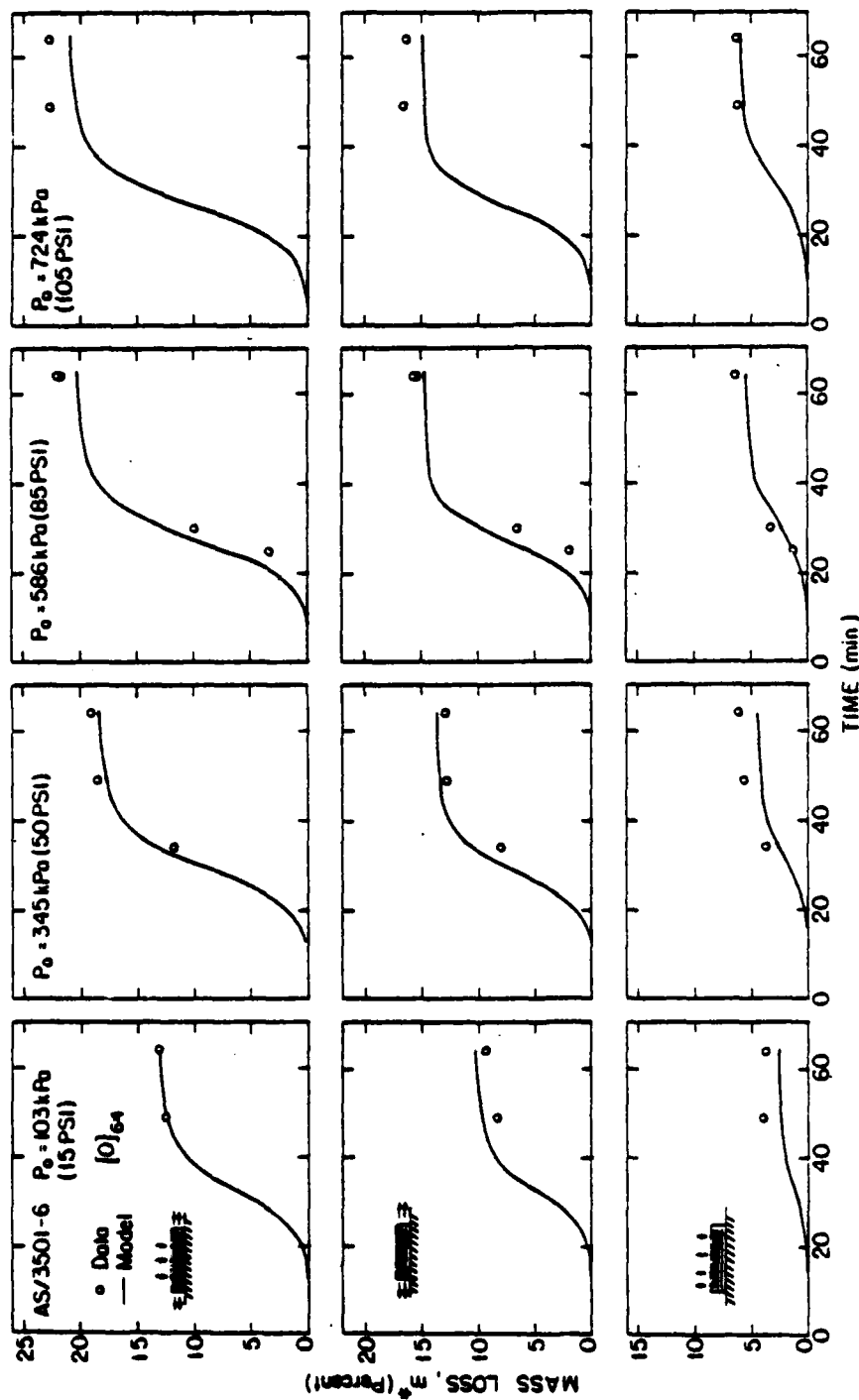


Figure 17 The Mass Loss, Normal to the Tool Plate (bottom), Parallel to the Tool Plate (center), and the Total Mass Loss (top) as a Function of Time for a 64-Ply Composite. Comparisons Between the Data and the Results Computed by the Model for Different Cure Pressures. The Temperature Cure Cycle is Shown in Figure 15. The Bleeder Pressure was Constant at 101 kPa (14.7 psi). The Initial Resin Content was 42%.

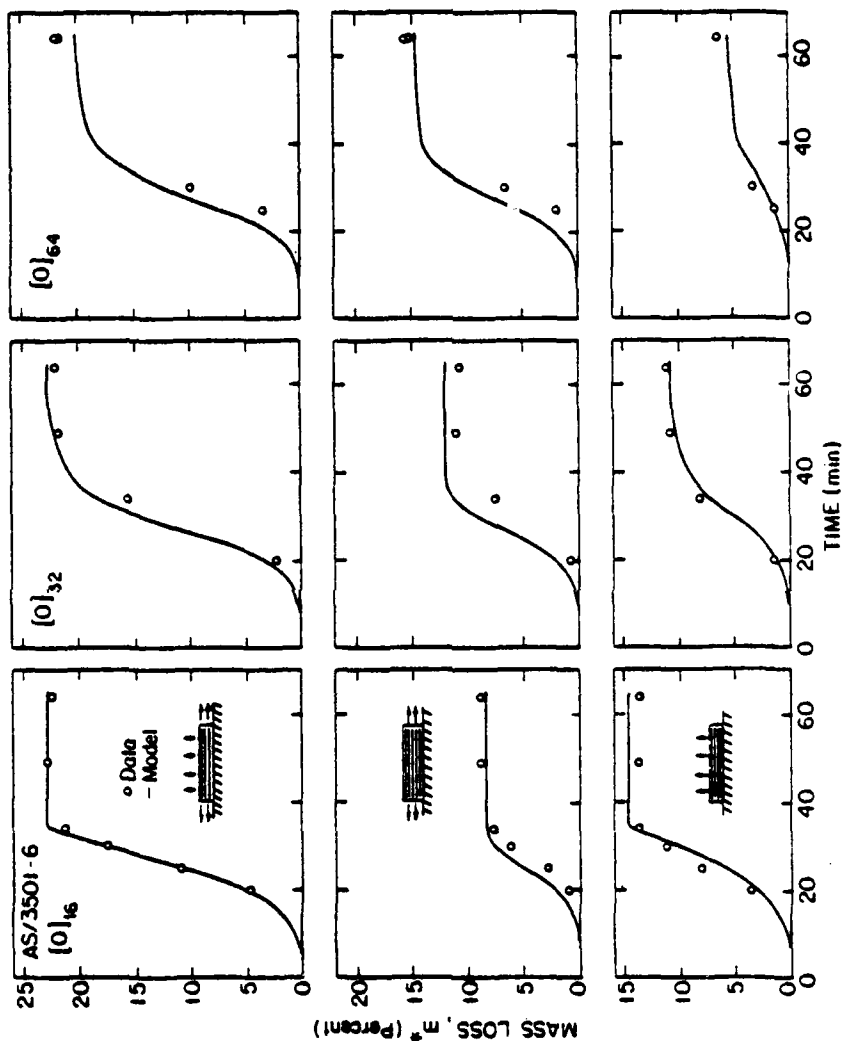


Figure 18 The Mass Loss, Normal to the Tool Plate (bottom), Parallel to the Tool Plate (center), and the Total Mass Loss (top) as a Function of Time. Comparisons Between the Data and the Results Computed by the Model for 16, 32, and 64-Ply Composites. The Temperature Cure Cycle is Shown in Figure 15. The Cure and Bleeder Pressures were Constant at 586 kPa (85 psi) and 101 kPa (14.7 psi) Respectively. The Initial Resin Content was 42%.

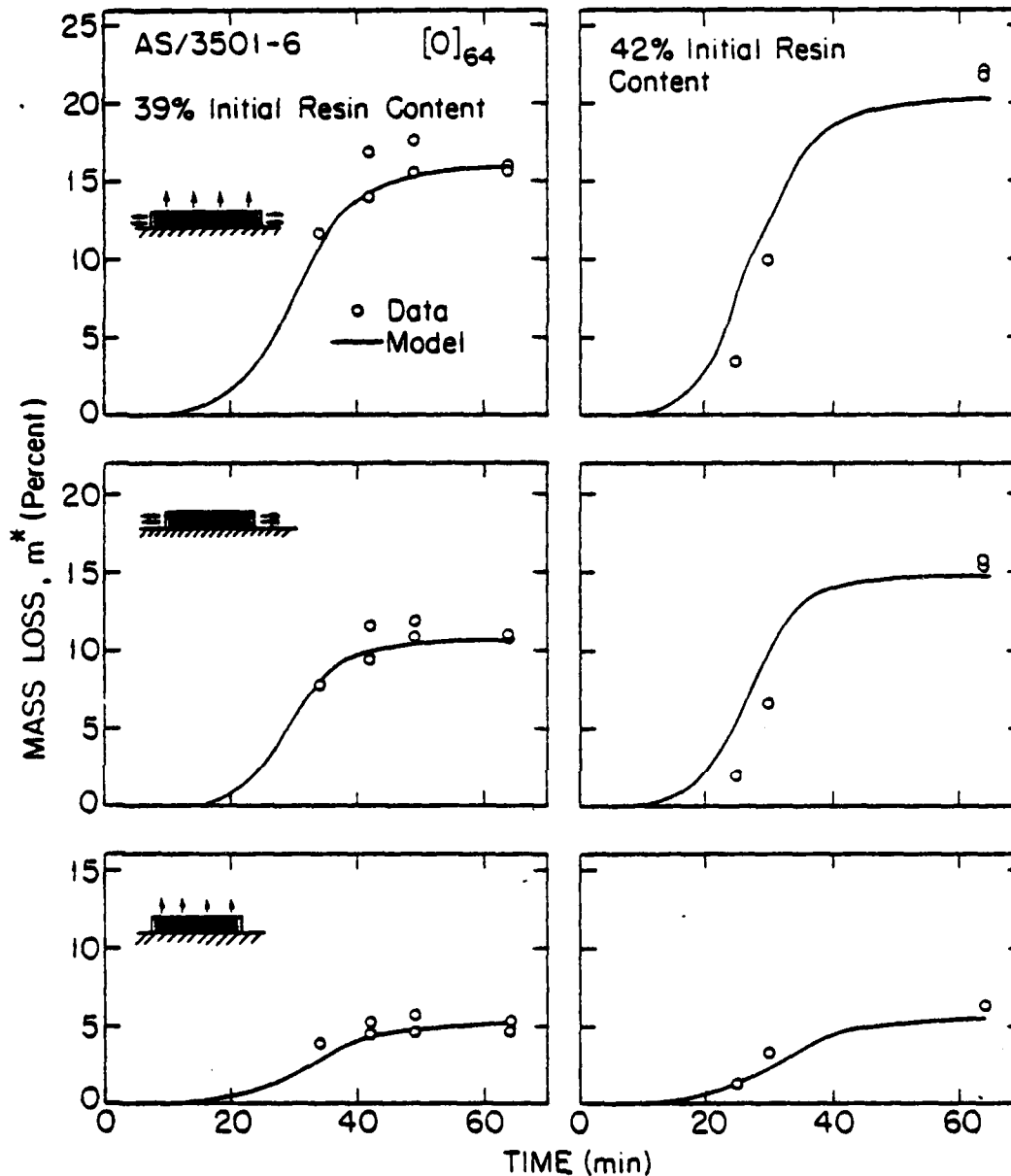


Figure 19 The Mass Loss, Normal to the Tool Plate (bottom), Parallel to the Tool Plate (center), and the Total Mass Loss (top) as a Function of Time for a 64-Ply Composite. Comparisons Between the Data and the Results Computed by the Model for Different Initial Resin Contents (39% and 42%). The Temperature Cure Cycle is Shown in Figure 15. The Cure and Bleeder Pressures were Constant at 586 kPa (85 psi) and 101 kPa (14.7 psi) Respectively.

6.2 Selection of the Cure Cycle

When curing a composite, the cure cycle should be selected in such a way that the following requirements are satisfied:

- a) the temperature at any position inside the material does not exceed a prescribed limit during the cure;
- b) the magnitude of the cure pressure is sufficiently high so that all of the excess resin is squeezed out from every ply of the composite before the resin gels at any point inside the composite;
- c) the pressure is applied before the viscosity of the resin, in the prepreg ply adjacent to the bleeder, becomes low enough to flow;
- d) the resin is cured uniformly and the degree of cure is above a specified limit throughout the composite at the end of cure; and
- e) the composite is cured in the shortest time.

The models and the corresponding computer code were used to generate results which illustrate the effects of cure temperature and cure pressure on the curing process for a given material. The calculations were performed for composites made of Hercules AS/3501-6 prepreg tape, bounded by the tool plate on one side and by the bleeder on the other side. The properties used in the calculations are given in Appendix B. In the calculations, only resin flow in the direction normal to the tool plate was considered. As was discussed in Section 2.3, the dimensions of the composite panel in commercial composite processing generally are such that resin flow along the plane of the composite is negligible.

The calculations were performed with the cure cycles shown in Figure 20. The cure temperature was increased at a constant heating rate, \dot{T}_0 , from room temperature until the maximum cure temperature, T_{\max} , was reached. For all calculations, it was assumed that the temperature on the upper and lower surfaces of the composite was equal to the applied cure temperature.

The cure pressure and the bleeder pressure used in the calculations are also shown in Figure 20. The cure pressure was applied at the beginning of the curing process ($t_p = 0$) and remained constant for the duration of the cure. The magnitude of the cure pressure is indicated on each figure showing the results. The pressure in the bleeder was taken to be constant at 16.7 kPa (25 in. Hg vacuum). This value is typical of the bleeder pressure in commercial composite processing using vacuum bagging procedures.

Calculations were also performed with the cure cycle recommended by the prepreg manufacturer for Hercules AS/3501-6 prepreg tape. This cycle is shown in Figure 21.

Maximum Temperature Inside the Composite. The maximum temperature reached inside a composite constructed from a given prepreg material depends on: a) the maximum value of the cure temperature, T_{\max} , b) the heating rate, \dot{T}_0 (i.e., the rate at which the cure temperature increases), and c) the thickness of the composite, L_j . Obviously, the temperature inside the composite will at some time reach the maximum cure temperature. Therefore, the cure temperature must not exceed the maximum temperature limit, T^* , prescribed for the prepreg. In the present parametric study, this limit was chosen arbitrarily to be 180°C.

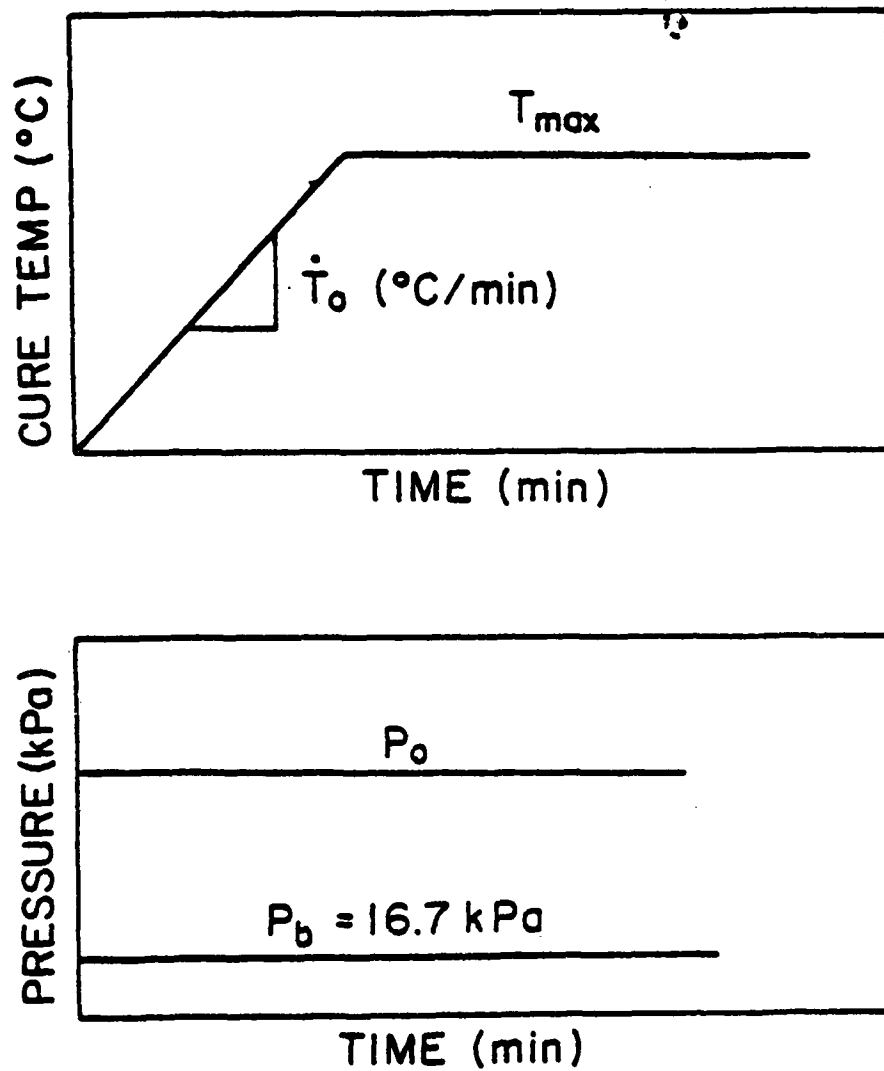


Figure 20 Illustration of the Cure Cycle Used in the Parametric Study.

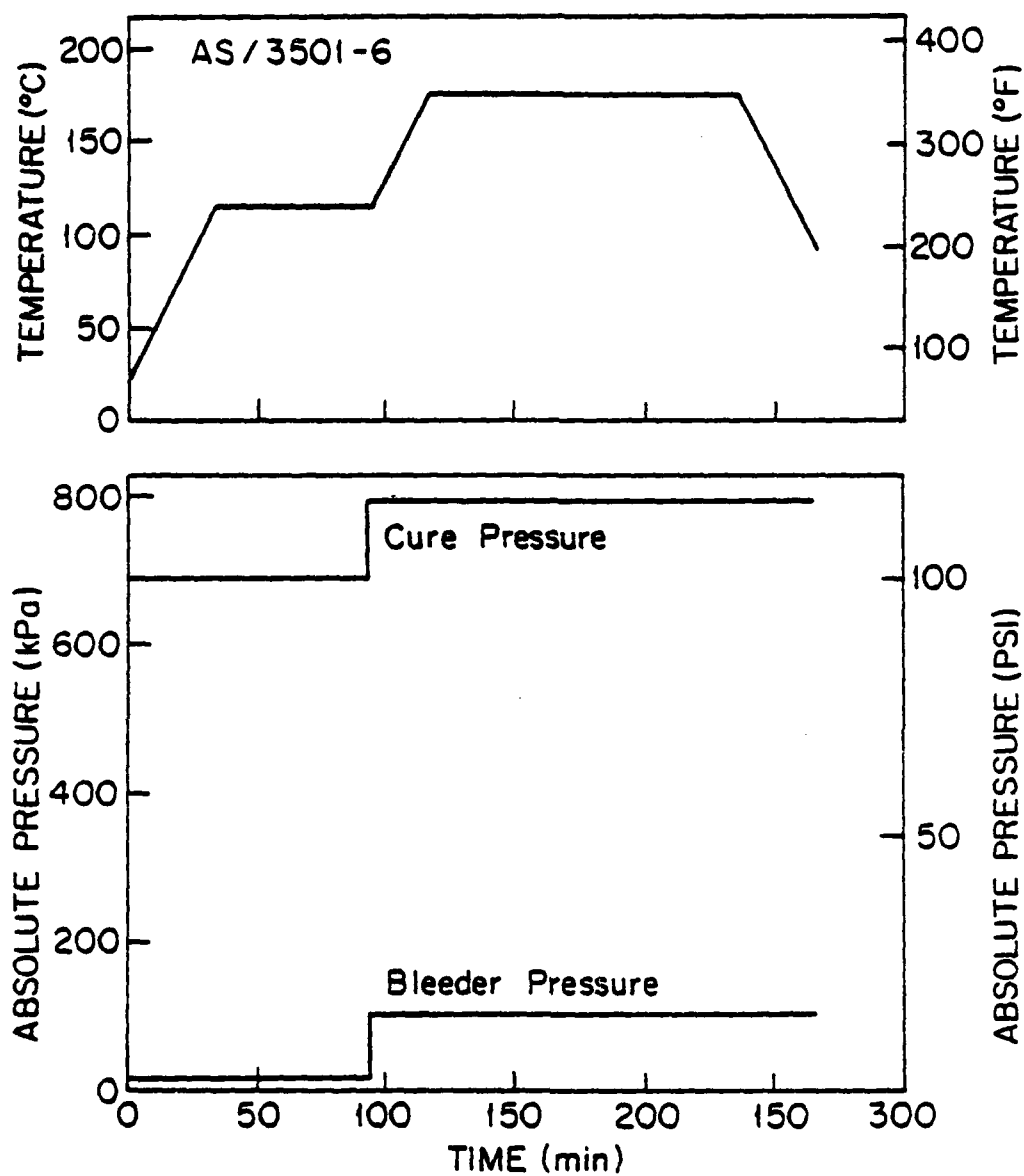


Figure 21 Manufacturer's Recommended Cure Cycle for Hercules AS/3501-6 Prepreg [38].

AD-A130 071

CURING OF GRAPHITE/EPOXY COMPOSITES(I) MICHIGAN UNIV
ANN ARBOR DEPT OF MECHANICAL ENGINEERING AND APPLIED
MECHANICS A C LOOS ET AL. MAR 83 AFWAL-TR-83-4040

UNCLASSIFIED

F33615-81-C-5050

F/G 11/4

NL

22

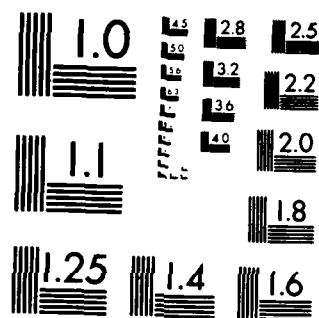
END

DATE

FILED

8 83

DTIC



MICROCOPY RESOLUTION TEST CHART
NATIONAL BUREAU OF STANDARDS-1963-A

The temperature inside the composite also depends on the heating rate and the thickness of the composite. At low heating rates, the temperature distribution inside the composite tends to remain uniform, as illustrated in Figure 22a. The results in this figure apply to a 64-ply composite where the cure temperature was increased from room temperature to the maximum cure temperature of 177°C at 2.8°C/min. When the heating rate was increased to 27.8°C/min, the temperature distribution became nonuniform, as shown in Figure 22b. However, at no time does the temperature at any place inside the composite exceed the maximum allowed temperature, T^* . On the other hand, when a 128-ply composite was cured using the same heating rate (27.8°C/min), the temperature inside the material exceeded both the boundary temperature and the maximum allowed temperature limit (Figure 22c). The temperature nonuniformity inside the material depends on the rate at which heat is transported through the composite and the rate at which heat is generated by chemical reactions. The temperature "overshoot" shown in Figure 22c occurs when heat is generated in the composite faster than it can be dissipated.

With the use of the computer code, results such as those in Figure 22 can be generated for a composite constructed from a given prepreg material and cured with a specified cure cycle. From these results, the temperature distribution inside the material can be established. This information can then be used to determine if the temperature distribution is uniform and if the local temperature at any point in the composite exceeds the maximum allowed temperature at any time.

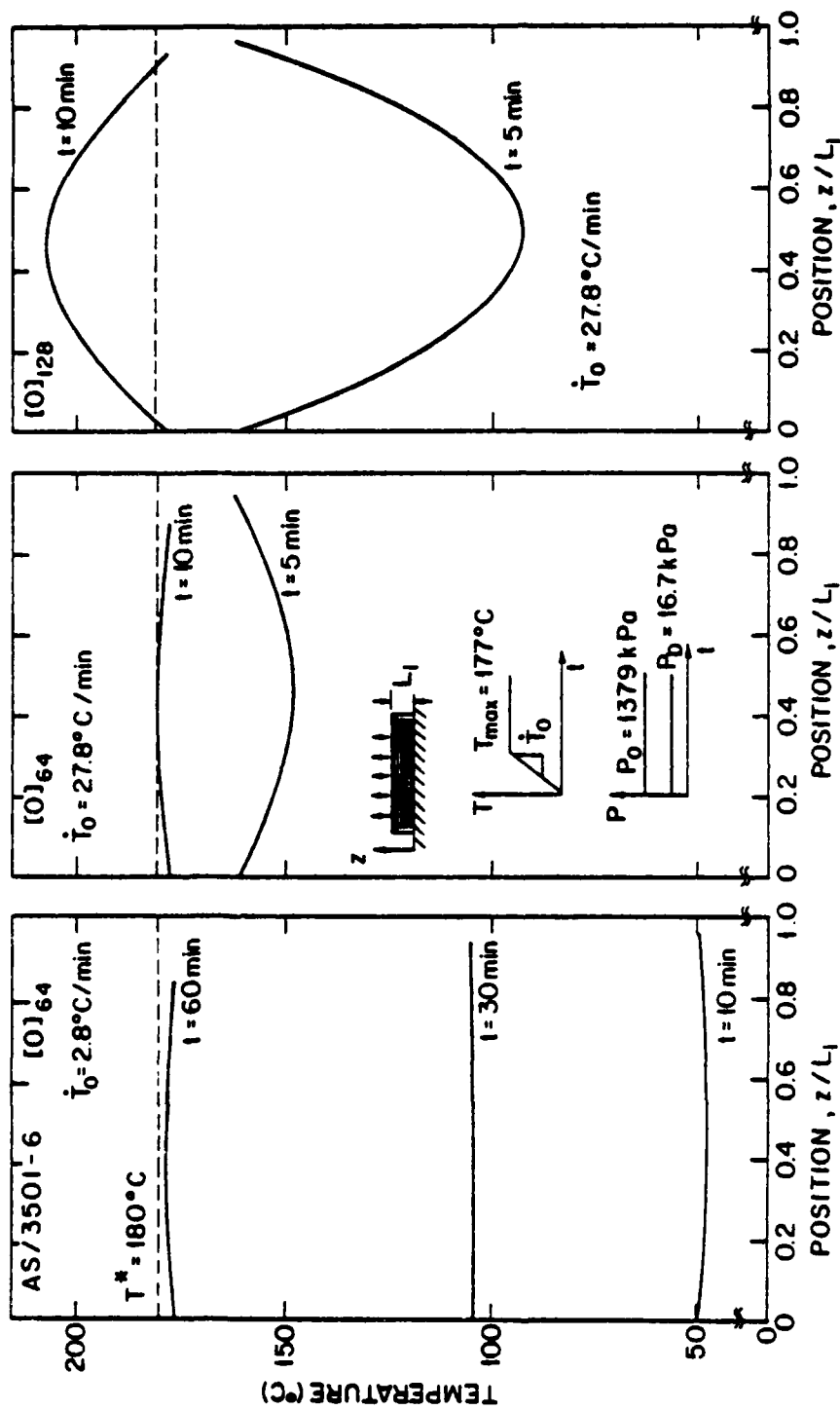


Figure 22 Temperature Distribution as a Function of Time for Different Heating Rates and Different Thicknesses. a) 64-Ply, $\dot{T}_0 = 2.8^\circ\text{C/min}$ (left), b) 64-Ply, $\dot{T}_0 = 27.8^\circ\text{C/min}$ (center), and c) 128-Ply, $\dot{T}_0 = 27.8^\circ\text{C/min}$ (right). Results Obtained by the Model.

Resin Flow The pressure applied during the cure must be sufficiently high so that the excess resin is squeezed out of every ply of the composite before the resin in any ply gels. The magnitude of pressure applied when curing a given material depends on the composite thickness and, to a lesser extent, on the cure temperature and heating rate. This is illustrated in Figure 23, where the number of compacted plies, n_s , is plotted as a function of time.

The curves in Figure 23 were generated by the computer code for different composite thicknesses (16, 32, and 64 plies). Results of the calculations show that cure pressures of 345 kPa (50 psi) and 1207 kPa (175 psi) are sufficient to squeeze all the excess resin out of 16-ply and 32-ply composites, respectively, before the gel point is reached (Figure 23). However, for a 64-ply composite, an applied pressure of 3447 kPa (500 psi) would squeeze excess resin out of only 55 plies, so that the 9 plies nearest to the tool plate would contain excess resin. These results apply to composites with a bleeder on one side only. If bleeders are placed on both sides of the composite and the same pressure is applied, excess resin can be squeezed out of approximately twice as many plies as with the single bleeder system.

For the cure cycles employed in this parametric study (Figure 20), a change in the maximum cure temperature does not significantly affect the number of compacted plies (Figure 24a). Similarly, variations in the applied heating rates have little effect on the number of compacted plies, unless the heating rate is so large that the resin gels before the excess resin is squeezed out of every ply. For example, the results in Figure 24b show that at a heating rate of 27.8°C/min, the resin gels

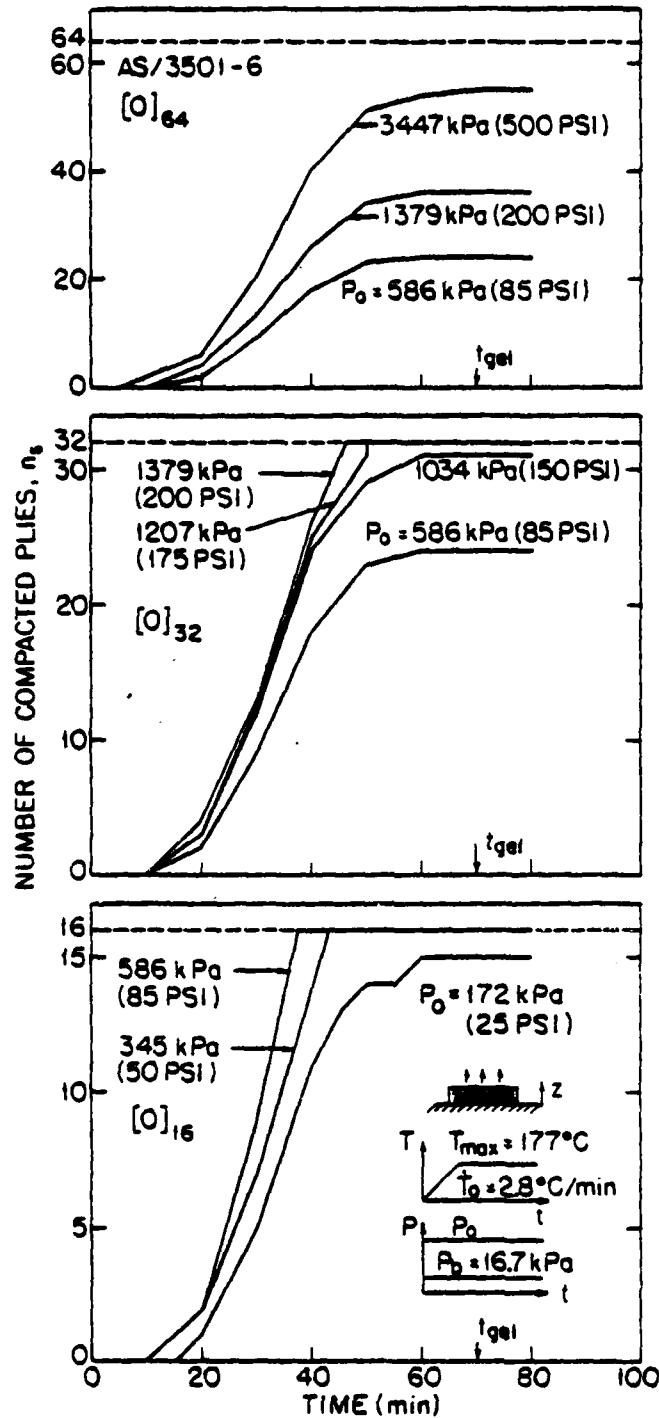


Figure 23 Number of Compacted Plies, n_s , as a Function of Time for Different Cure Pressures and Different Composite Thicknesses. a) 16-Ply (bottom), b) 32-Ply (center), and c) 64-Ply (top). Results Obtained by the Model.

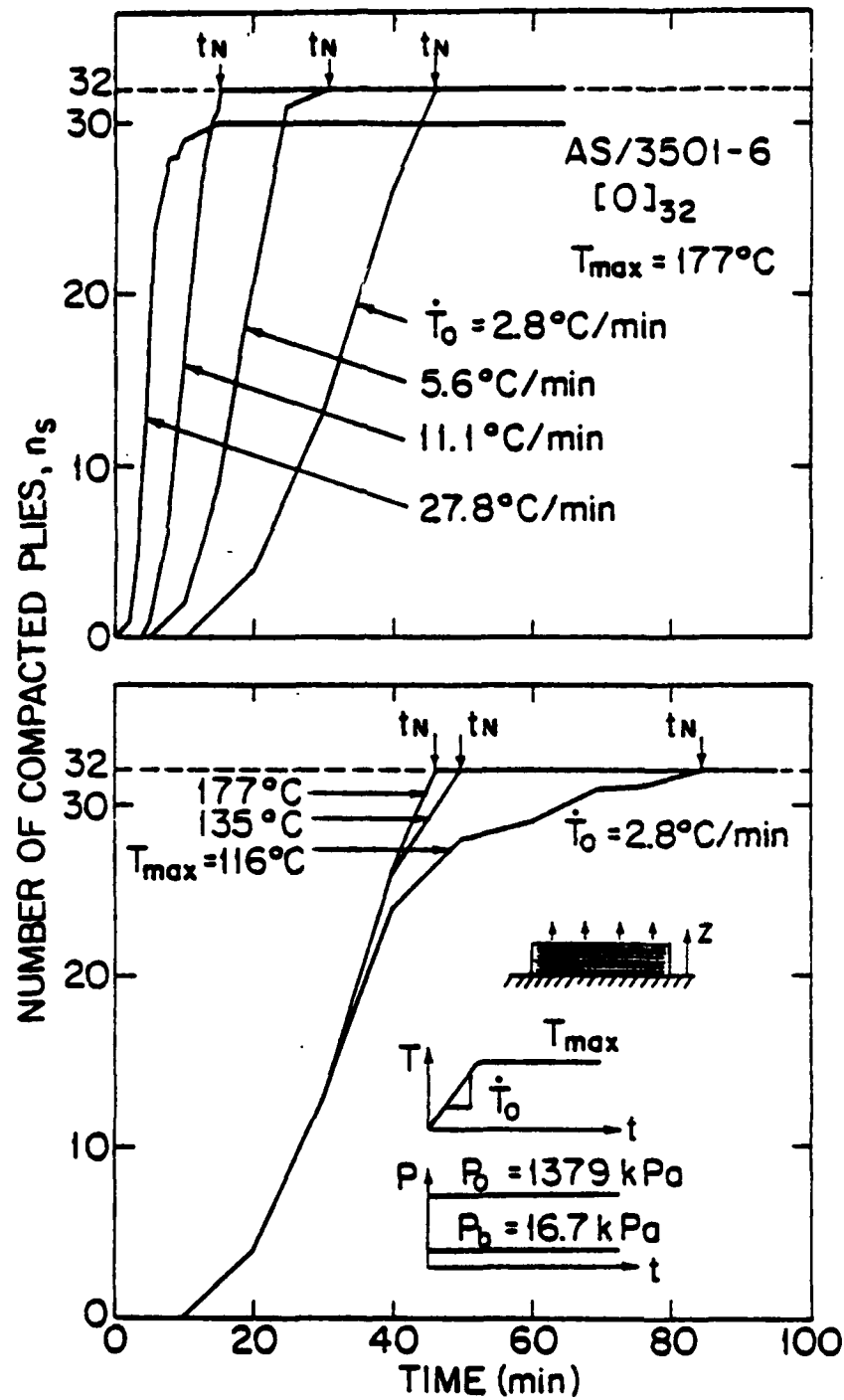


Figure 24 Number of Compacted Plies, n_s , as a Function of Time for
a) Different Maximum Cure Temperatures, T_{\max} (bottom) and
b) Different Heating Rates, \dot{T}_0 (top). Results Obtained
by the Model.

at a time when only 30 plies are compacted in a 32-ply composite. Thus, excess resin remains in two plies.

Although the maximum cure temperature and the heating rate have little effect on the total number of compacted plies, these two parameters do effect the amount of time required to squeeze excess resin out of every ply in the composite, t_N . The effect of cure temperature and heating rate on the time required to squeeze excess resin out of every ply of a 32-ply composite is shown in Figure 25. The time required to squeeze the excess resin out of every ply in the composite decreases with increasing cure temperature and increasing heating rate.

Calculations were also performed for the cure cycle recommended by the manufacturer for processing composites made of Hercules AS/3501-6 prepreg (Figure 21). The number of compacted plies, n_s , as a function of time is plotted in Figure 26. The results show that if the manufacturer's recommended cure cycle is used, excess resin could be squeezed out from only a 23-ply composite before the gel point is reached. If composites thicker than 23 plies are cured with the manufacturer's recommended cure cycle, then there would be resin rich plies adjacent to the tool plate at the end of cure. There is experimental evidence that the manufacturer's recommended cure cycle may not be appropriate when curing thick composites. Meade [39] presented microphotographs of a 96-ply composite, constructed from Narmco T300/-5208 unidirectional prepreg tape, and cured with the manufacturer's recommended cure cycle. These microphotographs reveal the existence of uncompact, resin-rich plies adjacent to the tool plate.

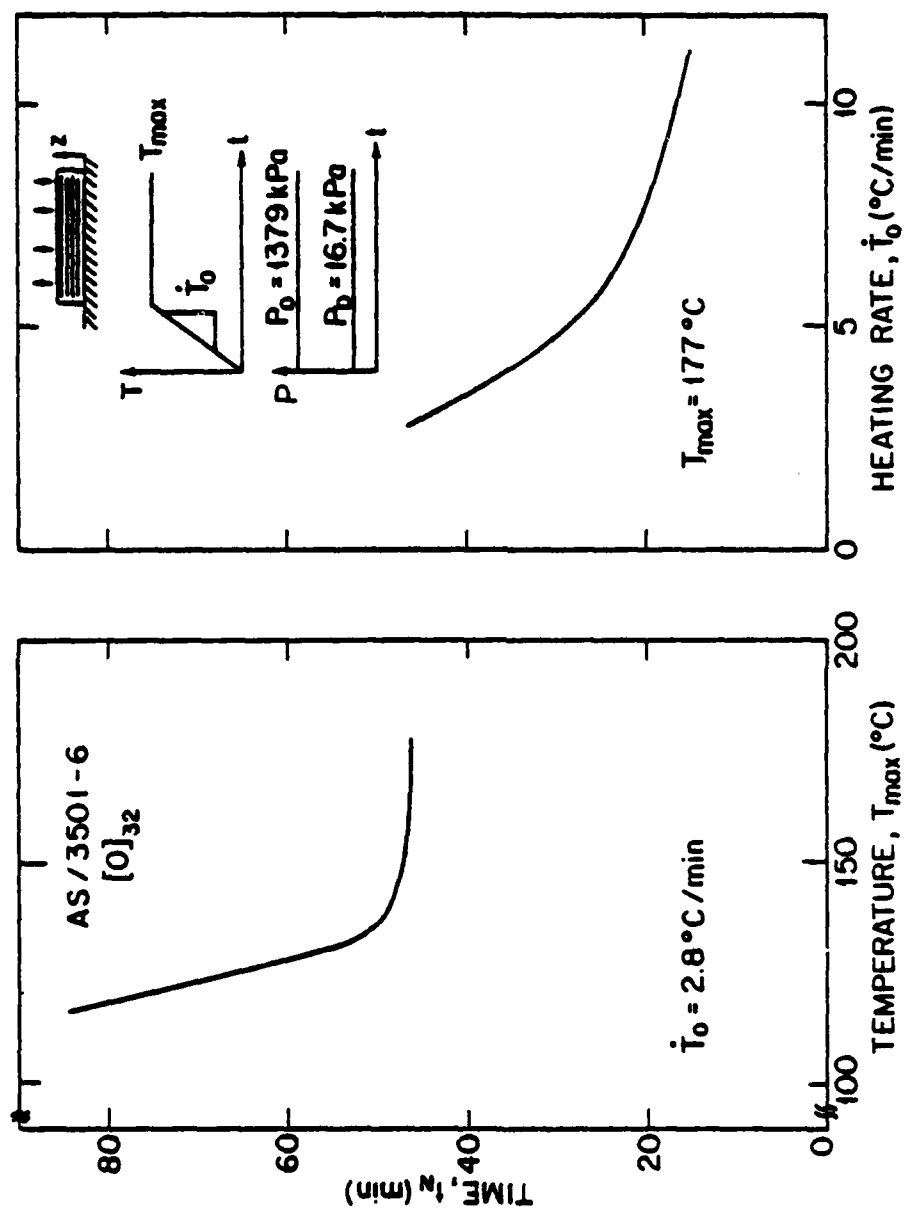


Figure 25 The Time Required, t_N , to Squeeze Excess Resin Out of Every Ply of a 32-Ply Composite at
a) Different Maximum Cure Temperatures, T_{max} (left) and b) Different Heating Rates, \dot{T}_0 (right). Results Obtained by the Model.

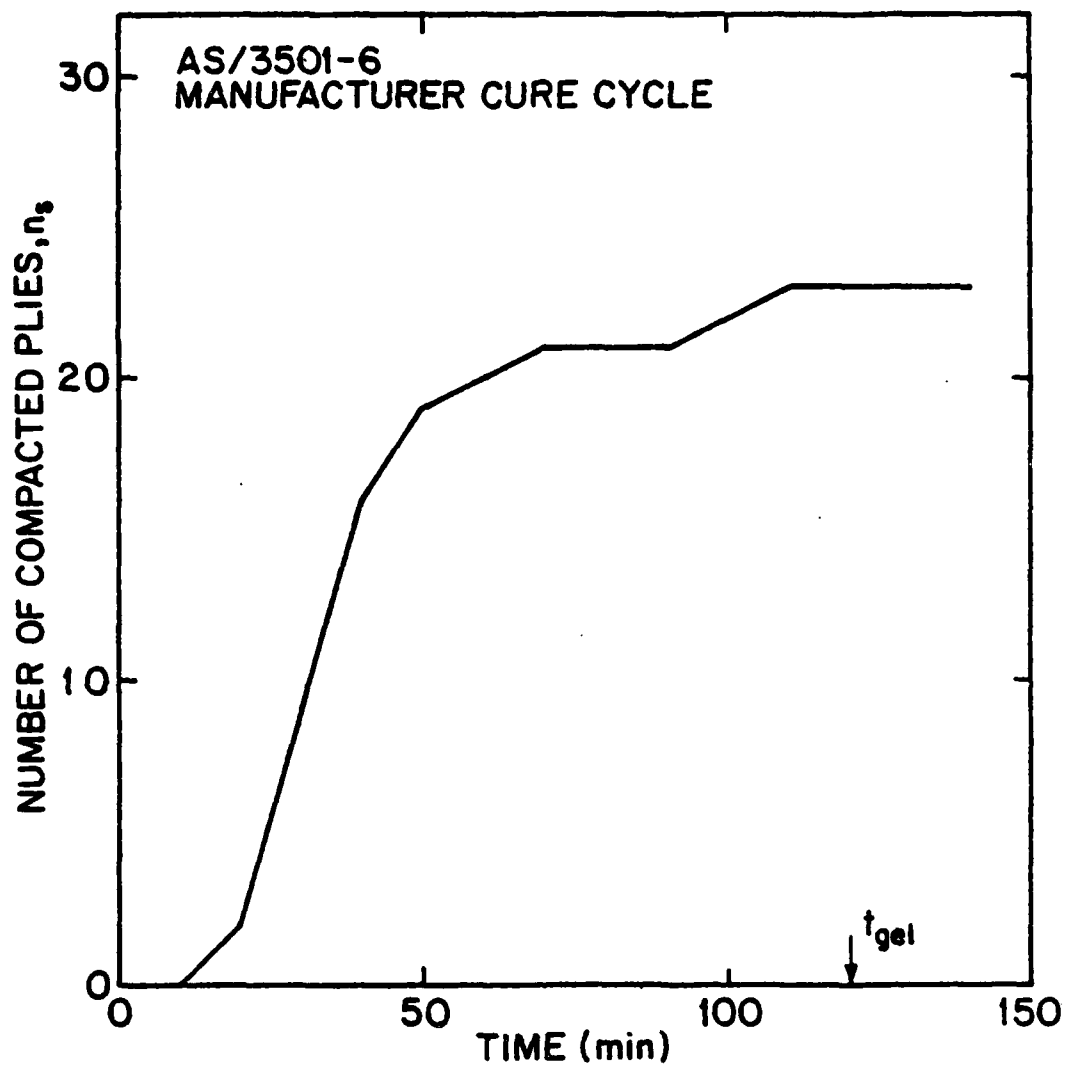


Figure 26 Number of Compacted Plies, n_s , as a Function of Time for a Composite Cured by the Cure Cycle Recommended by the Prepreg Manufacturer (Figure 21). Results Obtained by the Model.

The foregoing results illustrate a procedure which can be used to determine if the excess resin is squeezed out of every ply in the composite before the gel point is reached. This procedure requires that for a given cure cycle, the number of compacted plies, n_s , is calculated as a function of time. From a plot of n_s versus time, it can readily be seen how many plies are compacted before the gel point is reached.

By performing the calculations for different cure pressures, the maximum number of plies that can be compacted, $(n_s)_{\max}$, for a given pressure, P_0 , can also be determined. A plot of $(n_s)_{\max}$ versus pressure for Hercules AS/3501-6 prepreg is given in Figure 27. Such a plot can serve as a guide in selecting the pressure which is sufficient to squeeze the excess resin out of every ply of a given composite.

Gel Point As discussed previously, excess resin must be squeezed out of every ply before the gel point of the resin is reached at any point inside the composite. The computer code can be used to calculate the viscosity distribution inside the composite as a function of time (Figure 28). From this information, the maximum viscosity at any point inside the composite at any time can be determined and a plot of the maximum viscosity, μ_{\max} , versus time can be constructed (Figure 29). The gel point of the resin is assumed to occur when the viscosity of the resin reaches 100 Pa·s [40,41]. Thus, by knowing the viscosity corresponding to the gel point, the time when gel occurs can be determined from the maximum viscosity, μ_{\max} , versus time curve, as shown in Figure 29.

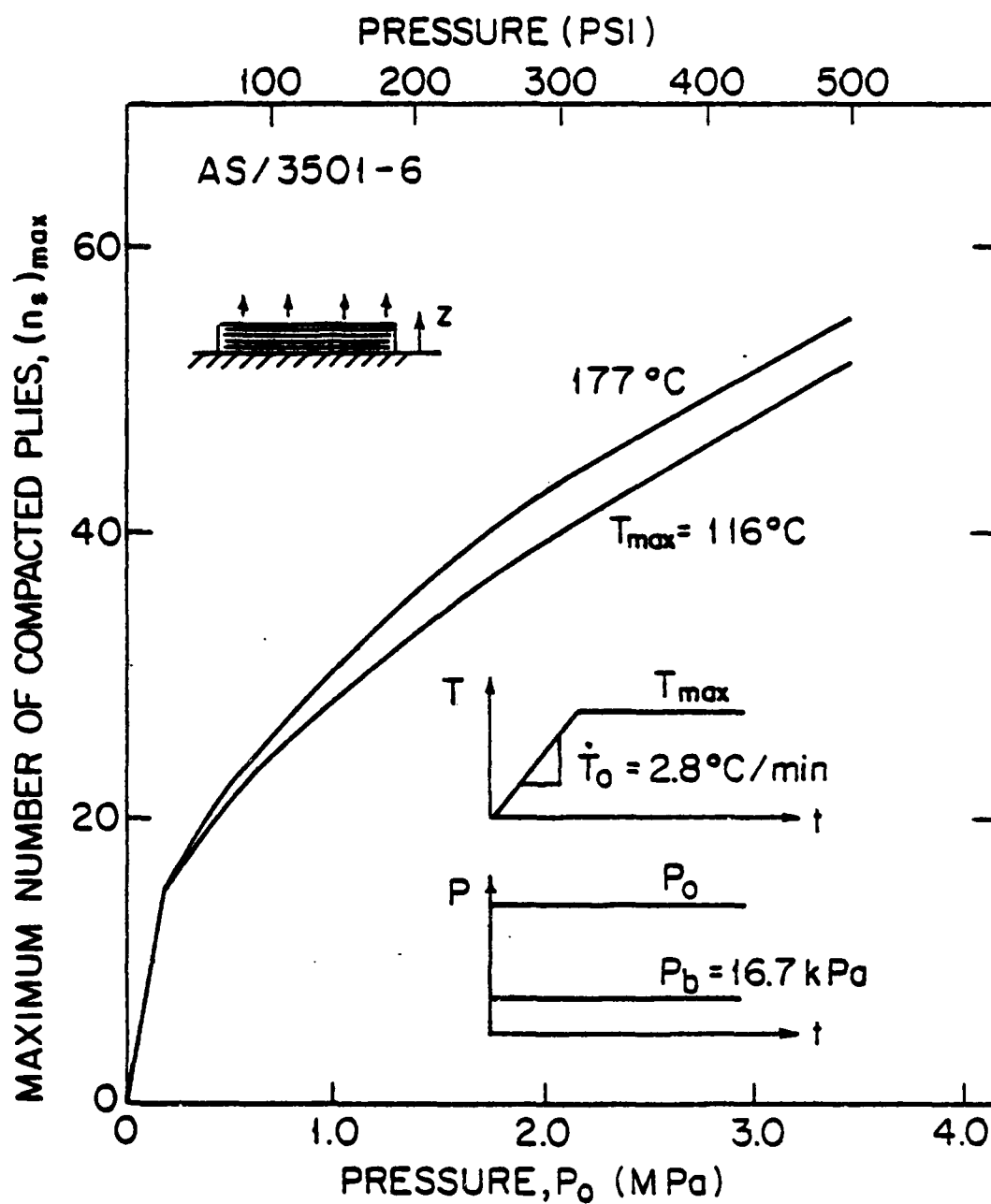


Figure 27 The Maximum Number of Compacted Plies, $(n_s)_{\max}$, at the End of the Cure as a Function of Cure Pressure, P_0 . Results Obtained by the Model.

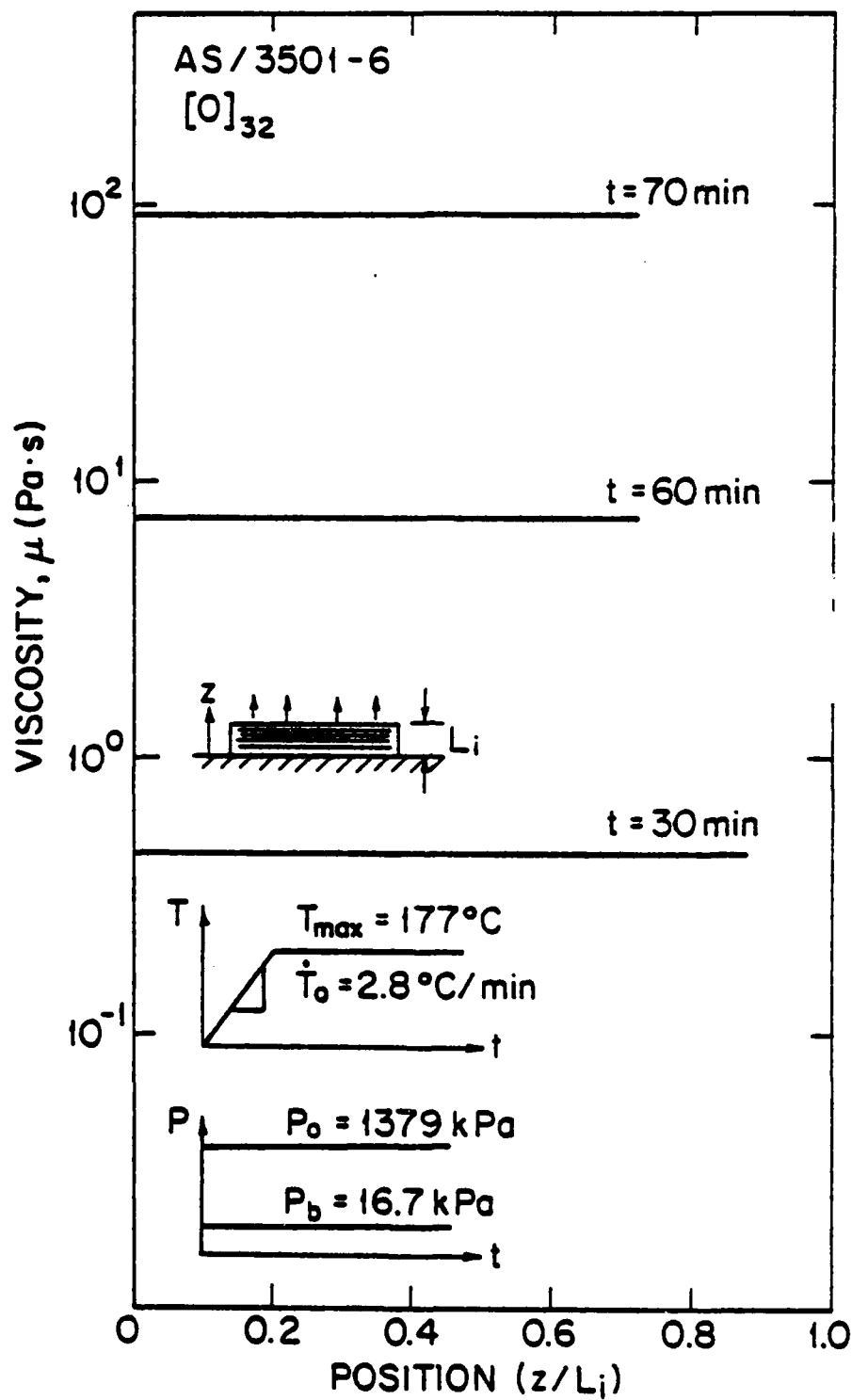


Figure 28 Viscosity Distribution at Different Times Inside a 32-Ply Composite. Results Obtained by the Model.

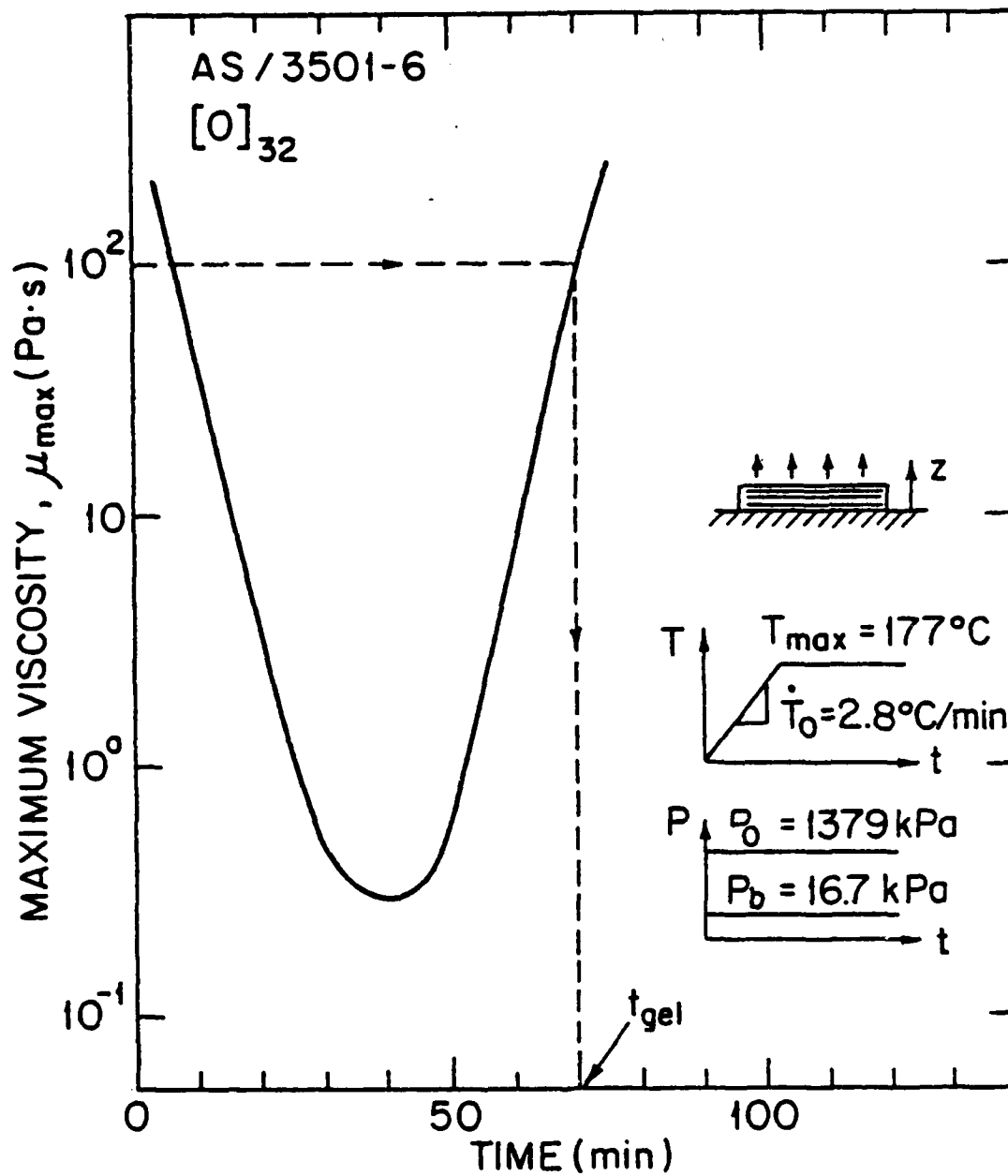


Figure 29 The Maximum Viscosity, μ_{\max} , Inside a 32-Ply Composite as a Function of Time. Gel is Assumed to Occur When the Viscosity Reaches 100 Pa·s. Results Obtained by the Model.

The above procedure was used to determine the gel point of a 32-ply composite cured at 177°C (Figure 20) with a cure pressure of 1379 kPa (200 psi), as shown in Figure 29. The intersection of the viscosity-time curve with the gel line (denoted as a dashed line on Figure 29) indicates that the resin would begin to gel in the composite 70 minutes after the cure temperature is first applied.

Time of Pressure Application The cure pressure should be applied before the viscosity of the resin in the first ply next to the bleeder becomes sufficiently low for resin flow to occur. This is the latest time at which the pressure should be applied. This time, referred to as the time of pressure application, t_p , can be determined from a plot of the number of compacted plies, n_s , versus time, t . The intersection of the n_s -versus-time-curve with the time axis is taken to be time of pressure application (Figure 30).

The time of pressure application depends on the magnitude of the applied pressure and on the heating rate as illustrated in Figure 30. The pressure may be applied, of course, at times which are less than t_p , but should not be applied at times greater than t_p . It should be emphasized that applying the cure pressure before t_p does not ensure that all the excess resin will be squeezed out of every ply of the composite before the gel point is reached.

Degree of Cure At the completion of the curing process, the resin in a composite should be cured uniformly, and the degree of cure must exceed a prescribed value, α^* , throughout the composite. The degree of cure will be uniform as long as the temperature distribution inside the composite is uniform, as illustrated in Figure 31a.

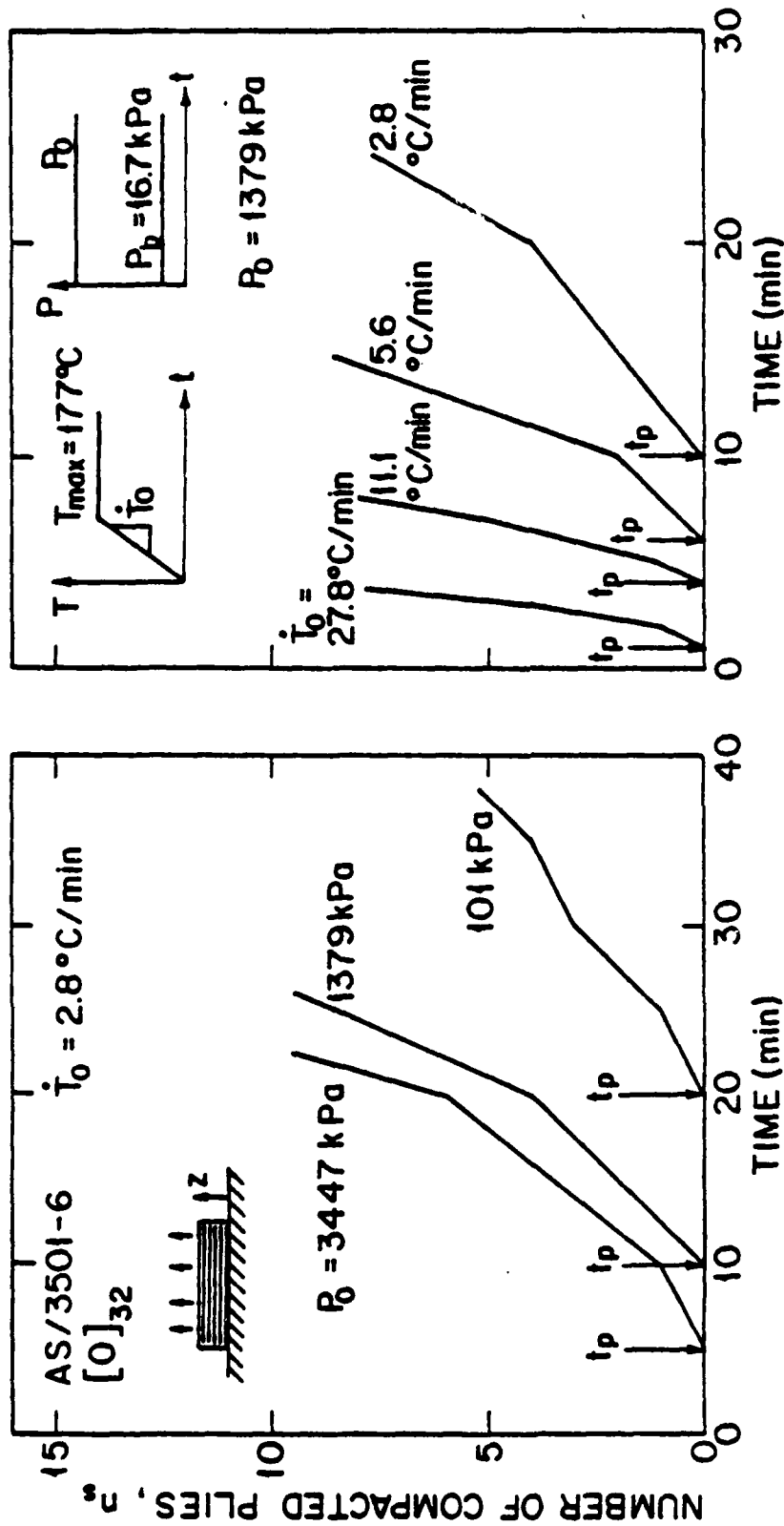


Figure 30 Number of Compacted Plies, n_s , as a Function of Time for a) Different Cure Pressures, P_0 , (left) and b) Different Heating Rates, \dot{T}_0 (right). The Pressure Should be Applied Before Time t_p . Results Obtained by the Model.

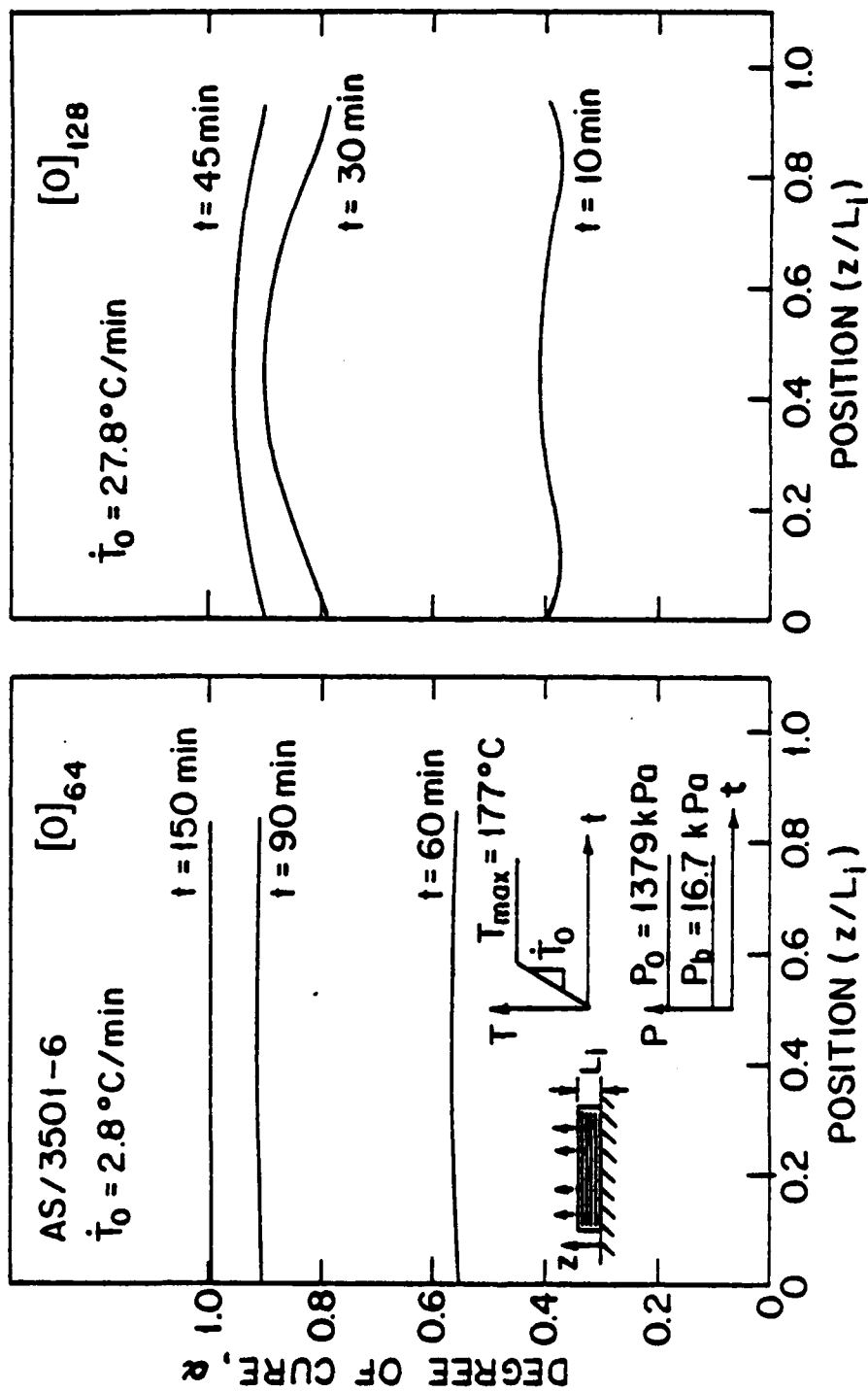


Figure 31 Degree of Cure Distribution as a Function of Time. a) 64-Ply Composite, $\dot{t}_0 = 2.8^\circ\text{C/min}$ (left). b) 128-Ply Composite, $\dot{t}_0 = 27.8^\circ\text{C/min}$ (right). Results Obtained by the Model.

Conversely, if the temperature distribution inside the composite becomes nonuniform, the degree of cure can also be expected to be nonuniform, as shown in Figure 31b. Therefore, cure cycles which result in uniform temperature distributions also result in composites that are cured uniformly.

The computer code can be used to generate results such as those shown in Figure 31. From these results, the degree of cure as a function of position inside the composite can be determined. Once this information is known, it can be determined if the composite was cured uniformly and if the degree of cure exceeds the prescribed value of α^* throughout the composite.

Cure Time When curing a composite, it is desirable that the curing process be completed in the shortest amount of time. The cure is considered complete when the degree of cure reaches a specified value, α^* , at every point in the composite. The time required to reach this value can be established by first plotting the degree of cure as a function of position and time, as shown in Figure 31. From this curve, the lowest value of the degree of cure, α_{\min} , in the composite at each time is determined and a plot of the lowest value of the degree of cure as a function of time can be constructed (Figure 32). The cure is considered complete when α_{\min} reaches the specified value α^* . Thus, from a plot such as that shown in Figure 33, the time required to complete the curing process can be determined.

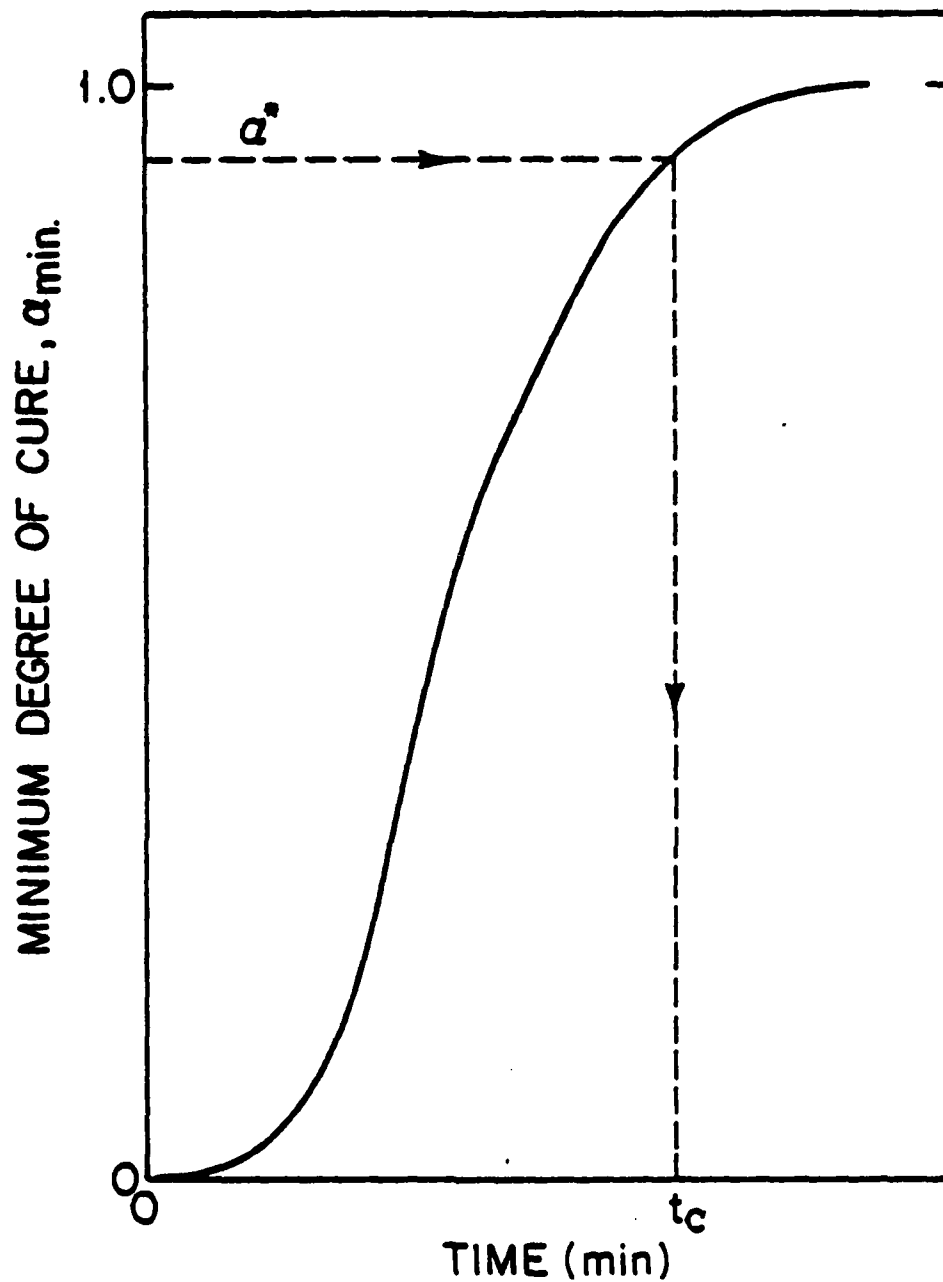


Figure 32 Illustration of the Minimum Value of the Degree of Cure, α_{\min} , Inside the Composite as a Function of Time. The Cure is Considered Complete When the Degree of Cure Reaches a Specified Value, α^* , at Every Point in the Composite.

The cure time, t_c , depends greatly on the applied cure temperature and on the heating rate, as illustrated in Figure 33. The results in these figures are based on the assumption that cure is complete when a degree of cure of 0.9 is reached at all points of the composite. For example, a 32-ply composite constructed from Hercules AS/3501-6 prepreg and cured using a heating rate of 2.8°C/min and a maximum cure temperature of 177°C, requires a cure time of 89 minutes (Figure 33a). If the maximum cure temperature is reduced to 135°C, the calculated cure time increases to 236 minutes.

The effect of heating rate on the cure time is illustrated in Figure 33b. Increasing the heating rate of a 32-ply composite (maximum cure temperature 177°C) from 2.8°C/min to 11.1°C/min results in a 37 minute reduction in cure time (Figure 33b).

The computer code can be used to calculate the cure time for different maximum cure temperatures and heating rates. A plot of cure time versus cure temperature, and a plot of cure time versus heating rate for Hercules AS/3501-6 prepreg is given in Figure 34. Results such as those shown in Figure 34 can be used to estimate the required cure time for a composite cured with a specified temperature cure cycle.

It is interesting to note that a 32-ply composite cured with the manufacturer's recommended cure cycle (Figure 21) requires a cure time of 146 minutes (Figure 35). Thus, use of the 177°C cure cycle with a heating rate of 2.8°C/min (Figure 33a) would result in a 57 minute (37%) savings in cure time. These results show that significant savings in cure time might be achieved by careful selection of the cure cycle.

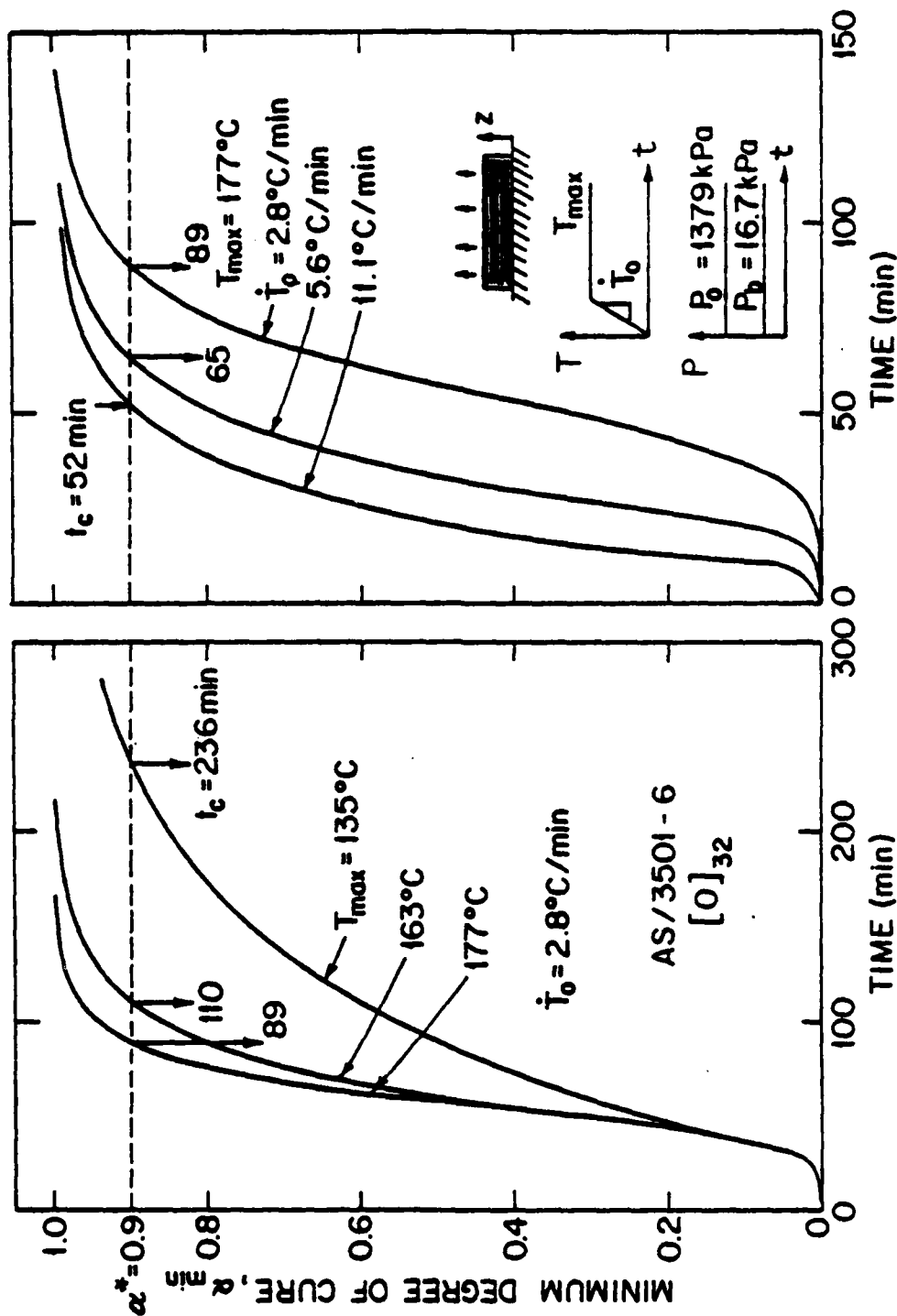


Figure 33 Minimum Degree of Cure, α_{min} , as a Function of Time for a 32-Ply Composite at a) Different Maximum Cure Temperatures, T_{max} (left) and b) Different Heating Rates, \dot{T}_0 (right). Results Obtained by the Model.

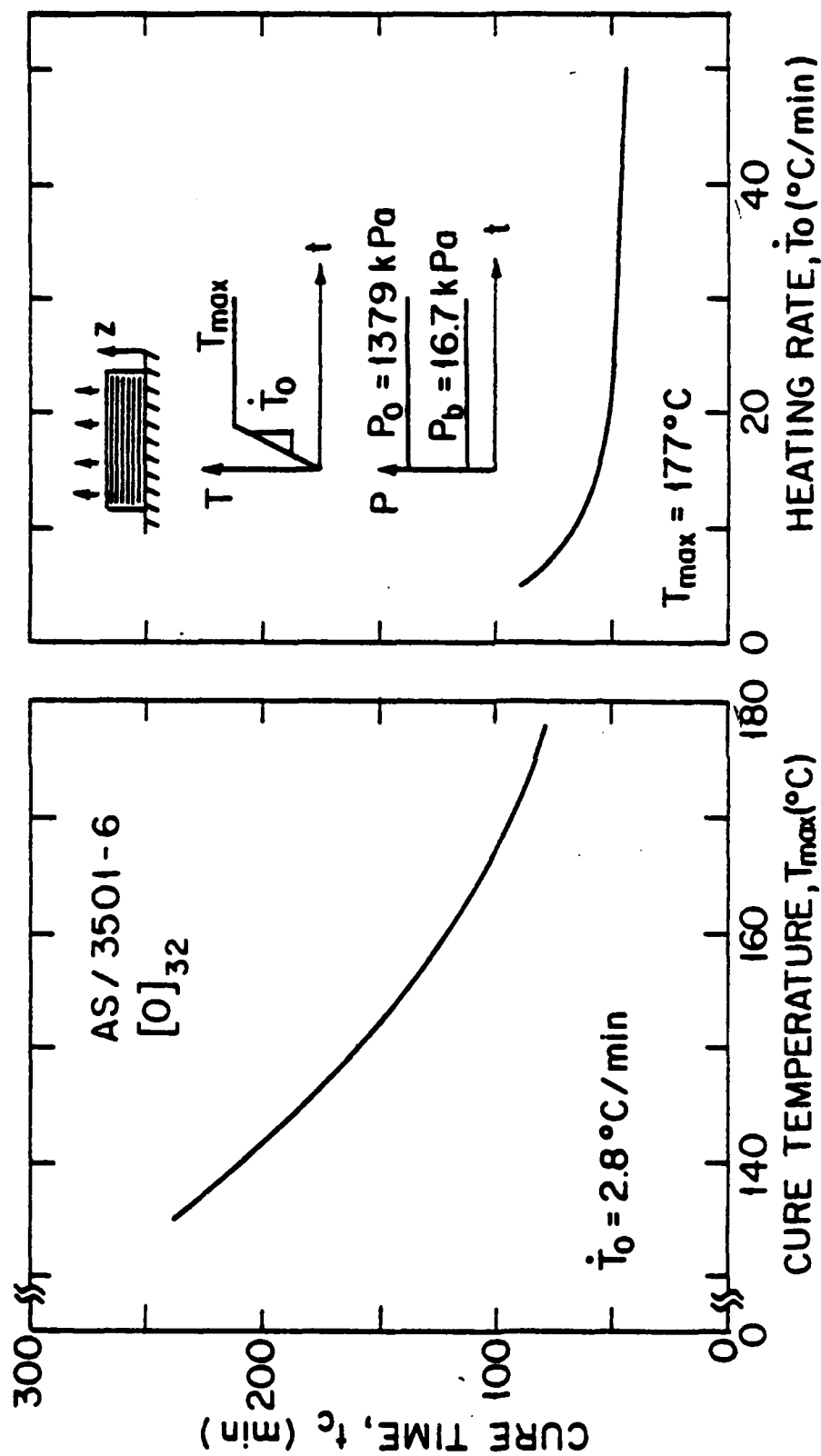


Figure 34 Cure Time, t_c , as a Function of a) Maximum Cure Temperature, T_{max} (left) and b) Heating Rate, \dot{T}_0 (right), for a 32-Ply Composite. Results Obtained by the Model.

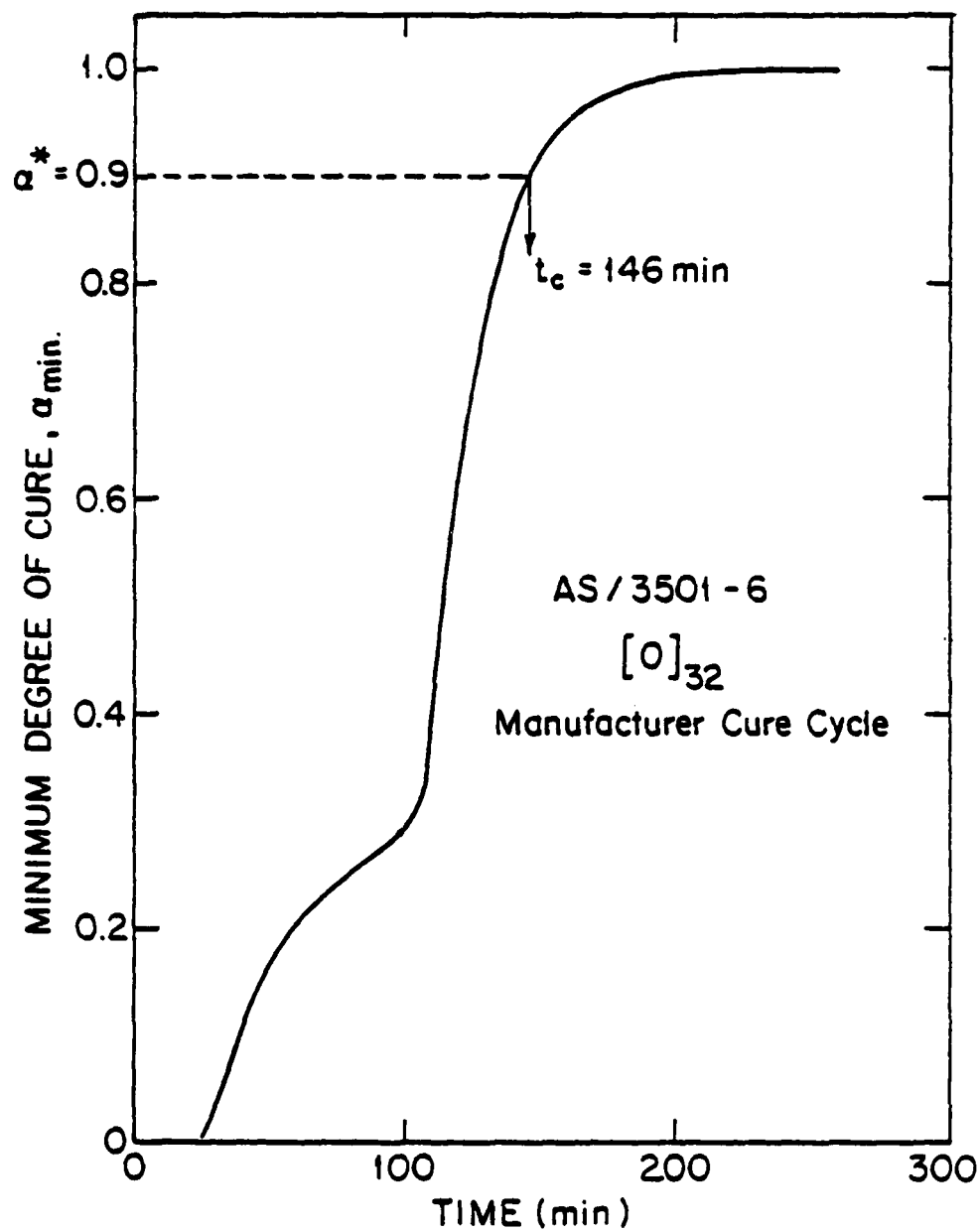


Figure 35 Minimum Degree of Cure, α_{\min} , as a Function of Time for a 32-Ply Composite Cured by the Manufacturer's Recommended Cure Cycle (Figure 21). Results Obtained by the Model.

SECTION VII

SUMMARY AND CONCLUSION

The following major tasks were completed during the course of this investigation:

- 1) Models were developed which simulate the curing process of composites constructed from continuous, fiber-reinforced, thermosetting resin matrix prepreg materials. The models relate the cure cycle to the thermal, chemical, and physical processes occurring in the composite during cure.
- 2) On the basis of the models, a computer code was developed which can be used to generate the following information for flat-plate composites cured by a specified cure cycle:
 - a) the temperature, T , inside the composite as a function of position and time;
 - b) the degree of cure of the resin, α , as a function of position and time;
 - c) the resin viscosity, μ , as a function of position and time;
 - d) the number of compacted prepreg plies, n_s , as a function of time;

- e) the amount of resin in the bleeder as a function of time; and
 - f) the thickness and the mass of the composite as a function of time.
- 3) The input parameters required in the computer code for the solution of the models were specified. The methods used to determine the parameters generally not known were described. These parameters included a) the thickness and resin content of a compacted ply, b) the apparent permeability and flow coefficient of the prepreg, c) the heat of reaction and the cure kinetics of the prepreg resin system, and d) the resin viscosity.
- 4) Experiments were performed measuring the temperature distribution in and the resin flow out of composites during cure. These measurements were made using test specimens constructed from Hercules AS/3501-6 prepreg material.
- 5) Calculations were performed with the computer code for the conditions employed in the experiments. The calculated results were compared with the experimental data and the results of the computer code showed that the model describes adequately the temperature distribution and resin flow of flat-plate, unidirectional composite panels during cure.
- 6) A parametric study was performed to illustrate how the model and the associated computer code can be used to determine the appropriate cure cycle for a given application which results

in a composite that is cured uniformly in the shortest amount of time.

In the present form, the computer code can be applied to flat-plate geometry only. It could, however, be readily extended to composites made in different shapes.

APPENDICES

APPENDIX A

HEAT OF REACTION AND DEGREE OF CURE MEASUREMENTS FOR HERCULES 3501-6 RESIN

In this appendix, the procedures used to obtain the heat of reaction and degree of cure for Hercules 3501-6 resin are described. The composition of the resin is given in Table A.1.

A.1 Experimental

The heat of reaction and the degree of cure were measured using a Perkin-Elmer DSC-2 differential scanning calorimeter. Prior to the tests, the DSC temperature (abscissa) and the DSC energy (ordinate) calibration was checked following the procedure recommended by the manufacturer [43].

A sample ranging in weight from 3 mg to 8 mg was encapsulated in a standard aluminum sample pan. The encapsulated sample was placed in the DSC sample holder and the rate of heat generation from the sample was measured as a function of time. An empty aluminum sample pan and cover was used as a reference. The weight of the sample was measured before and after the test. The weight losses during the tests were found to be negligible. The rate of heat generation dQ/dt was displayed on a strip chart recorder. The tests were performed in two different ways [11]: a) with the sample kept at constant temperature (isothermal

Table A.1

Composition of Hercules 3501-6 Resin.

Amounts given are in parts per hundred resin [42].

Epoxide No. 1 (H)	100
Curing Agent (DDS)	44
Epoxide No. 2 (H)	16
Epoxide No. 3 (H)	15
BF ₃	2

scanning), and b) with the sample heated at a constant scanning rate (dynamic scanning). Isothermal tests were performed at eight different temperatures: 400K, 425K, 430K, 440K, 450K, 465K, 470K, and 475K. The total time required for a test ranged from 15 min (at 400K) to 5 min. (at 475K). The time to reach the steady state was less than 30 seconds. The temperature was raised from room temperature to the test temperature at 320K/min.

In the experiments where dynamic scanning was applied, the temperature was raised from 320K to 590K at the rate of 20K/min. The heat of reaction was determined from the experiments using dynamic scanning. The rate of heat generation was plotted versus time and the area under the curve was determined (Figure A.1). The heat of reaction was calculated by the expression

$$H_r = \int_0^{t_f} (dQ/dt) dt \quad (A.1)$$

where t_f is the time required to complete the reaction.

The amount of heat released up to time t was determined using the rate of heat generations measured during isothermal scanning experiments. The rate of heat generation was plotted versus time and the area under the curve provided the amount of heat released (Figure A.1)

$$H = \int_0^t (dQ/dt) dt \quad (A.2)$$

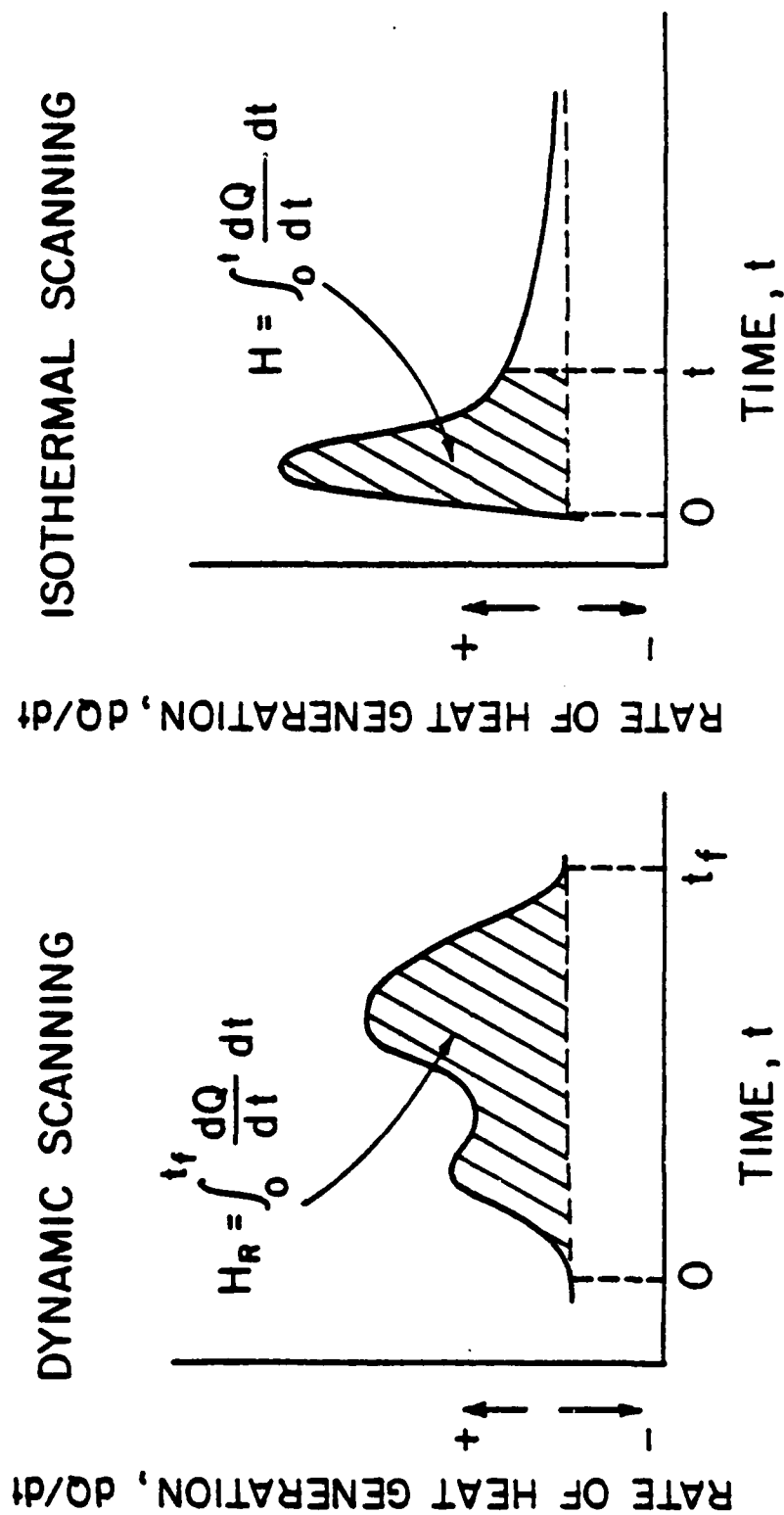


Figure A.1 Illustration of Rate of Heat Generation versus Time Curves Measured by Differential Scanning Calorimetry Using Dynamic Scanning and Isothermal Scanning.

The degree of cure is defined as

$$\alpha \equiv H/H_r \quad (A.3)$$

The cure rate is calculated by the expression

$$d\alpha/dt = (dQ/dt)/H_r \quad (A.4)$$

where the rate of heat generation dQ/dt is provided by the measurements.

A.2 Results

The heat of reaction of the resin was determined from the results of the dynamic scanning measurements. The tests were repeated four times. A typical result is shown in Figure A.2. Note that there are two "humps" in the dQ/dt versus time curve. These humps are caused by two different major reactions occurring during the cure. The measurements gave the following value for the heat of reaction

$$H_r = 473.6 \pm 5.4 \text{ kJ/kg} \quad (A.5)$$

The degree of cure α and the cure rate $d\alpha/dt$ were determined from the results of the isothermal scanning experiments. From the measured values of dQ/dt , the heat released H up to time t , the degree of cure α at time t , and the cure rate $d\alpha/dt$ at time t were calculated using Equations (A.2) - (A.5). The results are plotted in Figure A.3.

Efforts were made to describe the $d\alpha/dt$ versus α data with a modified Arrhenius type equation. In this investigation, the following equations were found to describe the data well [20, 23, 24]

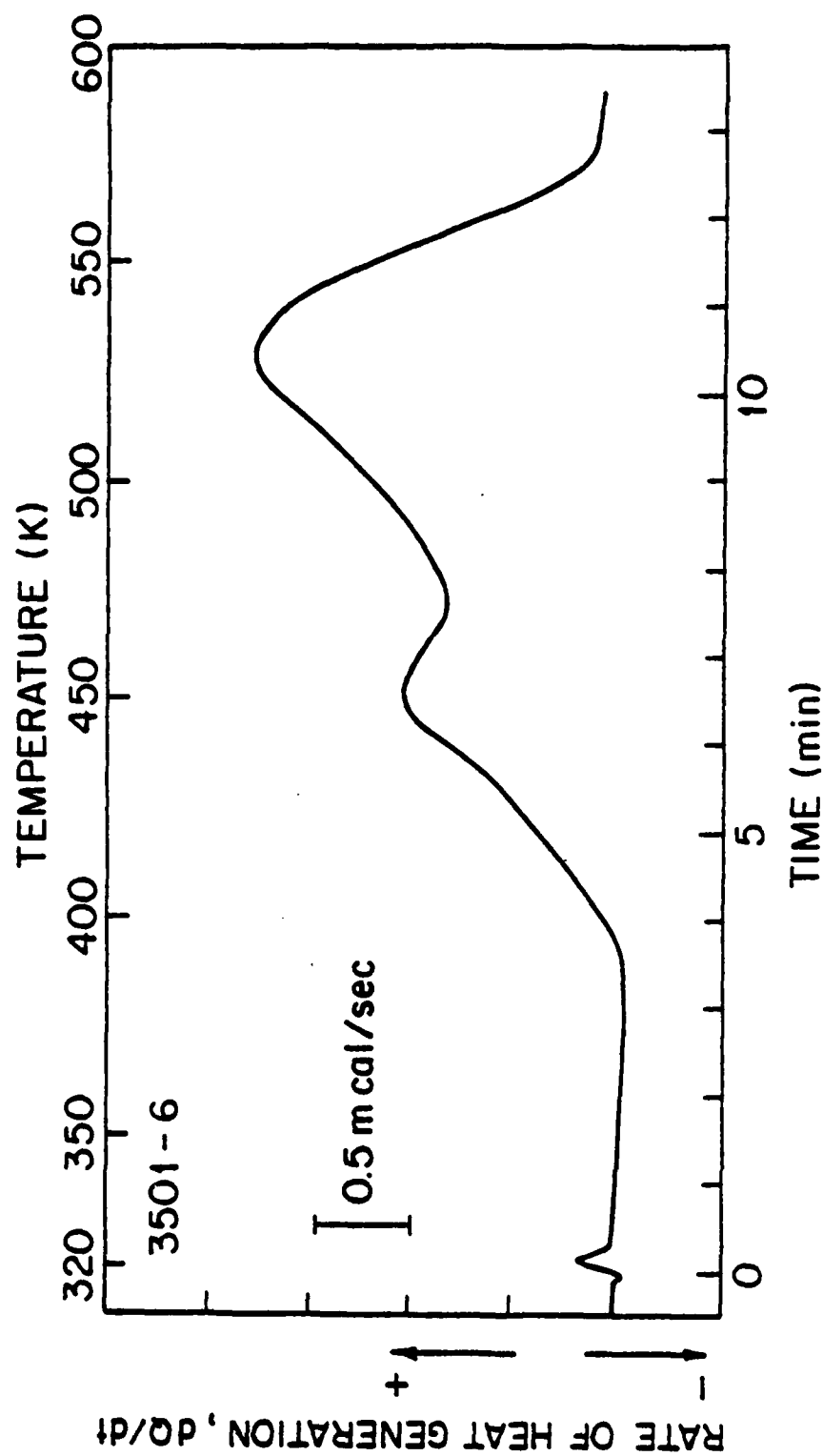


Figure A.2 A Typical Rate of Heat Generation versus Time Curve Provided by Dynamic Scanning Experiments. Sample Size 4.3 mg. Temperature Scale Constructed from the Known Value of the Scanning Rate which was 20 K/min.

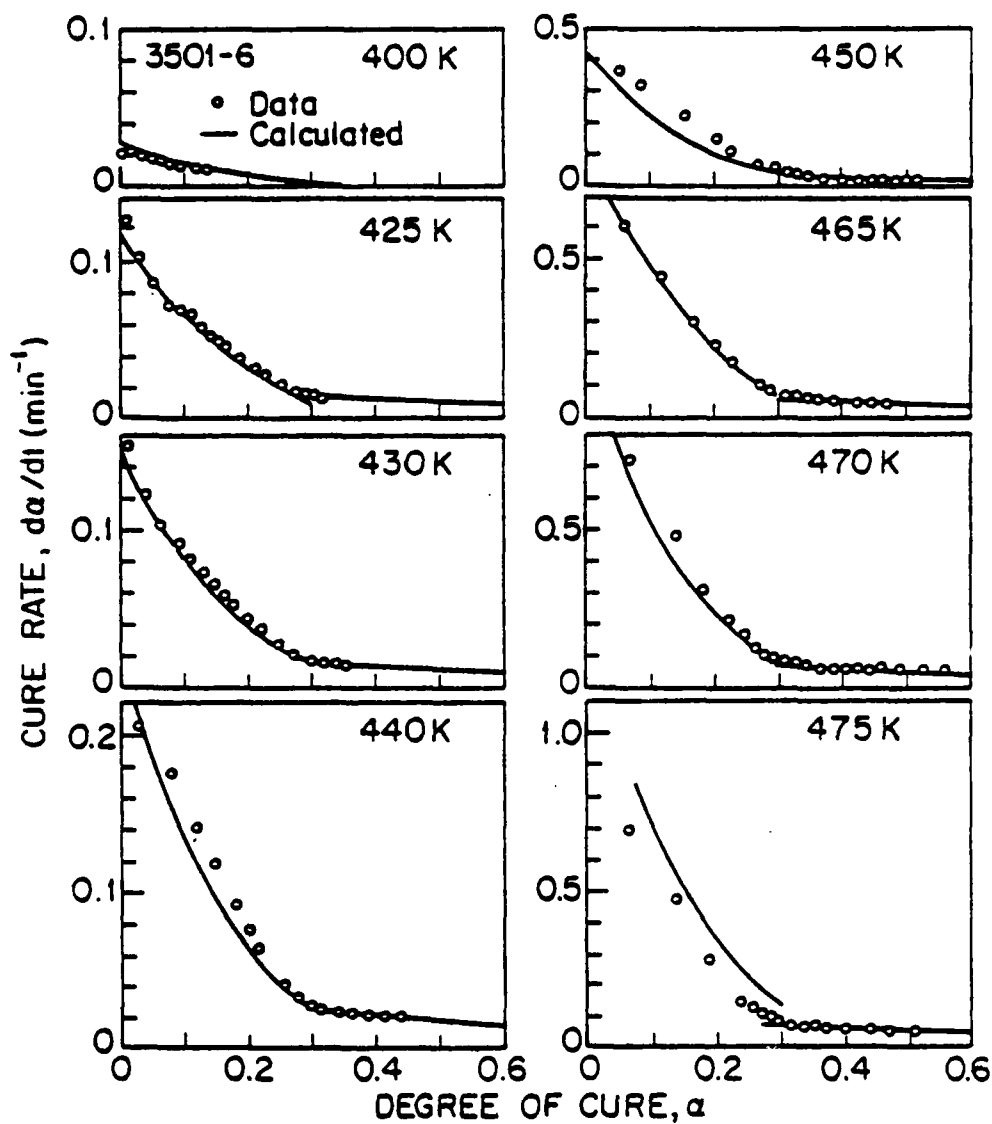


Figure A.3 Cure Rate versus Degree of Cure. Solid Lines were Calculated Using Equations (A.6)-(A.8) and the Constants given in Table A.2. Note the Difference in Scales on the Vertical Axes of the Figures on the Left and Right.

Table A.2

The Values of the Constants in Equation (A.8).

$$A_1 = 2.101 \times 10^9 \text{ min}^{-1}$$

$$A_2 = -2.014 \times 10^9 \text{ min}^{-1}$$

$$A_3 = 1.960 \times 10^5 \text{ min}^{-1}$$

$$\Delta E_1 = 8.07 \times 10^4 \text{ J/mol}$$

$$\Delta E_2 = 7.78 \times 10^4 \text{ J/mol}$$

$$\Delta E_3 = 5.66 \times 10^4 \text{ J/mol}$$

$$d\alpha/dt = (K_1 + K_2\alpha)(1-\alpha)(B-\alpha) \quad \alpha \leq 0.3 \quad (\text{A.6})$$

$$d\alpha/dt = K_3(1-\alpha) \quad \alpha > 0.3 \quad (\text{A.7})$$

where

$$\begin{aligned} K_1 &= A_1 \exp(-\Delta E_1/RT) \\ K_2 &= A_2 \exp(-\Delta E_2/RT) \\ K_3 &= A_3 \exp(-\Delta E_3/RT) \end{aligned} \quad (\text{A.8})$$

A_1 , A_2 , A_3 are the pre-exponential factors, ΔE_1 , ΔE_2 , ΔE_3 are the activation energies, R is the universal gas constant, and T is the absolute temperature. B is a constant independent of temperature. The constants K_1 , K_2 and B were determined by a non-linear least squares curve fit to the $d\alpha/dt$ versus α data using the Levenberg-Marquardt algorithm [44]. This procedure gave the following value of B

$$B = 0.47 \pm 0.07 \quad (\text{A.9})$$

Using the value $B = 0.47$, the values of K_1 and K_2 were calculated by a linear least squares curve fit to the data at α values less than 0.3. The K_1 and K_2 values thus calculated are plotted in Figure A.4. The value of K_3 was obtained by fitting a linear least squares curve to the $d\alpha/dt$ versus α data at α values greater than 0.3 ($\alpha > 0.3$). The resulting K_3 values are also shown in Figure A.4.

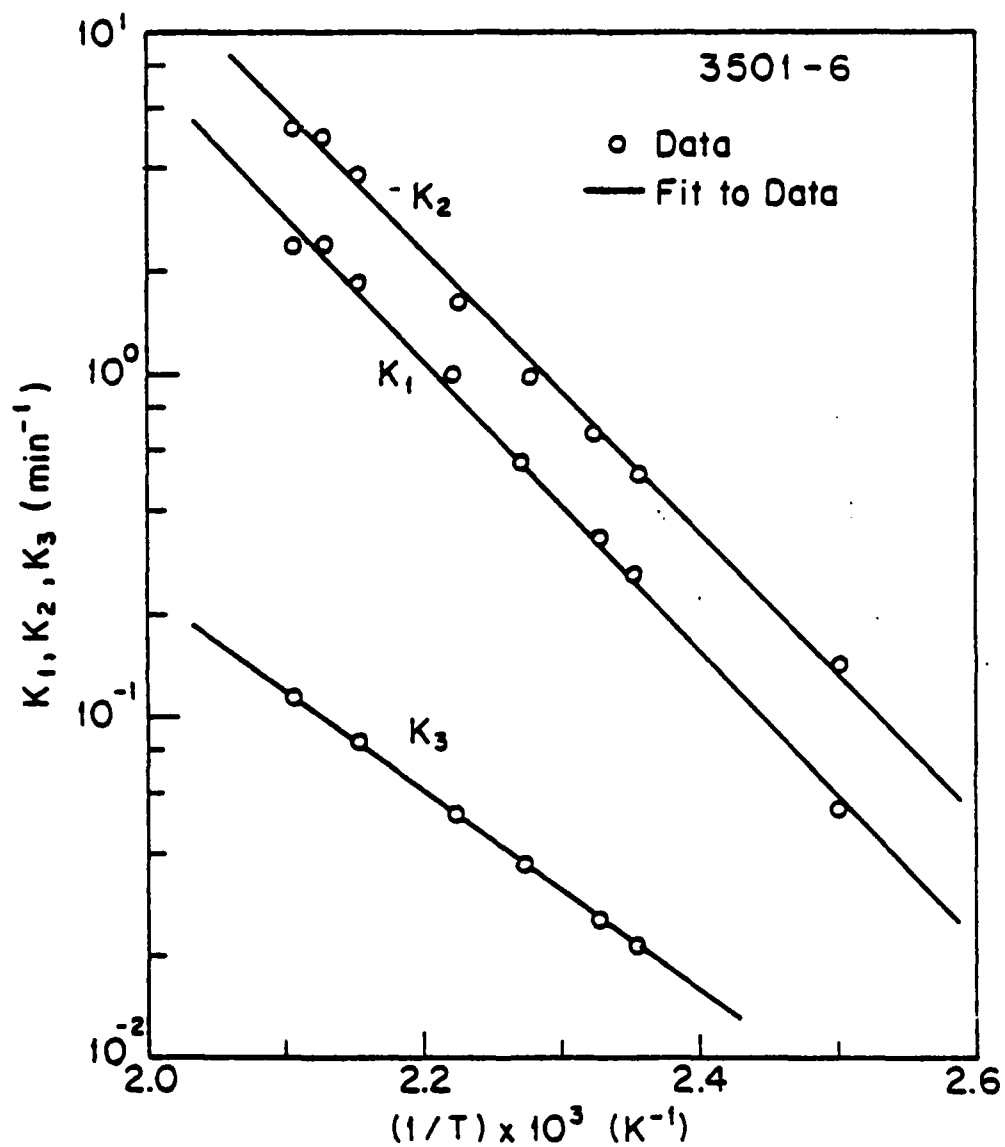


Figure A.4 The Parameters, K_1 , K_2 , and K_3 (Equations A.6-A.8), as a Function of Inverse Absolute Temperature. Solid Lines were Calculated by a Least Squares Curve Fit to the Data.

The values of A_1 , A_2 , A_3 and ΔE_1 , ΔE_2 , ΔE_3 were found by fitting straight lines to the K_1 , K_2 , K_3 versus $1/T$ data. The values of those constants are listed in Table A.2.

The reaction rate is described by two different equations (Equations (A.6) and (A.7)). The results of the dynamic scanning measurement showed that there are at least two dominant reactions occurring during the cure. These reactions (represented by the two "humps" in Figure A.1) cannot be correlated by a single equation, but must be described by different equations. This is the reason for the two equations employed here.

Comparisons between the measured values of $d\alpha/dt$ and the values calculated by Equations (A.6) - (A.8) are shown in Figure A.3.

By integrating Equation (A.6) and Equation (A.7), the following relationships between α and t are obtained

$$t = \frac{a_K}{K_2} \ln \left(1 + \frac{K_2}{K_1} \alpha \right) - b_K \ln(1 - \alpha) - c_K \ln \left(1 - \frac{\alpha}{B} \right) \quad (A.10)$$

$$t = -\frac{1}{K_3} \ln \left[\frac{1 - \alpha}{0.7} \right] + t_L \quad (A.11)$$

where

$$\begin{aligned} a_K &= K_2^2 (B - 1) / d_K \\ b_K &= (K_1 + K_2 B) / d_K \\ c_K &= -(K_1 + K_2) / d_K \\ d_K &= (K_1 + K_2) [K_1 B^2 + (K_1 - K_2) B - K_1] \end{aligned} \quad (A.12)$$

and t_L is the time given by Equation (A.10) for $\alpha = 0.3$ ($t = t_L$ at $\alpha = 0.3$).

A.3 Data

The data and the resultant calculated values are presented in Tables A.3 - A.10 of this section. The dQ/dt values given in the tables were obtained by taking the DSC output at selected times and applying a conversion factor to yield the tabulated results in kJ/(kg.min). Likewise, the H (amount of heat released) values obtained from the DSC output at selected times were converted to kJ/kg by a conversion factor.

The symbols used in the tables are explained below:

t = time, min.

dQ/dt = rate of heat generation, kJ/(kg.min).

H = amount of heat released (defined by Equation (A.2)), kJ/kg.

α = degree of cure calculated by Equation (A.3).

$d\alpha/dt$ = cure rate calculated by Equation (A.4), min^{-1} .

Table A.3

Hercules 3501-6

Temperature = 400K

Sample weight = 8.07 mg

t	dQ/dt	H	α	d α /dt
0.01	9.95	0.54	0.0011	0.0210
0.26	11.27	2.26	0.0048	0.0238
0.51	11.60	4.04	0.0085	0.0245
0.76	11.60	5.84	0.0123	0.0245
1.01	11.46	7.63	0.0161	0.0242
1.26	11.18	9.39	0.0198	0.0236
1.51	10.70	11.09	0.0234	0.0226
2.01	10.09	14.31	0.0302	0.0213
2.51	9.14	17.29	0.0365	0.0193
3.01	8.57	20.04	0.0423	0.0181
3.51	8.19	22.63	0.0478	0.0173
4.01	7.81	25.11	0.0530	0.0165
4.51	7.58	27.49	0.0580	0.0160
5.51	7.06	32.02	0.0676	0.0149
6.51	6.73	36.29	0.0766	0.0142
7.51	6.44	40.38	0.0853	0.0136
8.51	6.25	44.32	0.0936	0.0132
9.51	6.06	48.13	0.102	0.0128
11.51	5.59	55.35	0.117	0.0118
13.51	5.30	62.11	0.131	0.0112

Table A.4

Hercules 3501-6

Temperature = 425K

Sample weight = 6.12 mg

t	dQ/dt	H	α	d α /dt
0.115	59.67	5.35	0.0113	0.126
0.283	49.25	15.11	0.0319	0.104
0.533	40.35	25.81	0.0545	0.0852
0.783	36.09	35.61	0.0752	0.0762
1.03	32.96	44.19	0.0933	0.0696
1.28	32.39	52.10	0.110	0.0684
1.53	27.66	59.20	0.125	0.0584
1.78	25.20	65.83	0.139	0.0532
2.03	23.30	71.99	0.152	0.0492
2.28	21.69	77.67	0.164	0.0458
2.53	19.80	82.88	0.175	0.0418
2.78	18.33	87.62	0.185	0.0387
3.03	17.10	91.88	0.194	0.0361
3.53	15.20	99.93	0.211	0.0321
4.03	13.17	107.03	0.226	0.0278
4.53	11.70	113.19	0.239	0.0247
5.03	10.23	118.87	0.251	0.0216
5.53	9.33	123.61	0.261	0.0197
6.53	8.17	131.19	0.277	0.0173
7.53	7.39	137.82	0.291	0.0156
8.53	6.96	143.50	0.303	0.0147
9.53	6.77	148.71	0.314	0.0143

Table A.5

Hercules 3501-6

Temperature = 430K

Sample weight = 7.13 mg

t	dQ/dt	H	α	d α /dt
0.01	74.36	5.30	0.0112	0.157
0.28	58.25	18.04	0.0381	0.123
0.53	48.78	30.88	0.0657	0.103
0.78	43.81	42.48	0.0897	0.0925
1.03	38.83	53.04	0.112	0.0820
1.28	34.53	62.04	0.131	0.0729
1.53	30.88	70.09	0.148	0.0652
1.78	27.85	77.67	0.164	0.0588
2.03	25.29	84.30	0.178	0.0534
2.28	22.64	89.98	0.190	0.0478
2.53	20.46	95.67	0.202	0.0432
2.78	18.57	100.40	0.212	0.0392
3.03	16.95	104.67	0.221	0.0358
3.28	15.49	108.93	0.230	0.0327
3.53	14.30	112.72	0.238	0.0302
4.03	12.12	119.35	0.252	0.0256
4.53	10.89	125.03	0.264	0.0230
5.03	9.71	130.24	0.275	0.0205
5.53	9.05	134.98	0.285	0.0191
6.53	8.38	143.50	0.303	0.0177
7.53	8.05	151.55	0.320	0.0170
8.53	7.81	159.60	0.337	0.0165
9.53	7.44	167.18	0.353	0.0157

TABLE A.6

Hercules 3501-6

Temperature = 440K

Sample weight = 7.52 mg

t	dQ/dt	H	α	d α /dt
0.18	98.04	15.06	0.0318	0.207
0.43	83.35	38.03	0.0803	0.176
0.68	66.78	56.83	0.120	0.141
0.93	56.36	71.99	0.152	0.119
1.18	43.86	84.77	0.179	0.0926
1.43	36.42	94.72	0.200	0.0769
1.68	30.88	103.24	0.218	0.0652
1.93	26.19	110.35	0.233	0.0553
2.18	22.45	116.51	0.246	0.0474
2.43	19.65	121.72	0.257	0.0415
2.68	17.67	126.45	0.267	0.0373
2.93	16.06	130.71	0.276	0.0339
3.18	14.92	134.50	0.284	0.0315
3.43	13.88	137.82	0.291	0.0293
3.68	13.40	141.61	0.299	0.0283
4.18	12.74	147.76	0.312	0.0269
4.68	12.08	154.39	0.326	0.0255
5.18	11.60	160.08	0.338	0.0245
6.18	10.89	172.39	0.364	0.0230
7.18	10.32	184.23	0.389	0.0218
8.18	10.14	195.60	0.413	0.0214
9.18	9.99	206.49	0.436	0.0211

TABLE A.7

Hercules 3501-6

Temperature = 450K

Sample weight = 5.41 mg

t	dQ/dt	H	α	d α /dt
0.20	174.76	22.73	0.0480	0.369
0.31	152.03	41.49	0.0876	0.321
0.56	104.67	75.30	0.159	0.221
0.81	73.88	73.88	0.206	0.156
1.06	54.95	113.66	0.240	0.116
1.31	36.09	125.03	0.264	0.0762
1.56	32.39	133.56	0.282	0.0684
1.81	26.71	140.66	0.297	0.0564
2.06	23.77	147.29	0.311	0.0502
2.31	21.74	152.97	0.323	0.0459
2.56	20.08	158.18	0.334	0.0424
2.81	19.32	162.92	0.344	0.0408
3.06	18.71	167.65	0.354	0.0395
3.56	17.14	175.71	0.371	0.0362
4.06	16.58	182.34	0.385	0.0350
4.56	15.91	189.44	0.400	0.0336
5.06	15.11	195.60	0.413	0.0319
5.56	14.44	203.17	0.429	0.0305
6.56	13.83	213.59	0.451	0.0292
7.56	13.45	223.07	0.471	0.0284
8.56	12.98	233.96	0.494	0.0274
9.56	12.27	242.96	0.513	0.0259

Table A.8

Hercules 3501-6

Temperature = 465K

Sample weight = 4.22 mg

t	dQ/dt	H	α	d α /dt
0.13	284.63	27.00	0.0570	0.601
0.25	212.17	57.78	0.122	0.448
0.38	146.82	80.51	0.170	0.310
0.50	107.03	96.14	0.203	0.226
0.63	80.04	107.98	0.228	0.169
0.75	62.52	116.98	0.247	0.132
0.88	53.04	124.08	0.262	0.112
1.00	46.27	130.24	0.275	0.0977
1.13	42.77	135.92	0.287	0.0903
1.25	39.26	140.66	0.297	0.0829
1.50	35.05	150.13	0.317	0.0740
1.75	32.25	158.66	0.335	0.0681
2.00	30.12	166.23	0.351	0.0636
2.25	28.04	173.34	0.366	0.0592
2.75	25.91	187.07	0.395	0.0547
3.25	24.06	199.39	0.421	0.0508
3.75	22.64	211.23	0.446	0.0478
4.25	21.74	222.12	0.469	0.0459

TABLE A.9

Hercules 3501-6

Temperature = 470K

Sample weight = 3.67 mg

t	dQ/dt	H	α	d α /dt
0.13	340.04	31.73	0.067	0.718
0.25	231.12	67.25	0.142	0.488
0.38	146.34	90.93	0.192	0.309
0.50	104.19	106.56	0.225	0.220
0.63	77.20	117.45	0.248	0.163
0.75	62.52	126.45	0.267	0.132
0.88	53.99	133.56	0.282	0.114
1.00	48.31	140.19	0.296	0.102
1.13	45.99	145.87	0.308	0.0971
1.25	44.85	151.55	0.320	0.0947
1.50	42.62	162.44	0.343	0.0900
1.75	40.63	172.86	0.365	0.0858
2.00	37.89	182.81	0.386	0.0800
2.25	36.47	191.81	0.405	0.0770
2.50	34.76	200.81	0.424	0.0734
2.75	33.63	209.33	0.442	0.0710
3.00	32.82	217.86	0.460	0.0693
3.50	31.68	233.96	0.494	0.0669
4.00	31.12	249.59	0.527	0.0657
4.50	30.55	265.22	0.560	0.0645

TABLE A.10

Hercules 3501-6

Temperature = 475K

Sample weight = 3.3 mg

t	dQ/dt	H	α	d α /dt
0.11	329.15	29.03	0.0613	0.695
0.24	222.59	64.41	0.136	0.470
0.36	134.50	86.67	0.183	0.284
0.49	92.83	101.82	0.215	0.196
0.61	73.41	111.30	0.235	0.155
0.74	63.46	119.35	0.252	0.134
0.86	54.46	126.92	0.268	0.115
0.99	52.10	133.56	0.282	0.110
1.11	46.65	139.71	0.295	0.0985
1.36	41.35	150.60	0.318	0.0873
1.61	39.31	160.55	0.339	0.0830
1.86	34.67	164.81	0.348	0.0732
2.11	33.34	173.34	0.366	0.0704
2.61	32.02	189.44	0.400	0.0676
3.11	29.32	206.49	0.436	0.0619
3.61	27.99	220.70	0.466	0.0591
4.11	26.66	239.64	0.506	0.0563

APPENDIX B

PROPERTIES OF HERCULES AS/3501-6 PREPREG AND MOCHBURG CW 1850 THERMAL FIBER BLEEDER CLOTH

This appendix contains numerical values for the properties of Hercules AS/3501-6 prepreg and Mochburg CW 1850 thermal fiber bleeder cloth. The properties are tabulated in Table B.1.

TABLE B.1

Properties of Hercules AS/3501-6 Prepreg and Mochburg
CW 1850 Thermal Fiber Bleeder Cloth

AS/3501-6

Initial prepreg resin mass fraction ¹ .	42%
Initial thickness of the prepreg ¹ .	$1.651 \times 10^{-4} \text{ m}$
Resin content of one compacted ply ² .	$4.79 \times 10^{-2} \text{ kg/m}^2$
Thickness of one compacted ply ² .	$1.194 \times 10^{-4} \text{ m}$
Apparent permeability of the prepreg normal to the plane of the composite ³ .	$5.8 \times 10^{-16} \text{ m}^2$
Flow coefficient of the prepreg parallel to the fibers ³ .	1.7×10^2
Resin density ⁴ .	$1.26 \times 10^3 \text{ kg/m}^3$
Specific heat of the resin ⁵ .	$1.26 \text{ kJ}/(\text{kg} \cdot \text{K})$
Thermal conductivity of the resin ⁵ .	$1.67 \times 10^{-1} \text{ W}/(\text{m} \cdot \text{K})$
Heat of reaction of the resin.	See Appendix A
Fiber density ⁶ .	$1.79 \times 10^3 \text{ kg/m}^3$
Specific heat of the fiber ⁶ .	$7.12 \times 10^{-1} \text{ kJ}/(\text{kg} \cdot \text{K})$
Thermal conductivity of the fiber ⁶ .	$2.60 \times 10^{-1} \text{ W}/(\text{m} \cdot \text{K})$
Relationship between the cure rate, temperature, and degree of cure.	See Appendix A
Relationship between viscosity, temperature and degree of cure.	See Table 8.2

Mochburg Bleeder Cloth

Apparent permeability ⁷ .	$5.6 \times 10^{-11} \text{ m}^2$
Porosity ⁸ .	0.57

Table B.1 (cont.)

1. Specified by the manufacturer for each shipment of prepreg.
2. Determined by the procedures described in Section 3.1.
3. Estimated by fitting the computer model to the data in Figure 19, as described in Section 3.2.
4. Specified by Hercules for the 3501-6 resin.
5. Estimated from the data of Krehling and Kline [45].
6. Specified by the manufacturer [46].
7. Determined by the procedure described in Section 3.5. The volumetric flow rate per unit area for air through a single sheet of bleeder cloth, and the corresponding pressure drop across the bleeder, were specified by the bleeder cloth manufacturer.
8. Estimated by the procedure outlined in Section 3.5.

TABLE B.2

Empirical Expression for the Viscosity of
3501-6 Resin [29].

$$\mu = \mu_{\infty} \exp \left(\frac{E_{\mu}}{RT} + K_{\mu} \alpha \right)$$

$$\mu_{\infty} = 7.93 \times 10^{-14} \text{ Pa}\cdot\text{s}$$

$$E_{\mu} = 9.08 \times 10^4 \text{ J/mole}$$

$$K_{\mu} = 14.1$$

APPENDIX C

ADDITIONAL TEMPERATURE CONTROLLER INFORMATION

This appendix contains the information required to determine the relationship between temperature sensed by the RTD and the output voltage of the RTD circuit described in Section 5.3. The following curves were constructed using the procedures described in Section 5.3:

- a) The voltage output of the RTD circuit as a function of resistance (Figure C.1).
- b) RTD temperature versus RTD resistance (Figure C.2).
- c) The voltage output of the RTD circuit as a function of RTD temperature (Figure C.3).
- d) The relationship between the digital input to the D/A converter and the analog voltage output (Figure C.4).

A circuit diagram of the temperature controller is shown in Figure C.5.

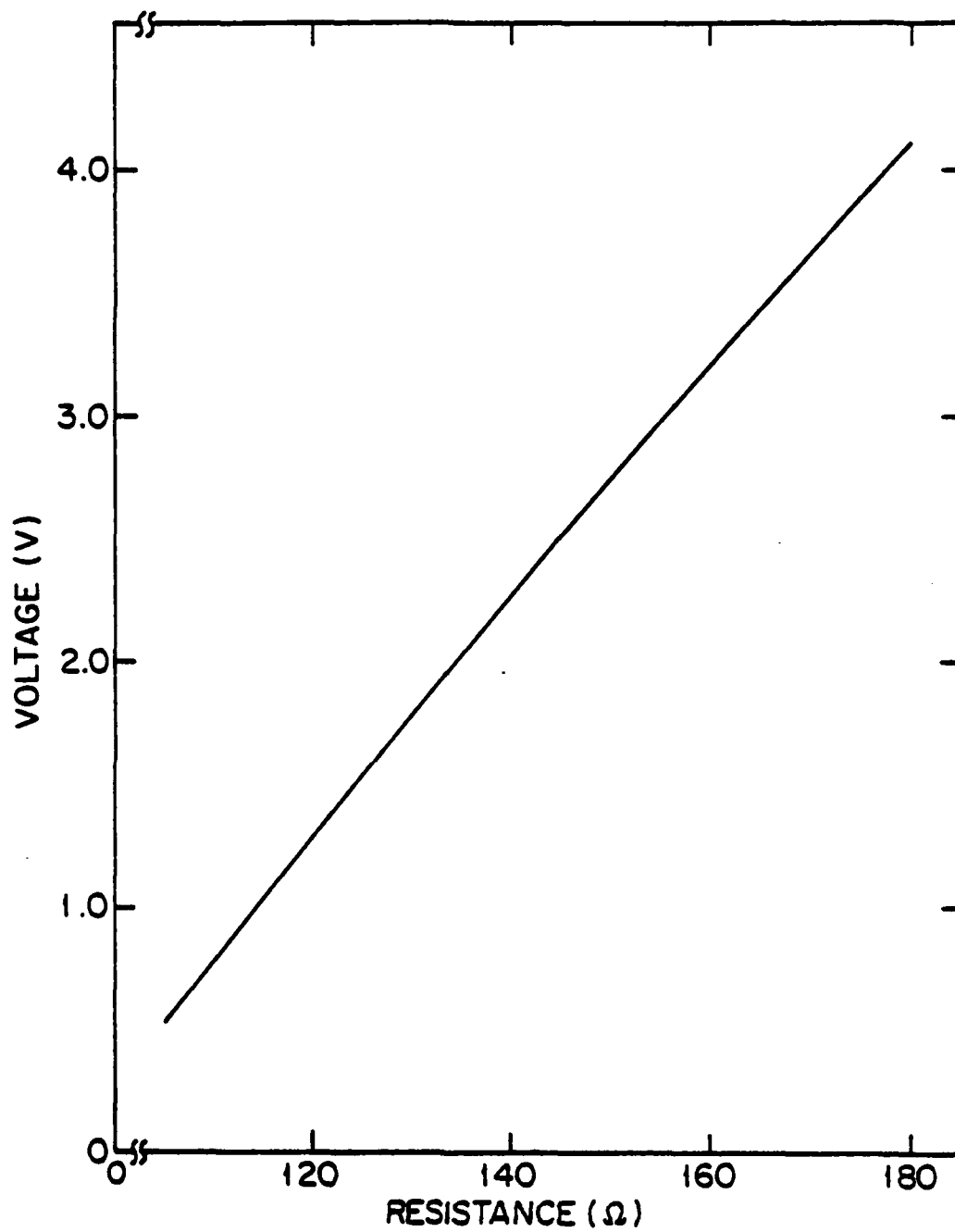


Figure C.1 Output Voltage of the RTD Circuit as a Function of Resistance.

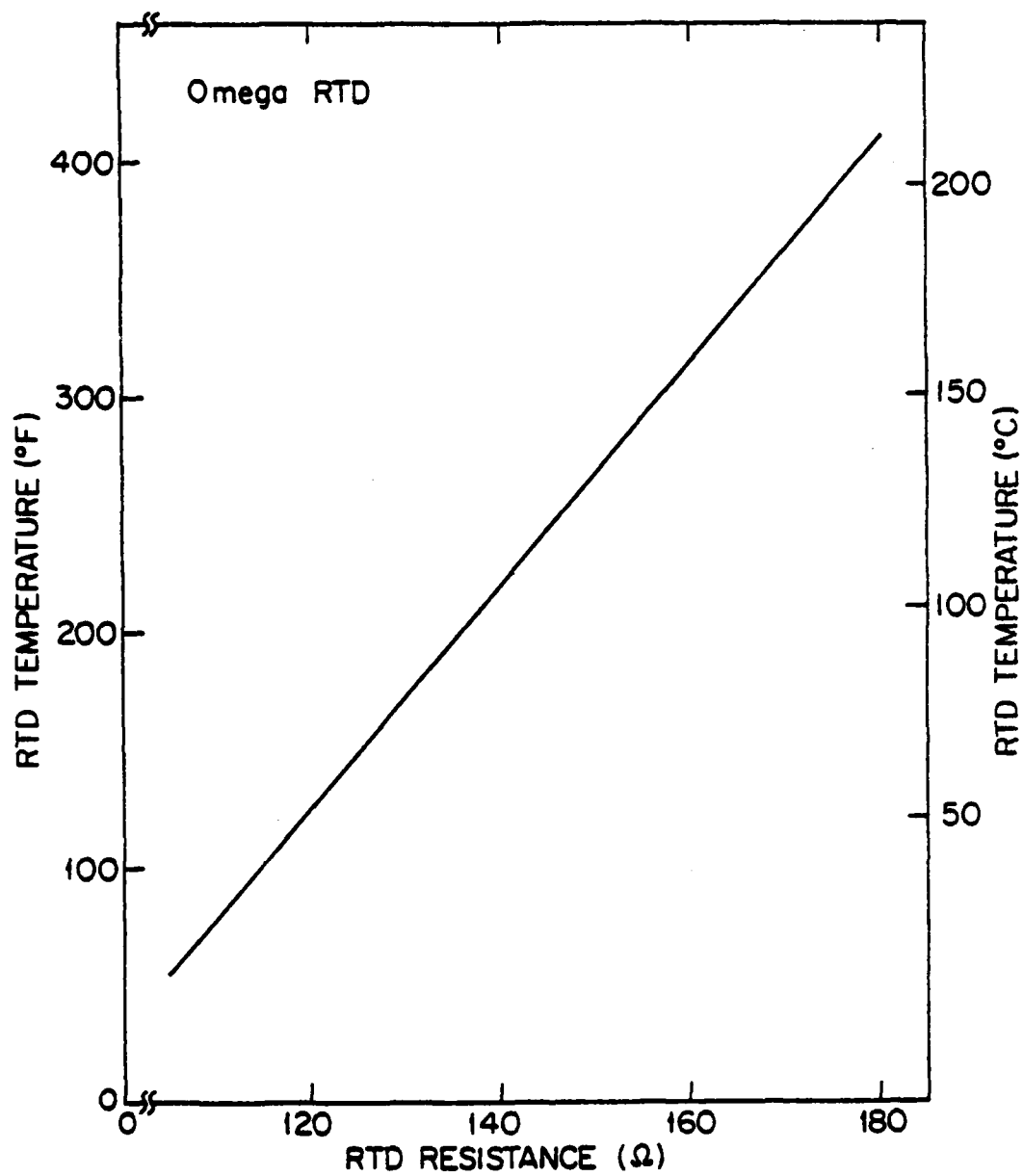


Figure C.2 RTD Temperature as a Function of RTD Resistance.
Calibration Curve was Constructed From Data Provided
by the RTD Manufacturer [47].

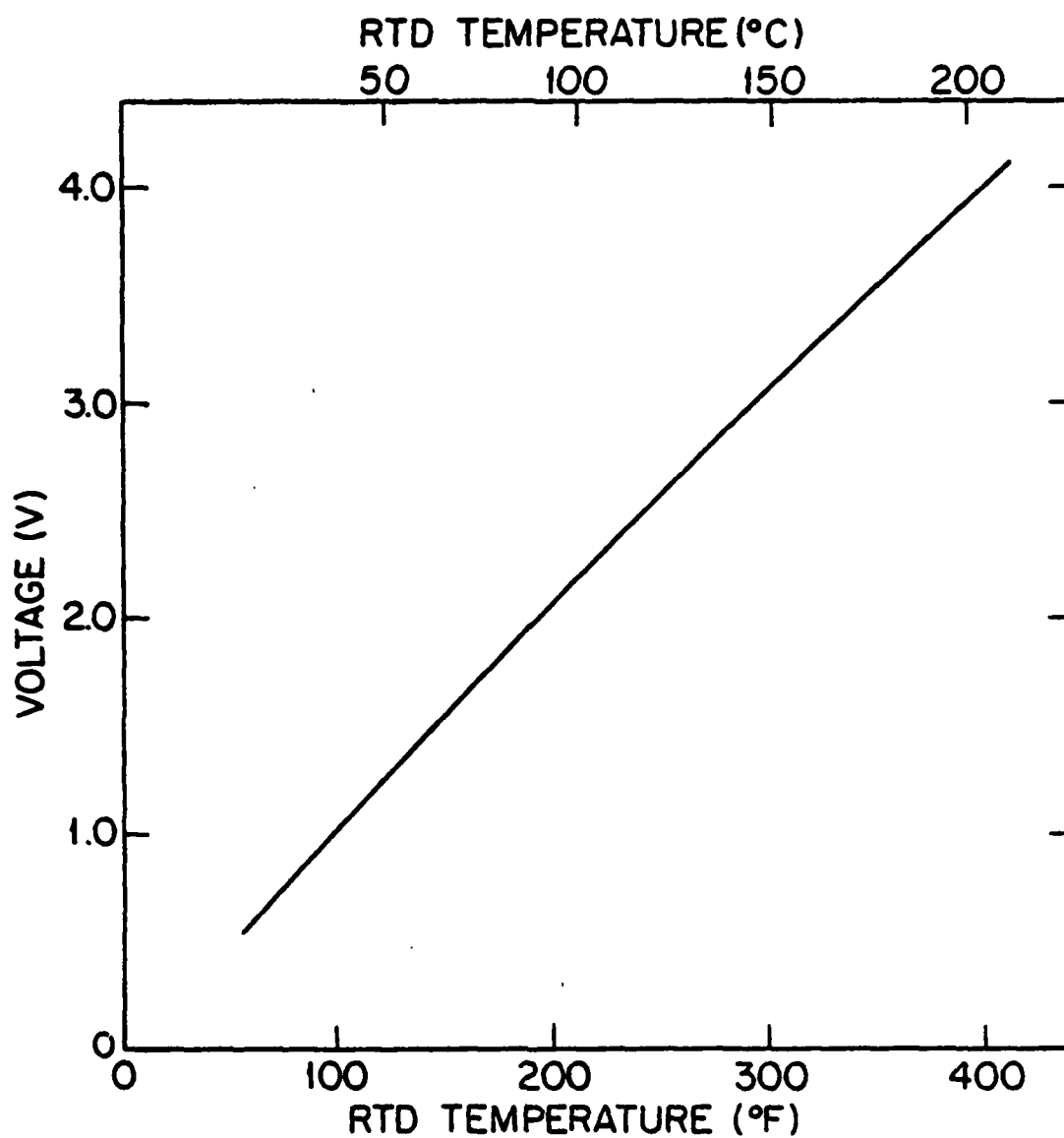


Figure C.3 Output Voltage of the RTD Circuit as a Function of RTD Temperature.

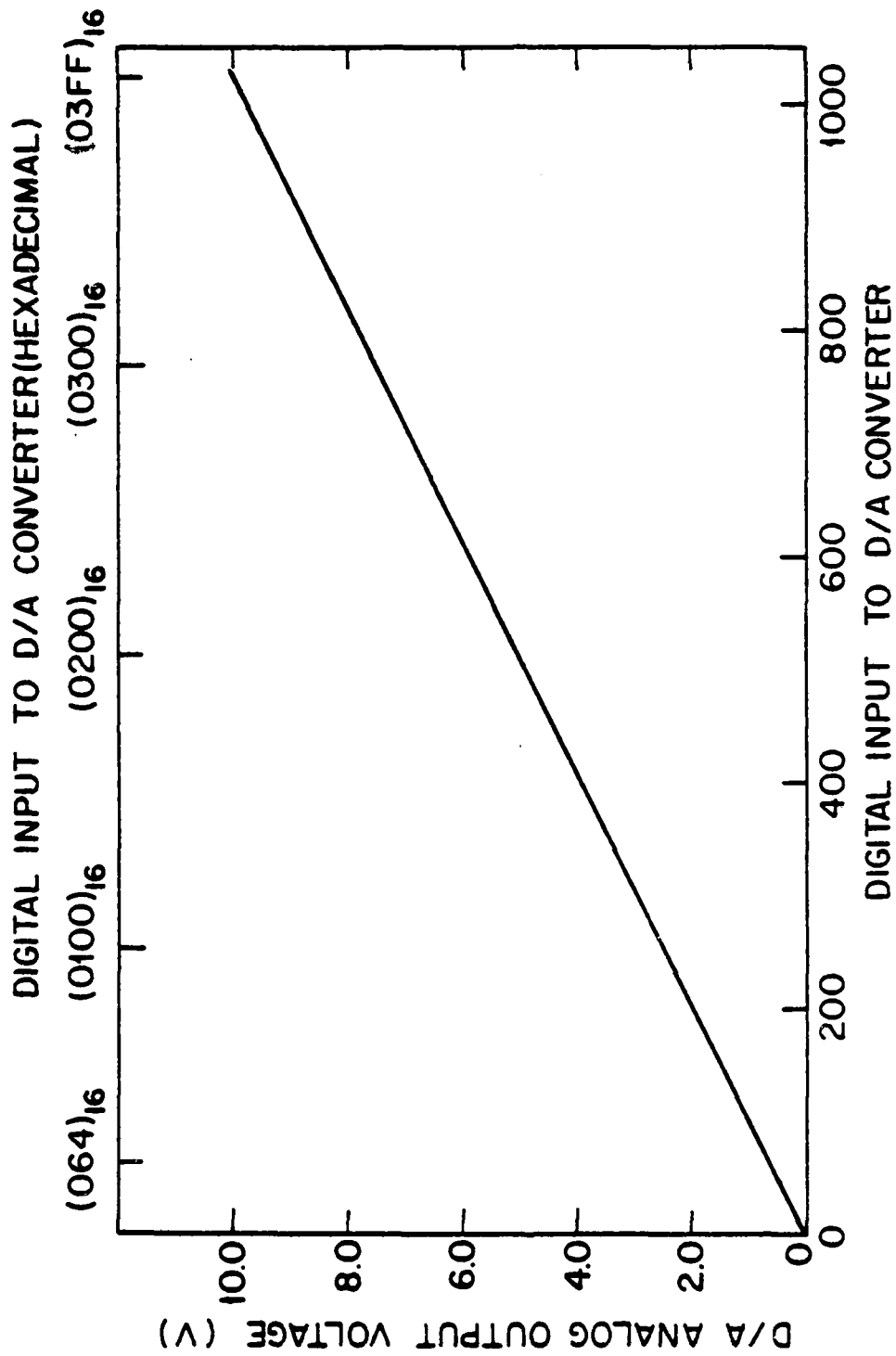


Figure C.4 Relationship Between the Digital Input to the D/A Converter and the Analog Voltage Output.

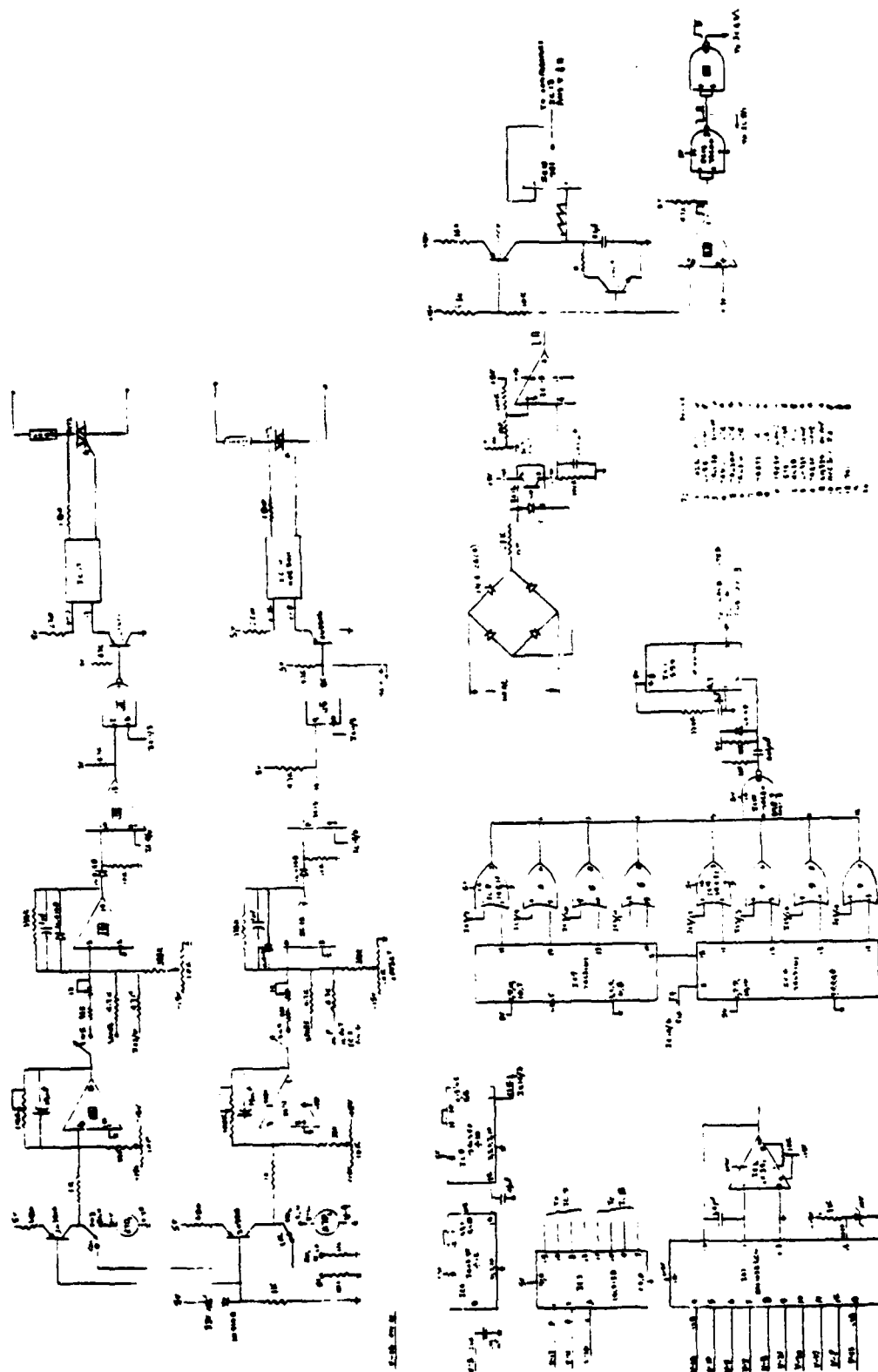


Figure C.5 Temperature Controller Circuit Diagram.

APPENDIX D

RELATIONSHIP BETWEEN PLATEN FORCE AND CYLINDER PRESSURE

The relationship between the force generated by the cylinder ram on the press platens and the indicated cylinder air pressure was determined using a calibrated load cell as described in Section 5.2. This relationship is shown in Figure D.1.

The load cell was calibrated by connecting a Baldwin (Model SR-4) 8.9 kN (2000 lbf) strain gage load cell to an Ellis Associates (Model BAM-1) bridge amplifier and meter. The output of the Ellis bridge amplifier was recorded on a Fluke digital voltmeter. Since the load cell is linear to within $\pm 0.25\%$ over its operating range (0 - 2000 lbf), only two points are necessary to construct a calibration curve [48].

The first calibration point was obtained by balancing the amplifier and bridge circuits of the Ellis bridge amplifier at the no load point (no force applied to the load cell). These circuits were adjusted so that the output voltage of the Ellis bridge amplifier was zero at the no load point. The second point of the calibration curve was obtained by loading the cell to 2000 lbf on a Tinius Olsen compression testing machine. With a force of 2000 lbf applied to the cell, the gain of the Ellis bridge amplifier circuit was adjusted to give a measured output voltage of 2.0 V. Thus, when the applied

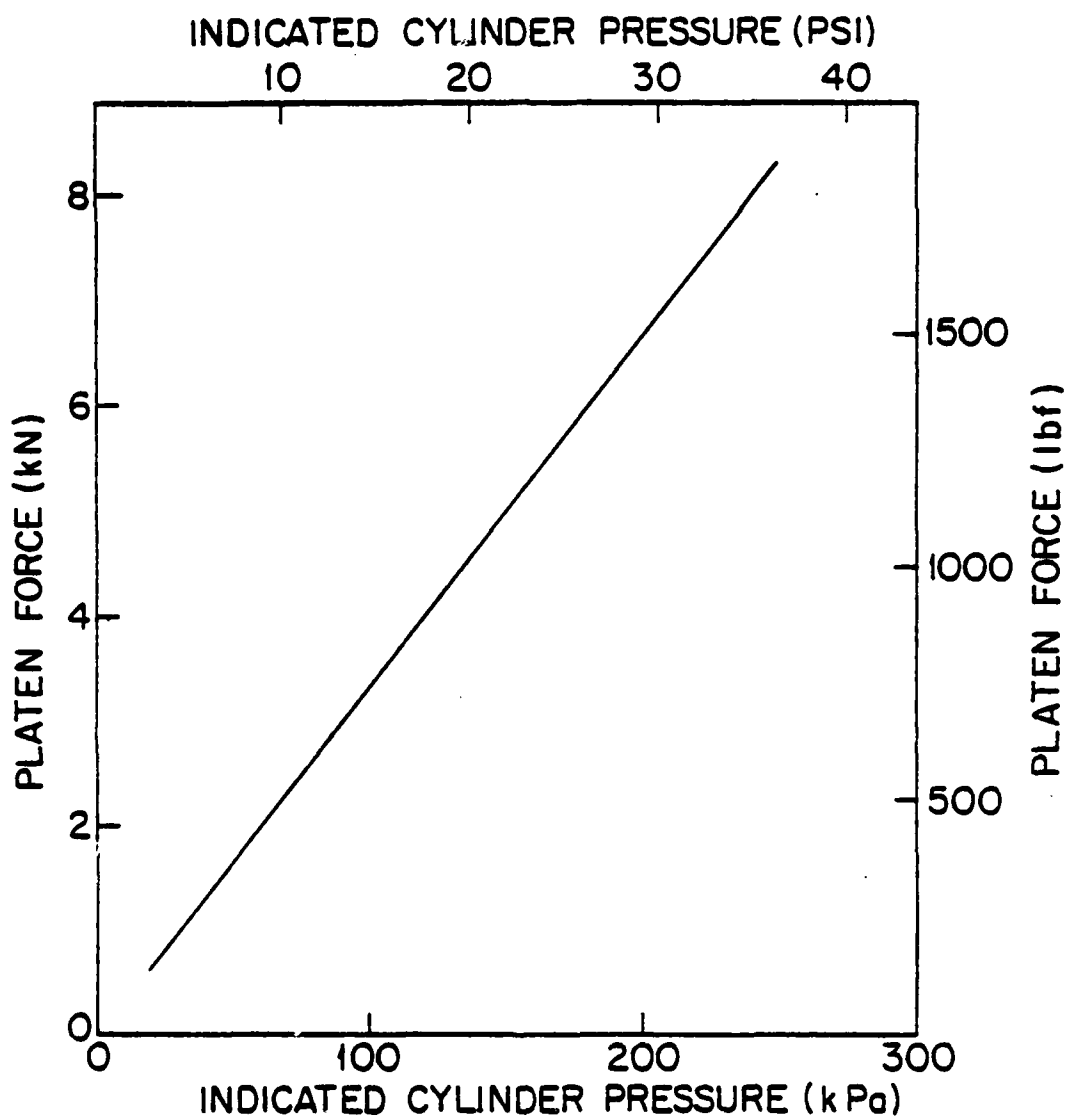


Figure D.1 Force Generated by the Cylinder Ram on the Press Platens as a Function of Indicated Cylinder Air Pressure.

force on the load cell ranged from 0 lbf to 2000 lbf, the output voltage of the Ellis bridge amplifier ranged from 0 V to 2.0 V. Therefore, the force on the load cell could be determined directly from the output voltage measurements of the Ellis bridge amplifier.

REFERENCES

1. Progelhof, R. C. and Throne, J. L., "Non-Isothermal Curing of Reactive Plastics," Polymer Engineering and Science, 15, 690-695 (1975).
2. Broyer, E. and Macosko, C. W., "Heat Transfer and Curing in Polymer Reaction Molding," AIChE Journal, 22, 268-276 (1976).
3. Adabbo, H. E., Rojas, A. J., and Williams, R. J. J., "Critical Parameters for Thermoset Curing in Heated Molds," Polymer Engineering and Science, 19, 835-840 (1979).
4. Stolin, A. M., Merzhanov, A. G., and Malkin, A. Ya., "Non-Isothermal Phenomena in Polymer Engineering and Science: A Review. Part 1: Non-Isothermal Polymerization," Polymer Engineering and Science, 19, 1065-1073 (1979).
5. Barone, M. R. and Caulk, D. A. "The Effect of Deformation and Thermoset Cure on Heat Conduction in a Chopped-Fiber Reinforced Polyester During Compression Molding," International Journal of Heat and Mass Transfer, 22, 1021-1032 (1979).
6. Pusatcioglu, S. Y., Hassler, J. C., Fricke, A. L., and McGee, Jr., H. A., "Effect of Temperature Gradients on Cure and Stress Gradients in Thick Thermoset Castings," Journal of Applied Polymer Science, 25, 381-393 (1980).
7. Lee, L. J., "Curing of Compression Molded Sheet Molding Compound," Polymer Engineering and Science, 21, 483-492 (1981).
8. Nied, H. A., "Cure Time Criterion With Application to Thermoset Polyesters," SPE Technical Papers, 27, 344-347 (1981).
9. Loos, A. C. and Springer G. S., "Calculation of Cure Process Variables During Cure of Graphite - Epoxy Composites," in Producibility and Quality Assurance of Composite Materials, ASTM STP, 1982, (in print).
10. Springer, G. S., "A Model of the Curing Process of Epoxy Matrix Composites," in Proceedings of the Fourth International Congress of Composite Materials, Tokyo, Japan (1982).
11. Fava, R. A., "Differential Scanning Calorimetry of Epoxy Resins," Polymer, 9, 137-151 (1968).
12. Abolafia, O. R., "Application of Differential Scanning Calorimetry to Epoxy Curing Studies," SPE Technical Papers, 15, 610-616 (1969).

13. Prime, R. B., "Dynamic Cure Analysis of Thermosetting Polymers," in Analytic Chemistry, edited by R. S. Porter and J. F. Johnson, Vol. 2, Plenum Press, New York (1970), pp. 201-210.
14. Acitelli, M. A., Prime, R. B., and Sacher, E., "Kinetics of Epoxy Cure: (1) The System of Bisphenol - A Diglycidyl Ether/M-Phenylene Diamine," Polymer, 12, 335-343 (1971).
15. Prime, R. B. and Sacher, E., "Kinetics of Epoxy Cure: 2. The System Bisphenol-A Diglycidyl Ether/Polyamide," Polymer, 13, 455-458 (1972).
16. Sourour, S. and Kamal, M. R., "Differential Scanning Calorimetry for Characterization of Thermoset Cure," SPE Technical Papers, 18, 93-98 (1972).
17. Gibboney, D. A., "Applications Research in the Thermal Analysis Laboratory," SPE Technical Papers, 18, 224-227 (1972).
18. Kamal, M. R. and Sourour, S., "Kinetics and Thermal Characterization of Thermoset Cure," Polymer Engineering and Science, 13, 59-64 (1973).
19. Kamal, M. R., Sourour, S., and Ryan, M., "Integrated Thermo-Rheological Analysis of the Cure of Thermosets," SPE Technical Papers, 19, 187-191 (1973).
20. Prime, R. B., "Differential Scanning Calorimetry of the Epoxy Cure Reaction," Polymer Engineering and Science, 13, 365-371 (1973).
21. Pappalardo, L. T., "DSC Evaluation of B-Stage Epoxy-Glass Prepregs For Multilayer Boards," SPE Technical Papers, 20, 13-16 (1974).
22. Kamal, M. R., "Thermoset Characterization for Moldability Analysis," Polymer Engineering and Science, 14, 231-239 (1974).
23. Sourour, S. and Kamal, M. R., "Differential Scanning Calorimetry of Epoxy Cure: Isothermal Cure Kinetics," Thermochimica Acta, 14, 41-59 (1976).
24. Pappalardo, L. T., "DSC Evaluation of Epoxy and Polyimide - Impregnated Laminates (Prepregs)," Journal of Applied Polymer Science, 21, 809-820, (1977).
25. Siegmann, A. and Narkis, M., "Thermal Analysis of Thermosetting Phenolic Compounds for Injection Molding," Journal of Applied Polymer Science, 21, 2311-2318 (1977).
26. Peyser, P. and Bascom, W. D., "Kinetics of Epoxy Resin Polymerization Using Differential Scanning Calorimetry," Journal of Applied Polymer Science, 21, 2359-2373 (1977).

27. Dutta, A. and Ryan, M. E., "Effect of Fillers on Kinetics of Epoxy Cure," Journal of Applied Polymer Science, 24, 635-649 (1979).
28. Pusatcioglu, S. Y., Fricke, A. L., and Hassler, J. C., "Heats of Reaction and Kinetics of a Thermoset Polyester," Journal of Applied Polymer Science, 24, 937-946 (1979).
29. Lee, W. I., Loos, A. C., and Springer, G. S., "Heat of Reaction, Degree of Cure, and Viscosity of Hercules 3501-6 Resin," (submitted for publication in Journal of Composite Materials, 1982).
30. Bartlett, C. J., "Use of the Parallel Plate Plastometer to Characterize Glass - Reinforced Resins: I. Flow Model," SPE Technical Papers, 24, 638-640 (1978).
31. Collins, R. E., Flow of Fluids through Porous Materials, Reinhold Publishing Corporation, New York (1961).
32. Springer, G. S., "Resin Flow During the Cure of Fiber Reinforced Composites," Journal of Composite Materials, (in print) (1982).
33. White, F. M., Viscous Fluid Flow, McGraw-Hill, New York (1974) pp. 336-337.
34. Springer, G. S. and Tsai, S. W., "Thermal Conductivities of Unidirectional Materials," Journal of Composite Materials, 1, 166-173 (1967).
35. Forsythe, G. E. and Wasow, W. R., Finite-Difference Methods for Partial Differential Equations, John Wiley & Sons, New York (1960), pp 184-190.
36. Carnahan, B., Luther, H. A., and Wilkes, J. O., Applied Numerical Methods, John Wiley & Sons, New York (1969), pp. 441-448.
37. Carslaw, H. S. and Jaeger, J. C., Conduction of Heat in Solids, Second Edition, Oxford Press (1959), pp. 99-102.
38. Hercules Incorporated, Aerospace Division, "Magnamite Graphite Fiber Presentation," Magna, Utah, (received 1981) p. 33.
39. Meade, L. E., "Fabrication of Thick Graphite/Epoxy Wing Surface Structure," in Proceedings of the 24th National SAMPE Symposium and Exhibition, San Francisco, CA (May 8-10, 1979), Vol. 24, Book 1, pp. 252-259.

40. Hollands, K. M. and Kalnin, I. L., "The Kinetics of Gelation of Some Accelerated Acid Anhydride Cured Epoxy Resins," in Epoxy Resins, Advances in Chemistry Series No. 92, American Chemical Society, Washington, D. C. (1970) pp. 60-69.
41. Roller, M. B., "Characterization of the Time-Temperature-Viscosity Behavior of Curing B-Staged Epoxy Resin," Polymer Engineering and Science, 15, 406-414 (1975).
42. Carpenter, J. F., "Test Program Evaluation of Hercules 3501-6 Resin," Final Report for Period 28 February 1977 to 28 February 1978 (NASC Contract No. N00019-77-C-0155), Mc Donnell Aircraft Company, St. Louis, Missouri (1978). Also available from NTIS order No. AD-A-054283/7GI.
43. Perkin-Elmer Corporation, "Model DSC-2 Differential Scanning Calorimeter Instruction Manual," Norwalk, Connecticut (1972).
44. International Mathematical and Statistical Libraries Incorporated, "IMSL Library Reference Manual," Vol. 3, Houston, Texas (1980).
45. Krehling, R. P. and Kline, D. E., "Thermal Conductivity, Specific Heat, and Dynamic Mechanical Behavior of Diglycidyl Ether of Bisphenol A Cured with m-Phenylenediamine," Journal of Applied Polymer Science, 13, 2411-2425 (1969).
46. Hercules Incorporated, Graphite Fiber Business Center, "MagnaMite Graphite Fibers," Magna, Utah (1979).
47. Omega Engineering Inc., "The Omega 1981 Temperature Measurement Handbook," Stamford, Conn., (1981) pp. A.38-A.40.
48. Baldwin Lima Hamilton Corp., Electronics Division, "Instructions SR-4 Load Cells," Bulletin 4360, Waltham, Massachusetts, March, 1961.

— 8
DTIC